A STUDY OF MOVEMENT OF IGS STATIONS DUE TO EFFECT OF HYDROLOGICAL WATER LOADING USING GPS AND GRACE DATA

(A CASE STUDY OF EAST AFRICA)

BY:

BAKARI MCHILA HEMEDI

A Thesis submitted to the School of Graduate Studies of Addis Ababa University in partial fulfillment of the requirements for the Degree of Masters of Science in Civil Engineering under Geodesy.

Addis Ababa, Ethiopia

July 2013

Addis Ababa University

Institute of Technology

Department of Civil Engineering

The undersigned hereby certify that they have read and recommended to the school of technology for acceptance of a thesis entitled "**A study of movement of IGS stations due to effect of hydrological water loading using GPS and GRACE data (A case study of East Africa)**" by Bakari Mchila Hemedi in partial fulfillment of the requirements for the degree of Masters of Science.

Supervisor/Advisor:

1._____ _____ _____

Signature Date

Co-Advisor(s):

1._____ _____ _____

2._____ _____ _____

Signature Date

Examiner(s):

1._____ _____ _____

2._____ _____ _____

3._____ _____ _____

Signature Date

DEDICATION

I would like to dedicate this thesis to my lovely mother Rafia Bakari who gave me great encouragement and support. I would also like to dedicate it to my lovely wife Amina Msangi for the courage and support she gave me. Lastly to my lovely daughter Lulu Abubakar Mchila, and all my family members.

AKNOWLEDGEMENTS

First I would like to thank the Almighty God for the health life, strength and ability to complete this research on time. Thanks to The Almighty Allah for giving me opportunity to study this program with great success from beginning up to end.

My special thanks goes to my parents Rafia Bakari and my late father Mchila Hemedi for the care and support since I was born, my lovely wife Amina Msangi for her toleration, support and encouragement she gave me from beginning up to end of this research.

Great thanks go to all M.Sc. Geodesy program coordinators Dr. Elias Lewi (Addis Ababa University-Ethiopia), Dr. Prosper Ulotu (Ardhi University-Tanzania), Dr. Elifuraha Mtalo (Bagamoyo University- Tanzania), Dr. R. G. Hipkin (Edinburgh University-UK) and Dr. Addisu Hunegnaw (Ethiopia) for their efforts in bringing this program to Ethiopia. I am expressing my gratitude to European Union through Edulink-program for funding this program, Addis Ababa University for their hospitality and acceptance of hosting the program.

My appreciation goes to my supervisor Dr. Addisu Hunegnaw for every step he made in developing my research, his valuable comments, suggestions and great supports which led to successful completion of my thesis. My sincere thanks also go to my Co-supervisor Dr. Tulu Bedada for his great ideas, comments and suggestions on developing and framing the structure and contents of the thesis which led to its quality and readability. Special thanks also go to Dr. R.G. Hipkin for valuable support in developing my thesis.

My deep appreciation also goes to Mr Saria for his helpful support, advices and suggestions which led me to obtain good results. I would like to extend my thanks to Ardhi University for giving me the chance to study in Addis Ababa University Ethiopia. I give also my sincere thanks to all Geomatics department staffs for their effort to make sure that we pursue this M.Sc. in Geodesy program.

Heart fully, I would like to thank all my fellow M.Sc. Geodesy students for their cooperation, toleration, support and encouragement they gave me to the completion of this work. To Mr Asmamaw Chanie and Berhanu Bekele, thanks for your excellence help you gave us when we were not in Ethiopia since you acted on behalf of us. Special thanks to my course mate Mr Leonard Bamuhiga for his helpful ideas, cooperation, courage, moral support and all

matters concerning discussions from the beginning of the course work to the thesis completion.

My last wishful thanks go to all my family members for their tireless support and encouragement, especially for taking care of my family when I was away and their inspirational love and pertinence which led me to complete successfully this research. Thanks to all who contributed in one way or another to my research for better completion.

ABSTRACT

This thesis studies the movement of GPS (IGS) stations due to elastic surface deformation of the earth caused by hydrological water loading as detected by the combined monthly Gravity Recovery and Climate Experiment (GRACE) and GPS data for a period of five years from June 2008 to March 2012. The GRACE data was obtained from four different data processing institutes which are Geoforschungszentrum (GFZ) Potsdam, Centre for Space Research (CSR) Texas, NASA Jet propulsion Laboratory (JPL) and Centre National d'Etudes Spatiales (CNES) to estimate total water storage anomalies over the whole of East African region as a case study involving Tanzania, Kenya, Uganda, Rwanda, Burundi and Ethiopia. Five IGS stations were used in this study in addition to six stabilization IGS sites in order to strengthen the network and get improved deformation estimates. Using 650 km half radius Gaussian smoothing, GRACE detected about 5 mm to 17 mm peak-to-peak of total water storage signal with maximum of 7.3 mm in May 2010 and minimum of ~ -17 mm in July 2011 with 2.88 cm mean standard deviation from the mean of the four standard deviations of the four GRACE data models. The derived water load estimates from GRACE were compared with 3D deformation estimates from GPS observations and found good agreement in areas with high and low hydrological signals at every GPS point with maximum correlation of 0.8 for horizontal and vertical components shown by MAL2 and RCMN stations considering enough data between the two signals being correlated. The monthly station positions were obtained with good repeatability computed as weighted root mean square of ~0 mm to 4 mm for horizontal component and ~3 mm to ~10 mm for vertical component. NKLG showed the largest repeatability of 4.6 mm and 18.4 mm for east component and vertical component respectively. The annual GPS signal for north and east components ranged from 1 mm to 4 mm and ~5 mm to ~9 mm for vertical component. However, ADIS and MBAR stations showed strong negative correlation with GRACE signal in north components while RCMN and MAL2 showed strong negative correlations in east components compared with other IGS stations. The analysis of the combined results revealed strong coincidence between GRACE and GPS signal on water loading effect to all studied IGS stations in the study area. The agreement was also observed when GARCE monthly solution signal from this study were compared with precipitation, rainfall and river water discharge from previous studies.

Key words: GRACE, GPS, hydrological water loading, IGS station movements

TABLE OF CONTENTS

LIST OF FIGURES

LIST OF TABLES

ACRONYMS AND ABBREVIATIONS

AEP	Architecture Evolution Plan
AFB	Air Force Base
AS	Anti-spoofing
CfA	Center for Astrophysics
CIS	Conventional Inertial Reference System
CNES	Centre National d'Etudes Spatiales
CORS	Continuous Operating Reference Stations
CSOC	Consolidated Space Operation Center
CSR	Centre for Space Research
CTS	Conventional Terrestrial Reference System
DASS	Distress Alerting Satellite System
DLR	Deutches Zentrum fur Luft- und Raumfahrt
DoD	Department of Defense
DORIS	Doppler Orbitography Radio Positioning Integrated by Satellite
EAR	East African Rift
EARS	East African Rift System
EGM	Earth Gravity Model
EGNOS	European Geostationary Navigation Overlay Service
EOP	Earth Orientation Parameters
EOW	End of Week
FOC	Full Operation Capability

GDGPS	Global Differential GPS
GFZ	Geoforschungszentrum
GGM	Global Gravity Model
GMT	Generic Mapping Tools
GNSS	Global Navigation Satellite System
GPS	Global Positioning System
GRACE	Gravity Recovery and Climatic Experiment
GRGS	Groupe de Recherches de Geodesie Spatiale
GRS	Geodetic Reference System
HOW	Hand over word
HWL	Hydrological Water Loading
ICGEM	IN Centre for Global Earth Models
IERS	International Earth Rotation Service
IGS	International GNSS service
InSAR	Interferometric Synthetic Aperture Radar
IOC	Initial Operation Capability
ISDC	Information System and Data Centre
ITRF	International Terrestrial Reference Frame
JPL	Jet propulsion Laboratory
MIT	Massachusetts Institute of Technology
NAVSTAR	Navigation Satellite Timing and Ranging
NDGPS	Nationwide Differential GPS System

NGA	National Geospatial-Intelligence Agency
OCS	Operation Control Segment
OCX	Next Generation Operational Control System
PO.DAAC	Physical Oceanography Distributed Active Archive Centre
PREM	Preliminary Reference Earth Model
RINEX	Receiver Independent Exchange Format
SA	Selective availability
SBAS	Space-Based Augmentation System
SINEX	Solution Independent Exchange Format
SIO	Scripps Institution of Oceanography
SLR	Satellite Laser Ranging
SST	Satellite-to-Satellite Tracking
TLM	Telemetry word
TRMM	Tropical Rainfall Measuring Mission
UTC	Coordinated Universal Time
VLBI	Very Long Baseline Interferometry
VMF	Vienna mapping functions
WAAS	Wide Area Augmentation System
ZTD	Zenith Tropospheric Delays

CHAPTER 1: INTRODUCTION

1.1 Background

The Gravity Recovery and Climate Experiment (GRACE) which is a joint mission of NASA in the USA and German Aerospace Center in German was launched in March 17, 2002 aiming at making detailed measurements of Earth's gravity field with spatial resolution of ~400 km. GRACE mission has two identical spacecrafts flying at about 220 kilometers apart in a polar orbit of 89º mean inclination at a mean altitude of 500 kilometers above the Earth. GRACE uses geodetic quality Global Positioning system (GPS) receivers and microwave ranging system to map the Earth's gravity field by making accurate measurements of the distance between the two satellites which provides efficient and cost-effective way to map the Earth's gravity field with unprecedented accuracy. GRACE has generated independent models at approximately one month interval of the Earth's gravitational field from which one can identify the pattern of changes in the surface mass anomalies with time which consists of sets of stokes coefficients which can be used to synthesize global grid of gravity anomalies, of geoid height or of surface mass density (Swenson and Wahr, 2002; Tapley et al., 2004; Wahr et al., 2004). Any of these can be transformed into a representation where the source of the gravity field is an equivalent layer of water on the Earth's surface with a variable thickness. Although GRACE lacks spatial resolution better than few hundred kilometers (spherical harmonic degree < 50) but, when averaged over regions of this size, it detects consistent water mass changes equivalent to the effect of few millimeters (~4.5 mm) of water thickness (Bedada, 2007), which is at least three times better than 15 mm accuracy of equivalent water thickness claimed by Tapley et al. [2004] when smoothed by 1000 km Gaussian filter. Wahr et al, [2006] also stated on the variation of errors in GRACE from one month to another depending on the size of the region and they decrease as smoothing radius increases falling from 38 mm to 15 mm at 500 km and 1000 km Gaussian smoothing radius respectively. This resolution and accuracy of elastic surface deformation as detected by GRACE can be directly observed by other space geodetic techniques such as GPS, VLBI and SLR. GPS can be used to monitor long-term geodynamical phenomena including crustal deformations, plate tectonics, postglacial rebound, and/or volcanic uplift by measuring the position of a fixed benchmark point continuously in time.

However, positioning time series from an individual GPS site commonly contains a significant displacement or movement associated with the response of the earth to surface mass loading (Van Dam and Wahr, 1998). Among the loads likely to be important are those due to changes in atmospheric pressure, tidal and non-tidal fluctuations in the ocean, and variations in the distribution of water, snow, and ice on land. One of the effects of hydrological loading (e.g. continental water storage) is the swelling of the soil below the basement of the pillar supporting the antenna resulting in GPS station uplift (Nahmani et al., 2012). For example, Rajner & Liwosz, [2011] showed that, continental water loading leads to crustal deformation which results in variation of GPS heights as well as variations in the horizontal positions though being affected by smaller amplitudes (1-2mm).

The main aim of this thesis is first to use GRACE solution time series to detect variations in the gravitational potential or equivalently changes in seasonal and inter-annual variability of continental water storage over the whole East Africa. Secondly, compare the elastic surface deformation derived from GRACE water load estimates with the three-dimensional deformation estimates computed directly from GPS time series solutions. The comparison is made for the period of five years between June 2008 and March 2012 to study the movement of IGS stations due to effect of hydrological water loading.

1.2 GRACE and GPS in studying changes in mass redistribution

The Earth's gravity field and its change depend on the mass redistribution which is constantly changing deep within, at or above the Earth. The large varying masses are caused by tides in the ocean and solid Earth at 12-hour and 24-hour periods, atmospheric disturbances associated with synoptic storms and seasonal climatic variations, and coupling of land and ocean through evaporation, precipitation and runoff. One of the key components of hydrological cycle is terrestrial water storage (Syed et al., 2008). A wide variety of geophysical processes involving change in mass distribution can be studied using either satellites or ground based instrumentation by observing the variation of Earth's gravity field that varies with time (Dickey et al., 1997) .To monitor these hydrological mass redistributions through their gravitational effect, Gravity Recovery And Climate Experiment (GRACE) satellite mission was launched for this purpose with spatial resolution close to 400km (Tapley et al., 2004; Kusche and Schrama, 2005). The unprecedented accuracy of these gravity field time variations enable us to monitor these geophysical processes especially water storage

change which is the dominant source of mass variation at seasonal time scale (Wahr et al., 2004; Schmidt et al., 2006).

In principle, gravity field changes sensed by the two GRACE satellites and surface loading observed by GPS networks include the combined direct and indirect effect of all mass redistributions within the earth and its atmospheric and fluid envelope. The gravity changes on timescales can be uniquely inverted into mass redistribution within a spherical shell at the surface. Since the atmospheric contribution to surface density change can be reasonably modelled using atmospheric pressure models, GRACE and GPS displacements allow detecting changes in the Earth's larger hydrological storage systems (Kusche and Schrama, 2005). To improve the reliability of estimates, solved-for mass, configurations are constrained either by low degree truncation, spatial averaging (Swenson and Wahr, 2002) or by regularization operations employing mathematically or physically motivated constraints. This is done so because the errors in GRACE or GPS derived spherical harmonic coefficients are not white over spectral domain but increase with higher resolution because load love numbers quickly loses their power and so the spectral sensitivity decreases (Kusche and Schrama, 2005).

1.3 Previous studies

GRACE has been adopted in global perspective in presenting information susceptible to aid flood forecasting (Reager and Famiglietti., 2009) and in estimating ground water variability in several major water basins such as Congo river basin (Crowley et al., 2006), the Mississippi river basin (Rodell et al., 2004), The Amazon river basin (Tapley et al., 2004; Syed et al., 2005), the Yangtze river basin (Hu et al., 2006) and the Zambezi river basin (Winsemius et al., 2006) to extract annual, semi-annual and long term trends of the continental water mass variations. Majority of these studies compared GRACE signals with hydrological land surface in predicting, validating and improving models. However, the main results of these global inter-comparison studies over major water basins (Ramillien et al., 2005; Schmidt et al., 2008; Syed et al., 2008; Han et al., 2010) showed high level of agreement regarding the magnitude of semi-annual and annual terms and of inter-annual variations with some underestimation of the seasonal amplitude of water storage in the model predictions (Nahmani et al., 2012). At monthly timescale, the models showed less variability and revealed a systematic phase advance in the annual term as compared to GRACE products in the range of 1 to 6 weeks (Schmidt et al., 2008). However, the discrepancies were

attributed to model deficiencies in surface water storage representation of runoff and horizontal transport terms (Nahmani et al., 2012). Other recent analysis of GRACE data indicated long term mass loss from Alaskan glacier system (Tamisiea et al., 2005) equivalent to 0.31±0.09 mm/year of geographically uniform sea level rise which agreed with estimates from earlier altimetry survey (Arendt et al., 2002).

The most recent studies were conducted in West Africa to study three-dimensional ground deformations measured with permanent GPS stations to investigate the hydrological loading deformations associated with West African Monsoon precipitation. The results showed that, weekly station positions were retrieved with repeatability (including unmodelled loading effects) of 1-2 mm in horizontal components and between 2.5 and 6 mm in the vertical component. This was modeled with a combination of hydrological, atmospheric and nontidal ocean models. The analysis of in situ hydrological data revealed a strong coincidence between transient signal detected in vertical component and the peak river discharge at three river sites located along river Niger (Timbuktu, GAO, and Niamey) and at Ouagadougou with the seasonal variations of the water Table depth. This was proposed to be a mechanism that involved a sequence of swelling/shrinking of clays combined with local loading effects associated with flooding of Niger River (Nahmani et al., 2012). Several studies have been used to examine the existing permanent GPS networks to compare and somehow validate the hydrological signals of GRACE products and/or model simulations (Davis et al., 2004; Kusche and Schrama, 2005; King et al., 2006; Van Dam et al., 2007; Tregoning et al., 2009; Steckler et al., 2010; Tesmer et al., 2011). Kusche and Schrama, [2005] found good agreement between the annual variations of continental water mass seen by GPS and GRACE and those predicted by a global hydrological model (Nahmani et al., 2012). Tregoning et al, [2009] computed elastic deformations using continental water storage variations derived from GRACE products and compared with 3-D deformations estimated from global reprocessed GPS network including 80 sites. They got good agreement for the two data with Root-Mean-Square (RMS) of GPS coordinate anomalies decreasing at ~50% of their sites when the derived deformations estimates were subtracted from their GPS solution. The good fit was obtained on European stations with 32 out of 36 stations which showed decrease in RMS anomalies which was in contrast with past results on the same area (Van Dam et al., 2007). Less or more same approach was used by Tesmer et al, [2011] over larger global network of 115 stations using longer data sets for both GRACE and GPS products i.e September 2002 to

April 2009. The results obtained improved compared with previous global studies where 80% of their stations showed decrease in RMS anomalies. Moreover, they estimated the precision of the GRACE-derived deformations at ~1.2 mm by comparing three different GRACE products. Another study is from Grippa et al, [2011] who focussed on West Africa by comparing land water storage estimates from six GRACE products (GFZ –v 04, JPL –v 04, CSR –v 4.1, DEOSS DMT V1, CNES –GRGS v2 and GSFC –Mascons) and soil moisture estimates from nine hydrological land surface models from year 2003 to 2007. The GRACE products were consistent with water maxima observed in September and minima in April (Nahmani et al., 2012).

1.4 Case study of the thesis

This research considers Eastern African countries which are Tanzania, Kenya, Uganda, Rwanda, Burundi and Ethiopia located approximately between 20ºS and 20ºN latitudes, and 30ºE and 53ºE longitudes (Figure 1.2). In this thesis, we construct a time series of monthly estimates of equivalent water thickness from GRACE and time series of GPS position estimates for each individual GPS site expected to contain displacement associated with the response of the earth to surface mass loading, mainly hydrological water loading from June 2008 to March 2012. The area includes all surface water sources such as rivers with all tributaries in their catchments, lakes, soil moisture and ground water. Five IGS stations used in this study include ADIS in Addis Ababa Ethiopia, MAL2 in Malindi Kenya, RCMN in Nairobi Kenya, NURK in Kigali Rwanda and MBAR in Uganda. The six stabilization IGS site used include NKLG (N'KOLTANG in Gabon), BAN2 (Bangalore), MAS1 (Maspalomas), SEY1 (Republic of Seyc), WTZR (Wettzell in German), and RAMO (Mitzpe_Ramon).

Figure 1.1: Some of IGS stations used in this study

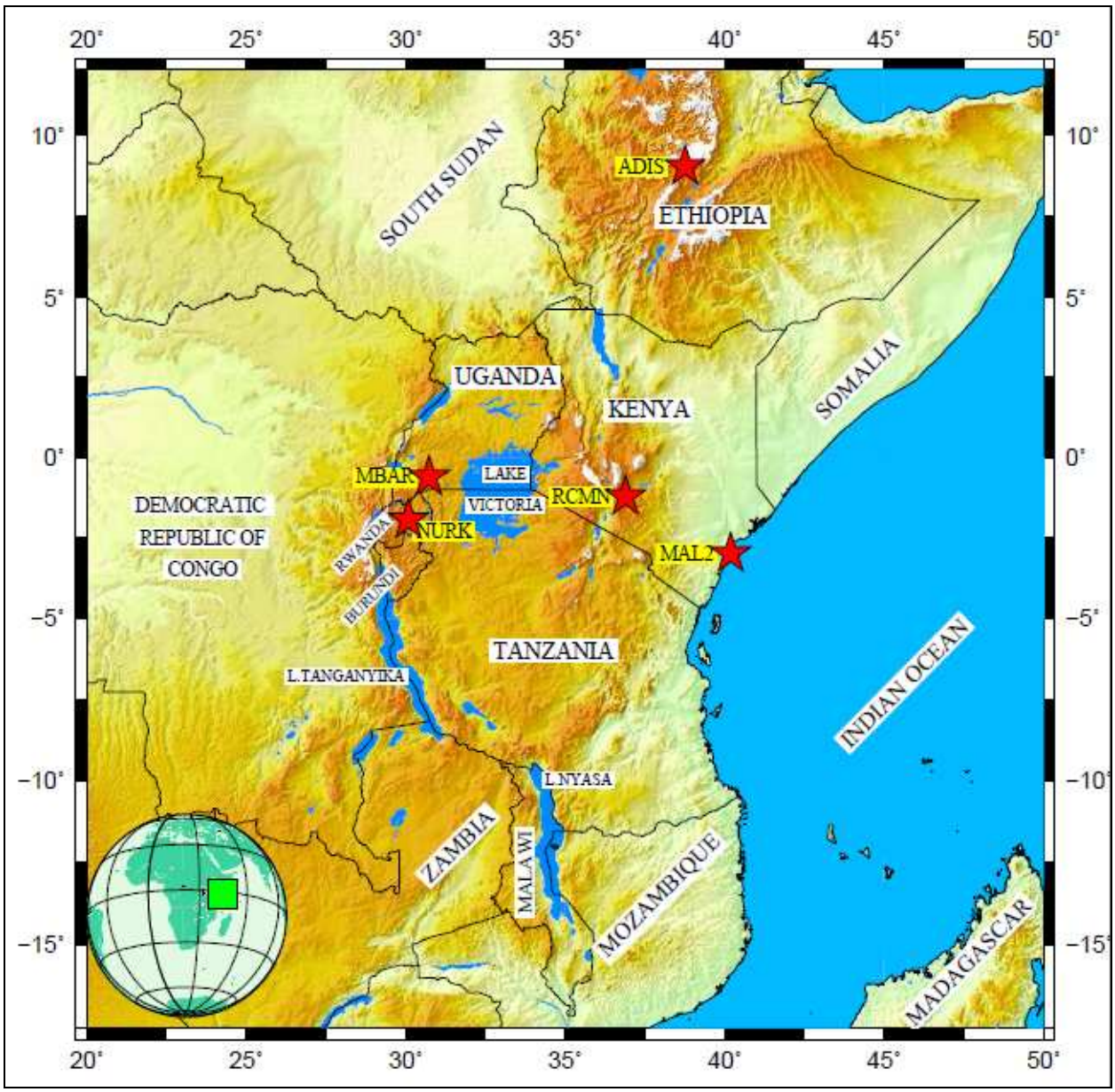

Figure 1. 2: Location map of the study area. The green square shows East Africa with respect to a globe; red stars represent the distribution of IGS station points used in this study; the blue features represent hydrological water bodies as they play an important role in hydrological cycle.

1.5 The Statement of the Research Problem

Temporal mass changes in the Earth system are reflected in both gravity field variations and the load deformations of the Earth's crust that is associated with the Earth's response to mass change. Global-scale gravity field variations are observed by the Gravity Recovery and Climate Experiment (GRACE) satellite mission. Space geodetic techniques such as the Global Positioning System (GPS), Very Long Baseline Interferometry (VLBI) and Satellite Laser Ranging allow the measurement of site position displacements (Zhang et al., 2005). Due to its high precision, 24 hours availability, operability under all weather conditions and automation, GPS technique has been widely used in monitoring ground movement, deformation and subsidence (He et al., 2004; King et al., 1995; Kogan et al., 2000; Zhang et al., 2005).

Recent studies have shown that, East Africa is undergoing on various deformation processes. For example, Saria, [2007] studied the kinematics of the Nubian and Somalian plates and sub-plates using GPS data in order to gain insight into the kinematics of East African Rift System (EARS). These studies and others such as studying the Surface Deformation in the East African Rift (EAR) using GPS data needs accurate and stable GPS station monuments. However, due to hydrological processes such as terrestrial water storage which is a key component of global hydrological cycles (Syed et al., 2008), there is a need to monitor the movement of these IGS stations due to hydrological water loading (HWL).

1.6 Objectives

1.6.1 Main objectives

The main objective of this thesis is to study the movement of permanent GPS (IGS) stations due to effect of hydrological water loading using GRACE and GPS data. The objective is to compare the GPS derived surface deformation estimates with GRACE based elastic surface water loading estimates over the entire East Africa from June 2008 to March 2012 and correlate the two signals.

1.6.2 Specific objectives

The specific objectives of this study are:

- To use GRACE statistical data to construct mean monthly GRACE gravity anomalies, standard deviations and root mean squares.

- To convert GRACE gravity anomalies to equivalent water thickness.
- To construct mean monthly GRACE solution time series of equivalent water thickness.
- To prepare GPS position time series from June 2008 to March 2012.
- To prepare velocity estimates for each IGS station in tabular format.
- To prepare the velocity map showing movement of all IGS stations.
- To correlate between continuous GPS time series with GRACE hydrological water loading signal.

1.7 Thesis structure

The thesis consists of five chapters. Chapter two covers the reviews in both GPS and GRACE measurements. It explains generally on theory and basic principles of GPS and the IGS site station status based on current International Terrestrial Reference system (ITRF) 2008. This chapter gives literature on how space geodesy with GPS can be used in monitoring earths' deformations based on reference systems and reference frames. It explains further on principles of GRACE measurements from space to ground, how it measures the time-variable gravity and how it is related to mass redistribution which affects different geophysical processes on the earth. It also gives the review on GRACE measurements and the associated errors in both, measurements and data processing. Finally it reviews on how the time varying gravity field is converted to an equivalent water thickness by applying different smoothing functions.

Chapter three presents data acquisition techniques, data processing techniques and the software packages for processing GPS and GRACE data.

Chapter four contains quantitative results and analysis of GRACE and GPS estimates. The first part of this chapter looks at the monthly average estimates of changes in equivalent water thickness over the whole East African region as acquired from the four GRACE processing institutes. It also shows the patterns of the obtained equivalent water mass described in the form of gravity anomaly maps. Additionally it looks at the comparison of the obtained results with the results in previous studies. The second part of the chapter looks at GPS results and analysis considering the position displacements and velocities for the 5 IGS stations with their accuracies based on repeatability. The results for velocities are depicted on the velocity map shown in Figure 4.7. Finally the chapter explains the results obtained after

combining GPS and GRACE results including accuracy, correlation analysis, and comparison of GPS and GRACE time series.

Chapter five discusses on the results obtained and conclusion. It explains on how the comparison of GPS coordinate anomalies and GRACE deformation estimates have shown high level of agreement on studying the effect of hydrological water loading on GPS stations. It further explains how their agreement has been coincided with other results from previous studies; and finally the conclusion from the discussion with recommendations in the future studies.

CHAPTER 2: REVIEW OF GPS AND GARACE MEASUREMENTS

2.1 Overview of theory of GPS geodesy

This section gives a theory of GPS system starting from its basic principles of positioning in an introduction part and its applications in monitoring deformations. It also explains how positioning is done in a suitable reference systems and frames. It also gives theory of satellites and satellite orbits and shows how satellite positions are determined using broadcast or navigation message based on Keplerian elements. Finally the section gives an overview on GPS signal structure, GPS observables and how the position of a GPS receiver is determined. The purpose of this section is to give knowledge to the reader in preparation for the next chapters.

2.1.1 Introduction to Global Positioning System

The aim of NAVSTAR Global Positioning System (GPS) which is a satellite-based radio navigation system is to determine precisely three dimensional position, navigation and time information to suitably equipped users in a common reference system anywhere on or near the earth on a continuous basis. It was developed by Department of Defense (DoD) under NAVSTAR satellite program to satisfy the requirements for military purposes but made available for civilian use in 1980's on a world-wide basis under all meteorological conditions. NAVSTAR GPS also contains the features that limit the accuracy for authorized users by protecting from malicious interface through Anti-spoofing (AS) method (Zhang, 2007).

The basic principle of GPS is based on simultaneous code-pseudorange and carrier phase observations between the user GPS receiver. At least four satellites in code-pseudorange measurements and four satellites at three epochs in carrier phase measurements are required to determine the user-receiver coordinates starting from the satellite of known coordinates in a suitable reference frame. A fourth observation which is a clock synchronization error and which is the reason for pseudorange is necessary since GPS uses the one-way range technique and the receiver clock is not synchronized with satellite clock (Seeber, 2003). Section 2.1.6 explains clearly how user position is determined using code-pseudorange and carrier phase measurements.

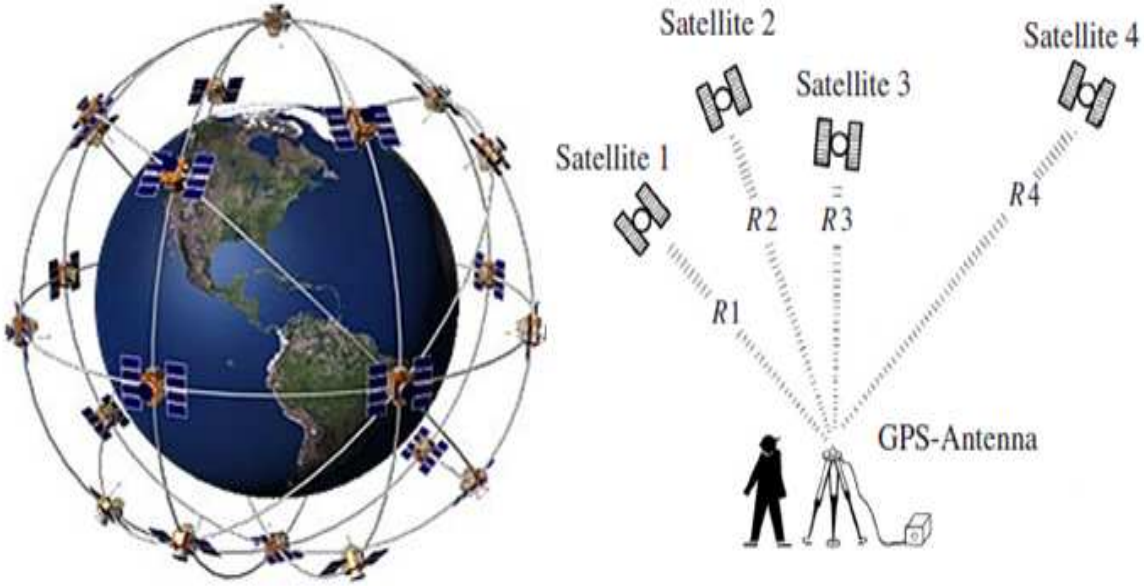

Figure 2. 1: Basic principles of positioning with GPS (source: Seeber, 2003).

GPS geodesy has been supported by a large permanent infrastructure which has revolutionized the way in which geodetic observations are planned, acquired and analyzed. The international GNSS service for Geodynamics (IGS) which is headed by the Central Bureau located at US Jet Propulsion Laboratory (JPL) provides precise orbits for all GNSS satellites starting from January, 1994 to date for the purpose of high precision geodynamical studies. GNSS in its space segment has a constellation of 27 satellites with mean altitude of 20,200 kilometres whereby, 24 are operational and three are spares (Hofmann-Wellenhof et al, 2008). This makes a total of 31 GNSS satellites in GPS constellation status up to May 2013 (Miller, 2013). The orbital constellation contains six equally-spaced orbital planes (A-F) surrounding the earth with 55 degrees inclination having four satellites per orbital plane. The arrangement of 24 satellites ensures that, there are at least four satellites in view from virtually any point on the planet. The full global coverage of satellites depends on the elevation mask whereby, four to eight satellites can be viewed simultaneously above 15 degrees at any time and occasionally up to ten satellites can be viewed if the elevation mask is reduced to 10 degrees. If the elevation mask is further reduced to 5 degrees, occasionally twelve satellites can be visible (Hofmann-Wellenhof et al, 2008). To maintain the full coverage whenever the baseline satellites are serviced or decommissioned, the US Air Force usually flies more than 24 GPS satellites by increasing extra satellites which increase performance but not considered as part of the core constellation. However, in June 2011, the

US Air Force successfully completed GPS constellation expansion by expanding the three of the 24 slots whereby, six satellites were repositioned so that, three of the extra satellites became part of the constellation baseline making GPS to effectively operate as a 27-slot constellation with improved coverage in most parts of the world. More information can be accessed through http://www.gps.gov/systems/gps/space/ site.

GNSS satellites can be categorized as Block I, Block II, Block IIA, Block IIR, Block IIR-M, Block IIF, and Block III satellites which are explained in details in Hofmann-Wellenhof et al, [2008], Seeber, [2003] and through http://www.gps.gov/systems/gps/modernization/ site. The first Block I satellite which is now not operational was successfully launched in the period of 1978 to 1985 from Vandenberg Air Force Base (AFB), California (Hofmann-Wellenhof et al, 2008). Compared to Block I constellation which has 63 degrees orbital planes inclination, Block II constellation has 55 degrees orbital planes inclination and the signals were restricted. The first Block II satellite weighing 1500 kg with life expectancy of 7.5 years was launched on February 14, 1989 while the first Block IIA satellite ("A" means advanced) which is an upgraded version of Block II satellites was launched in November 1990, and the last launch occurred in November 1997. Being equipped with mutual communication capability (Hofmann-Wellenhof et al, 2008), Block IIA satellites contain a total of 19 satellites but only 9 satellites are remaining up to May 2013 (Miller, 2013).

Block IIR satellite ("R" donating replenishment or replacement) whose first and last launch occurred in July 23, 1997 and November 2004 respectively weigh more than 2000kg with total of 13 satellites in the constellation. All the satellites in this Block have a life expectancy of 10 years and carry improved communication and inter-satellite tracking capabilities (Hofmann-Wellenhof et al, 2008). The IIR series satellites were produced in order to replace the II/IIA series satellites which have gradually degraded or have exceeded their intended design life. However, there were only 12 satellites remaining in the GPS constellation as of May 2013 forming the backbone of today's GPS along with the IIR-M series.

Block IIR-M ("M" denoting modernized) which is an upgraded version of IIR series contains 8 satellites in the GPS constellation. However, there were only 7 health satellites in the constellation up to May 2013 where the final one was set to unusable status. Its first satellite was launched on September 25, 2005, and the last launch occurred in August 2009 with new features of civil L2C-code on L2 frequency with an improved performance in commercial

applications allowing for ionospheric corrections, and a military M-code on L1 and L2 carrier signals which provides enhanced military jam-resistance (See section 2.1.6 for more information on signal structure). However, the initial operation capability (IOC) under the new codes is expected in 2014 while the full operation capability might be archived in 2015 (Hofmann-Wellenhof et al, 2008).

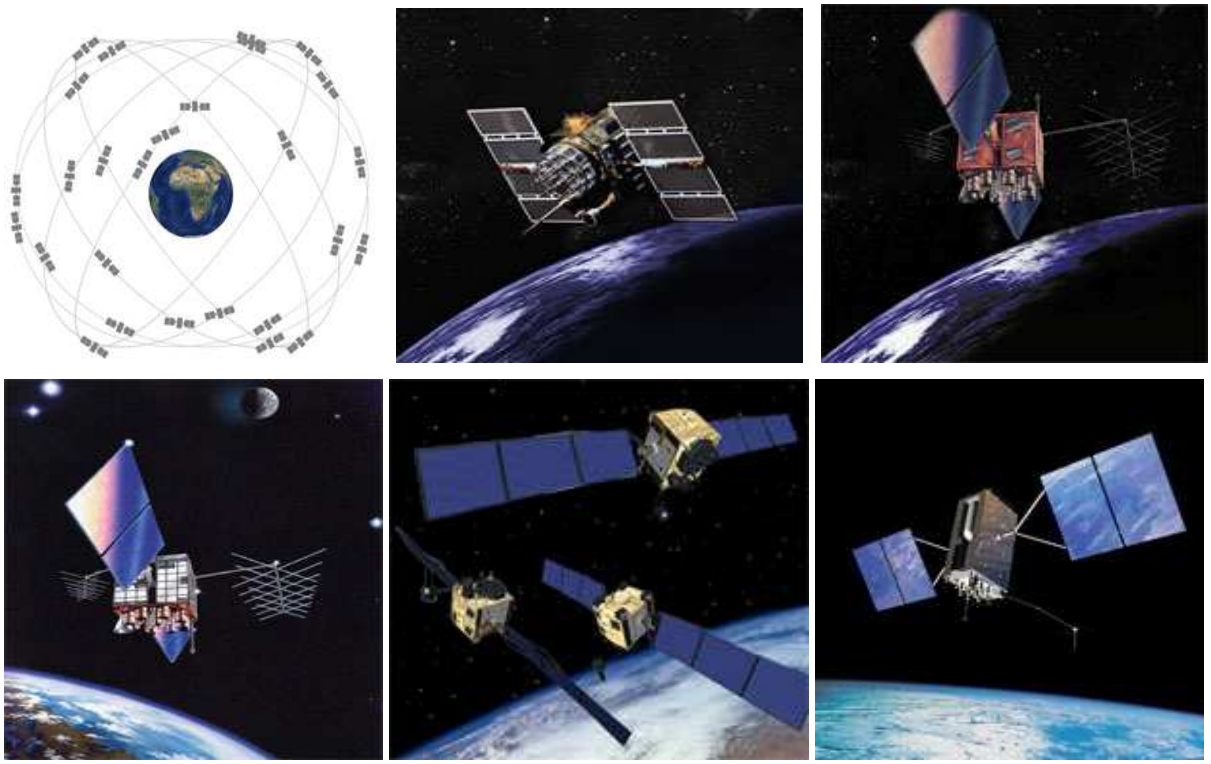

Figure 2. 2: GPS space segment showing GPS satellite constellation (top left), GPS Block IIA (top middle), GPS Block IIR (top right), GPS Block IIR-M (bottom left), GPS Block IIF (bottom middle), and GPS Block III satellite (bottom right). (Source: http://www.gps.gov/systems/gps/space/).

After Block IIR-M, the next generation will be Block IIF satellites ("F" denoting follow-on) which will be added with a third civilian signal designated as L5C-code in a frequency protected for safety-of-life transportation, and the two military M-code signals. These satellites will be equipped with improved onboard capabilities such as initial navigation systems and are expected to weigh more than 2000 kg with longer life expectancy of 12 years. The Block IIF series will improve the accuracy, signal strength, and quality of GPS since its spacecraft uses a mix of rubidium and caesium atomic clocks to keep the time to

within 8 billionths of a second per day. The first Block IIF satellite was launched in May 2010 making a total of 12 satellites in the GPS constellation but, up to May 14, 2013 only three satellites were operational whereby, the fourth one was successfully launched into orbit on May 15, 2013. More studies are being undertaken recently under DoD for the next generation satellite block called Block III satellites which are expected to carry GPS starting from 2015 to 2030 and beyond (Hofmann-Wellenhof et al, 2008). As the newest block of satellites, GPS III will provide more powerful signals in additional to enhanced signal reliability, accuracy, and integrity all supporting high precision, navigation, and timing services. GPS III series will be featured with a fourth civilian GPS signal (L1C) for international interoperability, Distress Alerting Satellite System (DASS) for search and rescue (in the future), and satellite laser retroreflectors (in the future) with increased design life span of 15 years. The future versions' will increase capabilities to meet demands of military and civilian users alike. More can be accessed through http://www.gps.gov/systems/gps/ site.

GNSS satellites are tracked in GPS control segment under Operational Control Segment (OCS) which consists of a global network of ground facilities that track the GPS satellites, monitor their transmissions, perform analyses, and send commands and data to the constellation. Currently OCS has a master control station, an alternate master control station, 12 command and control antennas, and 16 monitor sites located throughout the world which includes six stations from the Air Force and 10 from the National Geospatial-Intelligence Agency (NGA) as shown in Figure 2.3. Visit **http://www.gps.gov/systems/gps/control/** for more information.

Apart from tracking GNSS satellites for orbit and clock determination and prediction, OCS synchronises the time of satellites and uploads the navigation data message to the satellites as well as imposing selective availability (SA) on broadcast signals. Monitor stations under OCS send tracking data to the Consolidated Space Operations Center (CSOC) which then calculates the satellite orbit and clock parameters using Kalman estimator and pass it to the four ground antennas which are under master control station and located at Ascension Island, Diego Garcia, Kwajalein, and Cape Canaveral in Florida for eventual upload to the GPS satellites via S-band radio links. Each of monitor stations is equipped with a precise atomic time standard and receivers which continuously measure pseudoranges to all satellites in view at every 1.5 seconds. The pseudoranges are then smoothed using the ionospheric and

meteorological data to generate 15-minute interval data transmitted to master control station (Hofmann-Wellenhof et al, 2008).

GNSS satellite constellation observation capability by 2005 has been improved under GPS modernization program by incorporating into the control segment six new monitor stations located in Washington, DC (the US Naval Observatory), Argentina (Buenos Aires), Bahrain (Manama), United Kingdom (Hermitage), Ecuador (Quito), and Australia (Adelaide) which has lead to improved data and new data upload strategy with an increased update rate of the navigation data to the GPS satellites at three uploads per day for each satellite. Five more monitor stations located in Alaska (Fairbanks), Tahiti (Papeete), South Africa (Pretoria), South Korea (Osan), and New Zealand (Wellington) were also added by 2006 (Hofmann-Wellenhof et al, 2008).

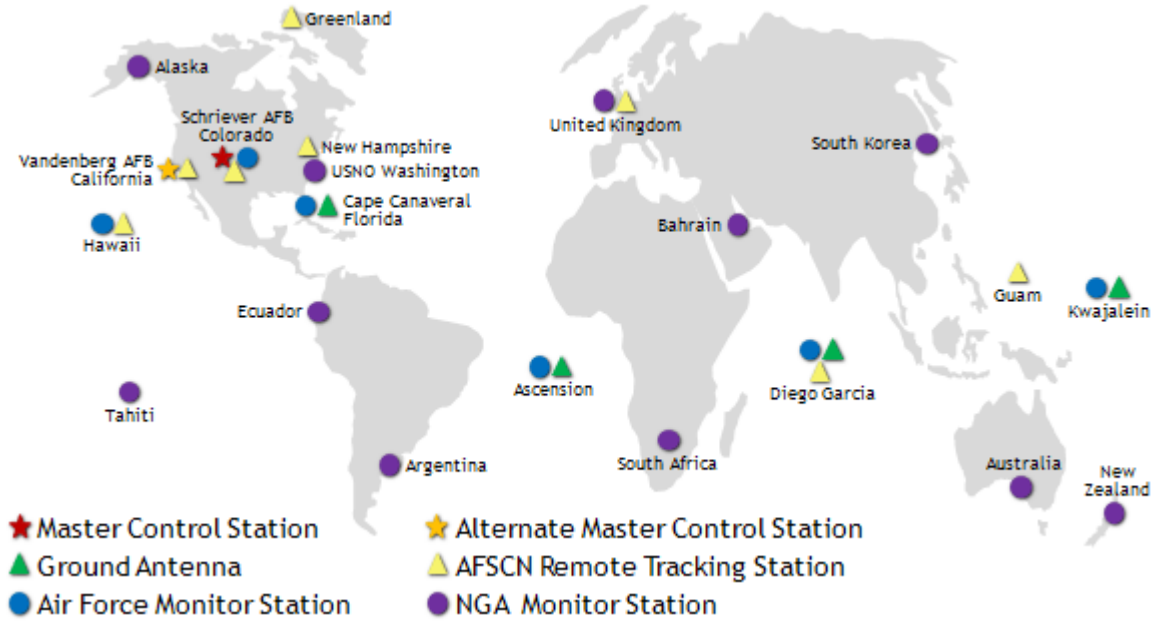

Figure 2. 3: GPS control segment (source: http://www.gps.gov/systems/gps/control/).

Apart from consecutive satellite acquisition including GPS IIR-M, GPS IIF, and GPS III and increase monitor stations, GPS modernization program has improved its GPS control segment through the Architecture Evolution Plan (AEP) and the Next Generation Operational Control System (OCX) as shown in its space and control segment upgrade schedule in Figure 2.4. Visit http://www.gps.gov/systems/gps/control/) for more information.

Figure 2.4: GPS space and control segment schedule up to May 2012 (source: http://www.gps.gov/systems/gps/control/).

Other improvements under GPS modernization program include accuracy of the Kalman filter state estimates which are necessary for calculating accurate satellite orbits, accuracy of the broadcast ephemerides and clock parameters, and the ability to observe the performance of the GPS satellites. The accuracy improvement has been archived by installing new software packages on the Operational Control System (OCS) and by implementing the National Geospatial-Intelligence Agency (NGA) monitor station network in which, both have yielded improvements in monitoring the signal integrity and constellation performance and the data used for satellite position and time estimation which has resulted in more accurate predicted satellite orbital positions and clock data (Hofmann-Wellenhof et al, 2008).

The high accuracy and reliability of orbit determination for GNSS satellites has been obtained through the global tracking networks based on observations at monitor stations of the respective control segment. The tracking sites are either distributed regularly around the global or each network site is surrounded by a cluster of additional points in order to facilitate ambiguity resolution and hence strengthening the solution of the orbital parameters. Several global orbital tracking networks have been established including 8 stations in North America, Europe and Japan in 1988 whereby, the number increased to 20 stations by 1991, and 30 more satiations were incorporated in the network by 1994 (Hofmann-Wellenhof et al, 2008). Up to August 2006, the IGS tracking network was based on more than 330 globally distributed active tracking sites (Figure 2.3) with coordinates and velocities related to International Terrestrial Reference Frame (ITRF) (Hofmann-Wellenhof et al, 2008) which

has expanded from 410 to 440 stations since 2008 to 2012 from 200 contributing organizations in 80 countries of which 84% are actively transmitting data (IGS Progress Report, 2012; Neilan et al., 2012). Although not yet integrated through the IGS network and being under experimental basis, the number of stations delivering real-time streamed data to IGS has increased from approximately 40 in 2008 to 188 currently (IGS Progress Report, 2012). The IGS network which collects code ranges and carrier phases from all GNSS satellites in view using dual-frequency receivers has a mission of providing the highest quality GNSS data, products, and services in support of ITRF, Earth observations and research, positioning, navigation and timing, and other applications that benefit the scientific community and society. After being collected, the data are analyzed independently by agencies and are achieved daily in RINEX and SINEX formats by global and regional data centers. The IGS service also provides raw tracking data, satellite clock parameters, the earth orientation parameters (EOP), and other data like ionospheric and tropospheric information. The IGS service can be accessed via the following website, http://igscb.jpl.nasa.gov.

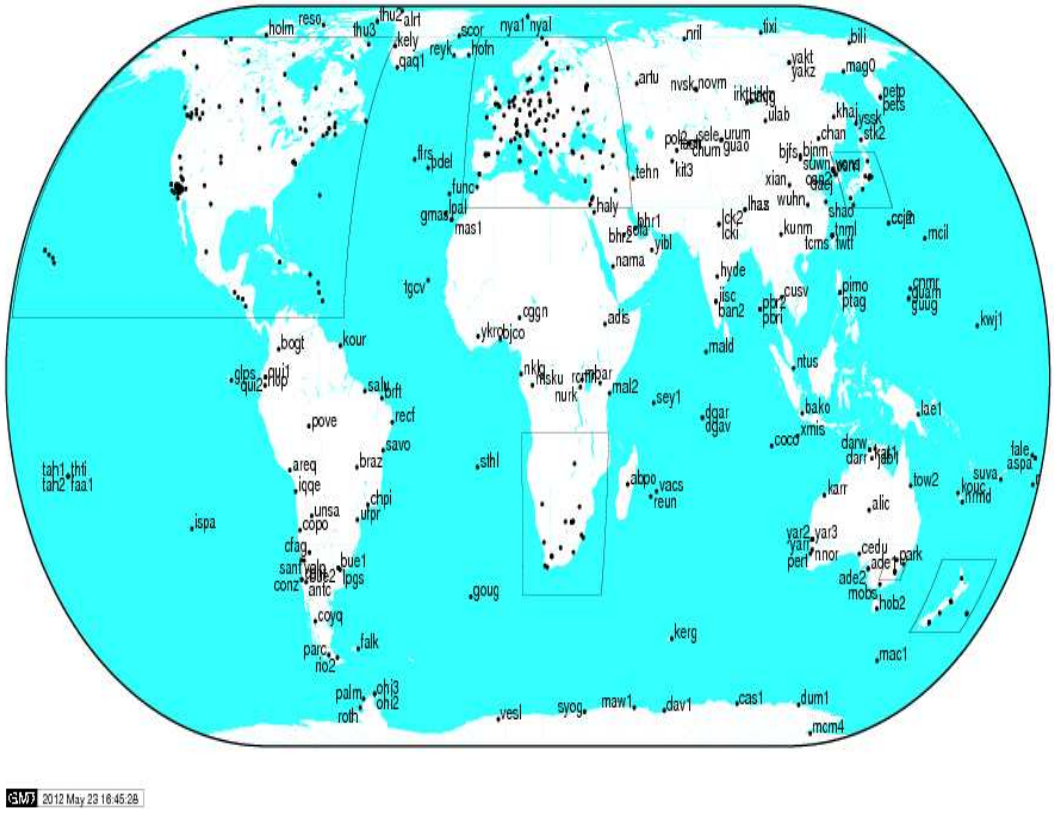

Figure 2. 5: The current global IGS tracking network of IGS site stations.

2.1.2 Space Geodesy with GPS in monitoring Deformations

GPS and other geodetic observation techniques such as GRACE and Interferometric Synthetic Aperture Radar (InSAR) allows for validation of the individual time series. The combination of velocities derived from GPS and gravity data, allows us to monitor continuously in space and time crustal movements which is important in understanding the processes responsible for the observed deformations (Zerbin et al., 2007). Zerbin et al, [2007] for instance derived long-term trends which enabled mapping of the behavior of subsidence with high spatial resolution in the Southern Po Plain (Italy) in which, they identified the uplifting behavior of Apennines chain bordering the Po Plain together with a narrow zone separating the contrasting vertical crustal movement.

In present days, Space Geodesy technology is used in conjunction with terrestrial techniques to monitor land-surface deformations with high spatial and temporal resolution as referred to a global reference system by measuring positions of geodetic monuments to a better than centimeter accuracy even for sites which are more than thousands of kilometers apart. The advantage of using these combined techniques is that, large area is covered than it would for with traditional geodesy which is restricted to sites which are in view of each other. More-over, the accuracy of using individual space geodetic technique is mainly limited by the systematic errors of the individual techniques themselves as well as by our understanding of geo-dynamic driving mechanism at the observational timescales. Combined systematic techniques extended over a certain period of time allows validation and inter-comparison of the individual observations enabling us in identifying problematic data and provide the basis for exploiting the potential of each single technique (Zerbin et al., 2007).

2.1.3 The Reference Systems and Frames in Space Geodesy

A reference system is conceptually showing how a coordinate system is formed by defining the origin and the orientation of fundamental planes or axes of the system including the underlying fundamental mathematical and physical models. A reference frame is the practical realization of the reference system through observations consisting of a set of fiducially identifiable points on the sky (e.g. stars) or on Earth's surface (e.g. fundamental stations). Reference frame is described by a catalogue of precise positions and motions at a specific epoch. The two fundamental systems required in space geodesy are space-fixed (Conventional Inertial Reference System (CIS)) for describing satellite motion and an Earth-fixed (Conventional Terrestrial Reference System (CTS)) describing positions of the

observation stations and for describing results from space geodesy. The latter must be connected to the earth's crust in a well defined way and can be realized through a set of Cartesian coordinates of the fundamental stations or markers within a global network (Seeber, 2003).

Reference coordinate systems are crucial in describing the satellite motion, the modelling of observables, and representation and interpretation of results. Increase in accuracy of satellite observation techniques, requires increase in accuracy of reference systems. The reference systems are global in nature since they refer to the centre of mass of the Earth. Since terrestrial measurements are local in nature and are usually described in local reference coordinate systems; there must be a common relationship between all systems in use and must be known with sufficient accuracy due to change of relative position and orientation with time. However, it should be clear that, different observation methods refer to a particular reference coordinate systems which relate to the individual method. The relationship between these particular systems is known with accuracy which is lower than the accuracy of individual observation techniques. The most important task is the transformation formulas between the systems (Seeber, 2003).

In 1988, International Earth Rotation Service (IERS) which provides with highly accurate earth orientation parameters with high temporal resolution used modern space techniques such as SLR, VLBI, GPS and DORIS (Doppler) to establish and maintain both the celestial and terrestrial Reference systems and frames. The retained and refined reference frames are Inter-national Celestial Reference Frame (ICRF), based on Interferometric radio observations, and the International Terrestrial Reference Frame (ITRF) based on different space techniques. The International Terrestrial Reference System (ITRS) which was established and maintained by IERS is a conventional terrestrial system realized through International Terrestrial Reference Frame (ITRF) (Seeber, 2003). The realization of ITRF is formed through Cartesian coordinates and linear velocities of global set of sites equipped with various space geodetic observing systems. However GRS80 frame is recommended if geographic coordinates (ellipsoidal latitude, longitude and height) instead of Cartesian coordinates (X, Y, Z) are used. A new ITRF based on new observations with geodetic space techniques was realized nearly each year starting with ITRF88 and ending with ITRF2000 (Altamimi et al., 2011) and the results were published under the denomination ITRFxx, where xx means last digits of the year whose data were used in the formation of the frame

(Seeber, 2003). Later on ITRF was realized at the interval of five years starting with ITRF2000, ITRF2005 and the latest being ITRF2008 (Altamimi et al., 2011). In this case, the future ITRF is planned to be published in late 2013 or early 2014. Beginning with ITRF2000, each particular ITRF is assembled by combining sets of results from independent techniques as analyzed by a number of separate groups. By using many different techniques as possible helps in minimizing significant systematic errors. The most recent solution which is ITRF2008 is a refined version of International Terrestrial Reference Frame based on reprocessed solutions of the four space geodetic techniques which are Very Long Baseline Interferometry (VLBI), Satellite Laser Ranging (SLR), Global Navigation Satellite Systems (GNSS) and Doppler Orbitography Radio positioning Integrated by Satellite (DORIS), spinning 29, 26, 12.5 and 16 years of observations respectively (Altamimi et al., 2011).

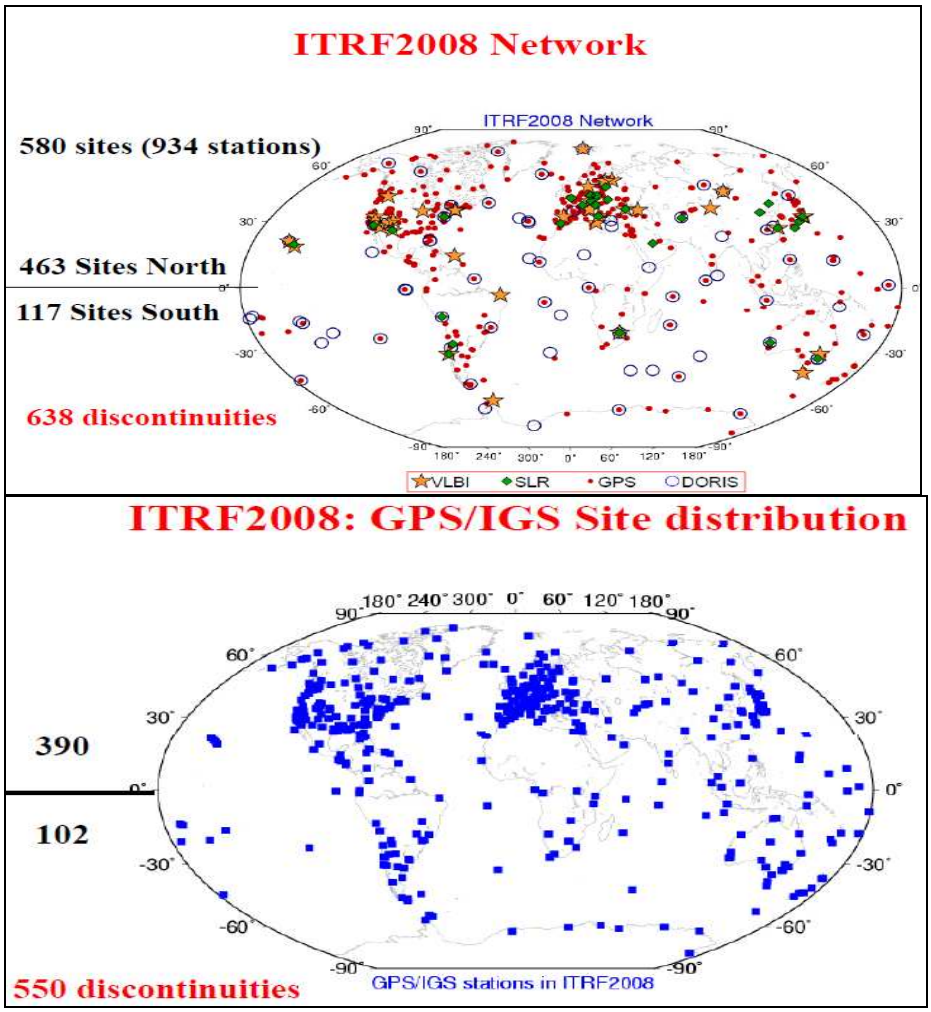

Figure 2. 6: ITRF2008 network (top) and GPS/IGS Site distribution (bottom) (Altamimi, 2010).

2.1.4 GPS satellites and satellite orbits

GPS applications depend on knowing satellite orbits which move as a result of earth's gravitational attraction and other forces. The orbits of GPS satellites along with other thousand detectable objects as reported by NASA are governed by three laws of orbital motion as discovered by astronomer Johannes Kepler in 17^{th} century. As a first law, he discovered that; all planets move in elliptical orbits with the sun at one focus. He further discovered his second law governing the motion of planets that; a line joining the sun to the planet sweeps out equally sized areas in a given interval of time regardless of the position of the planet in its orbit. Finally in his third law he stated that; the square of the time taken by a planet to complete its orbit is proportional to the cube of its means distance from the sun. To calculate accurately the position of satellite in its orbit, gravity and other small forces acting on satellite need to be carefully taken into account. Given the position and velocity of the satellite at a given initial epoch, the future satellite position can be determined based on six Kepler elements. Starting with two Keplerian elements which define the size and shape of an orbital ellipse which are semi-major axis (a) and eccentricity (e), other three Kepler elements which define the orientation of the orbit in space with respect to the fixed stars are inclination (i) which is the angle between satellite orbit and the earth's equatorial plane; right ascension of ascending node (Ω) which is the angle measured in the equatorial plane between the reference direction in space called vernal equinox (which coincides with the position of the sun the instant spring begins in the Northern Hemisphere) and the ascending node which is the point on the satellite orbit where the satellite crosses the plane of the equator moving from below the equator above it; and the argument of perigee (ω) which is the angle measured in the plane of the orbit between the ascending node and the perigee (the point on the orbit that is closest to the earth's centre). The last Keplerian element which shows where the satellite is on the orbit at a certain time is the true anomaly (f) which is the angel between the perigee and the satellite. Figure 2.4 shows the orbital orientation defined by the six-Keplerian elements where, the x-axis points towards the vernal equinox, the z-axis coincides with the celestial pole and the y-axis completes the right hand coordinate system in the equator. The coordinate system (q_1 and q_3) defines the orbital plane with its origin at the focal point of the ellipse that coincides with the centre of earths' mass while ξ defines the principle axis of the ellipse in the equatorial plane. This system is called Earth Centred Inertial system (ECI) which uses earth's centre as the origin (Hunegnaw, 2011).

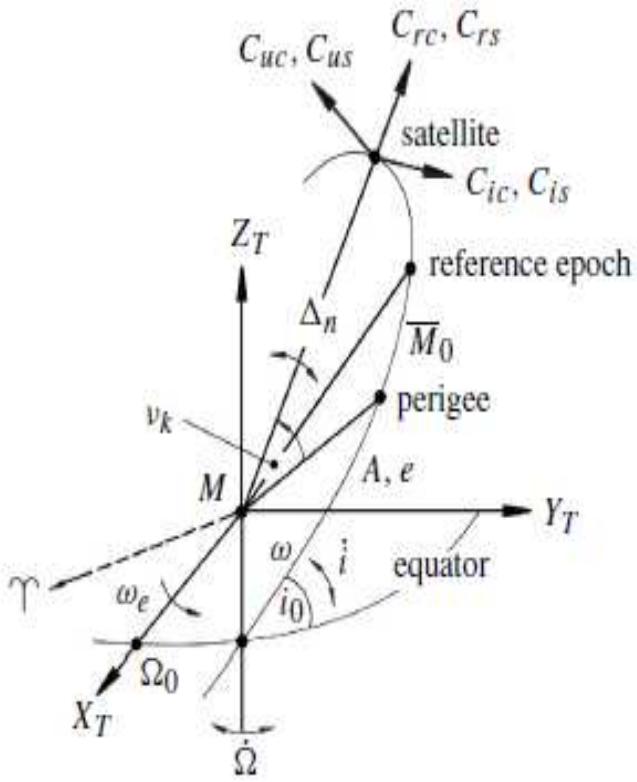

Figure 2.7: Keplerian and disturbance parameters contained in the navigation message.

Using Keplerian elements with additional perturbation parameters, satellite positions can be estimated in the Kalman filter process (Seeber, 2003). All parameters which refer to a given epoch t_{oe} and clock t_{oc} represent satellite orbit and the state of the satellite clock as shown in Table 1.1. These parameters are broadcasted at every observation epoch and renewed on every two hours causing small steps between the different overlapping representations (Seeber, 2003). However, they must not be used out of prescribed time which is about four hours since the extrapolation error grows exponentially beyond the given period. To compute the satellite time and the satellite coordinates, the parameters in Table 1.1 are used in groups by following some steps which can reach a few decimeters but may be smoothed by suitable approximation techniques. For more information on approximation techniques, refer Seeber [2003]. The parameters are arranged in three groups such that, the first group is used to correct satellite time, second group determines a Keplerian ellipse at reference epoch and the third group contains nine perturbation parameters (Figure 2.4).

Table 1. 1: GPS broadcast ephemerides

Time Parameters	Explanation
to_e	Reference time, ephemeris parameter (s)
to_c	Reference time, clock parameters (s)
a0, a1, a2	Polynomial coefficients for clock correction [bias (s), drift(s/s), drift-rate (ageing) (s/s^2)]
IODC	Issue of Data, Clock, arbitrary identification number
Keplerian parameters	
$\sqrt{a}$	Square root of semi-major axis ($m^{1/2}$)
e	Eccentricity
ω	Argument of perigee
i_o	Inclination at reference epoch
M_o	Mean anomaly at reference epoch
Ω_o	Longitude of ascending node at reference epoch
IODE	Issue of Data, Ephemeris, arbitrary identification number
Perturbation parameters	
Δn	Mean motion difference from computed value
Dot i	Rate of change of inclination
$\dot{\Omega}$	Rate of change of right ascension
Cus, Cuc	Amplitude of the sine and cosine harmonic correction terms to the argument of latitude respectively.
Crs, Crc	Amplitude of the sine and cosine harmonic correction terms to the orbit radius respectively.
Cis, Cic	Amplitude of the sine and cosine harmonic correction terms to the angle of inclination respectively.

2.1.5 Calculation of GPS satellite position and time

The main characteristics of GPS system time are a week number which varies between 0 at the beginning of a week and 604800 at the end of a week; and the number of seconds since the beginning of the current week. The initial epoch of GPS was on January 5, 1980 at 0^h UTC which makes the GPS week to start at midnight (Universal Time) between Saturday and Sunday. The GPS week number which is included in sub-frame 1 of the navigation message and represented by 10 bits has the largest possible week number of 1023 which rolls over to zero at the end of the week (EOW). The end of the first cycle was on August 21, 1999 and the second runs from August 22, 1999 and will end on April 6, 2019 (Seeber, 2003). However, numbering of the GPS week is continuous (no rollover) for RINEX data (Seeber, 2003).

GPS system time is defined by the weighted mean of the atomic clocks in the monitor stations and the satellites. Although it is a continuous time scale, GPS system time differs from UTC due to drift in the GPS clocks, the difference which is continuously monitored by the control segment and is broadcast to users in the navigation message. For example the difference was about 13 seconds (GPS time ahead) on January 1, 2003. Satellite oscillators (rubidium or caesium) have constant and irregular frequency errors which makes satellite clock readings to differ from GPS system time. This behaviour of individual satellite clocks is monitored by control segment and predicted in the form of a second degree polynomial. Seeber [2003] showed that, the individual satellite time t_{SV} is corrected to GPS system time t using equation 2.1.

$$t = t_{SV} - \Delta t_{SV} \tag{2.1}$$

In which;

$$\Delta t_{SV} = a_0 + a_1(t - t_{0c}) + a_2(t - t_{0c})^2 \tag{2.2}$$

Where t_{0c} is the reference epoch for the coefficients a_0 , a_1 and a_2 .

By differentiating (2.2) with respect to time, expression for drift of satellite clock is obtained as:

$$\dot{\Delta} t_{SV} = a_1 + 2a_2(t - t_{0c}) \tag{2.3}$$

The elapsed time t_k from ephemerides reference epoch t_{0e} (all expressed in seconds in GPS

week) is given by equation 2.4. In this case, the correct time of ephemeris (t_{0e}) must first be found in the navigation file.

$$t_k = t - t_{0e} \tag{2.4}$$

The mean anomaly is given by:

$$M_k = M_0 + n(t - t_{0e}) = M_0 + \left(\sqrt{\frac{\mu}{a^3}} + \Delta n \right) t_k \tag{2.5}$$

Where:

$\mu = GM = 3986005\, x10^8\, m^3\, \sec^{-2}$ is the WGS84 value of the geocentric gravitational constant, n is the corrected mean motion, Δn is the correction to the mean motion, and a is the semi-major axis.

Solving iteratively, the Kepler equation for eccentric anomaly E_k is given by:

$$E_k = \overline{M}_k + e \sin E_k \tag{2.6}$$

Since the value of eccentricity of GPS orbit is very small $(e < 0.001)$, two iterations are usually sufficient.

$$E_0 = \overline{M}, \;\; E_i = \overline{M} + e \sin E_{i-1}, \;\; i = 1,2,3,..... \tag{2.7}$$

The true anomaly v_k is computed by:

$$v_k = \arctan\left(\frac{\sqrt{1 - e^2 \sin E_k}}{\cos E_k - e} \right) \tag{2.8}$$

Using argument of perigee ω, true anomaly v_k, corrections C_{uc} and C_{us}, the corrected argument of latitude u_k is given by:

$$u_k = \omega_0 + C_{uc} \cos 2(\omega + v_k) + C_{us} \sin 2(\omega + v_k) \tag{2.9}$$

The corrected radial distance r_k considering corrections C_{rc} and C_{rs} is given by:

$$r_k = a(1 - e\cos E_k) + C_{rc}\cos 2(\omega + v_k) + C_{rs}\sin 2(\omega + v_k) \tag{2.10}$$

The corrected inclination i_k of the orbital plane from inclination i_0 at reference time t_{0e} and corrections C_{ic} and C_{is} is given by:

$$i_k = i_0 + \dot{i}t_k + C_{ic}\cos 2(\omega + v_k) + C_{is}\sin 2(\omega + v_k) \tag{2.11}$$

The corrected longitude of ascending node Ω_k (referring to Greenwich) using its right ascension Ω_0 at the beginning of the current week corrected from the apparent sidereal time variation in Greenwich between the beginning of the week and reference time t_k and the change in longitude of ascending node from the reference time t_{0e} is given by:

$$\Omega_k = \Omega_0 + (\dot{\Omega} - \omega_e)t_k - \omega_e t_{0e} \tag{2.12}$$

Where $\omega_e = 7.2921151467\ x10^{-5}\ rad/\sec$ is Earth rotation rate in WGS84.

The position of satellite in orbital plane is given by:

$$\begin{pmatrix} X_k' \\ Y_k' \\ Z_k' \end{pmatrix} = \begin{pmatrix} r_k \cos u_k \\ r_k \sin u_k \\ 0 \end{pmatrix} \tag{2.13}$$

Finally, the position of satellite (satellite coordinates) X_k, Y_k, Z_k with respect to Earth-fixed geocentric frame are given by:

$$\begin{pmatrix} X_k \\ Y_k \\ Z_k \end{pmatrix} = \begin{pmatrix} X_k' \cos \Omega_k - Y_k' \sin \Omega_k \cos i_k \\ X_k' \sin \Omega_k + Y_k' \cos \Omega_k \cos i_k \\ Y_k' \sin i_k \end{pmatrix} \tag{2.14}$$

For more information on the steps in satellite position determination, refer Seeber [2003].

2.1.6 The structure of GPS signal and navigation data

The GPS navigation data is organized in data frame which is subdivided in five subframes. Each subframe has six seconds duration (corresponding to 300 bits each) and contains ten data words of 30 bits each, six of them being control bits. This makes total information content of navigation data set to be 1500 bits with a bit-rate of 50 bps and a cycle of 30 seconds. The first two words of each subframe are the telemetry word (TLM) which contains a synchronization pattern to facilitate the access to the navigation data and C/A- to P-code called hand over word (HOW) (Seeber, 2003).

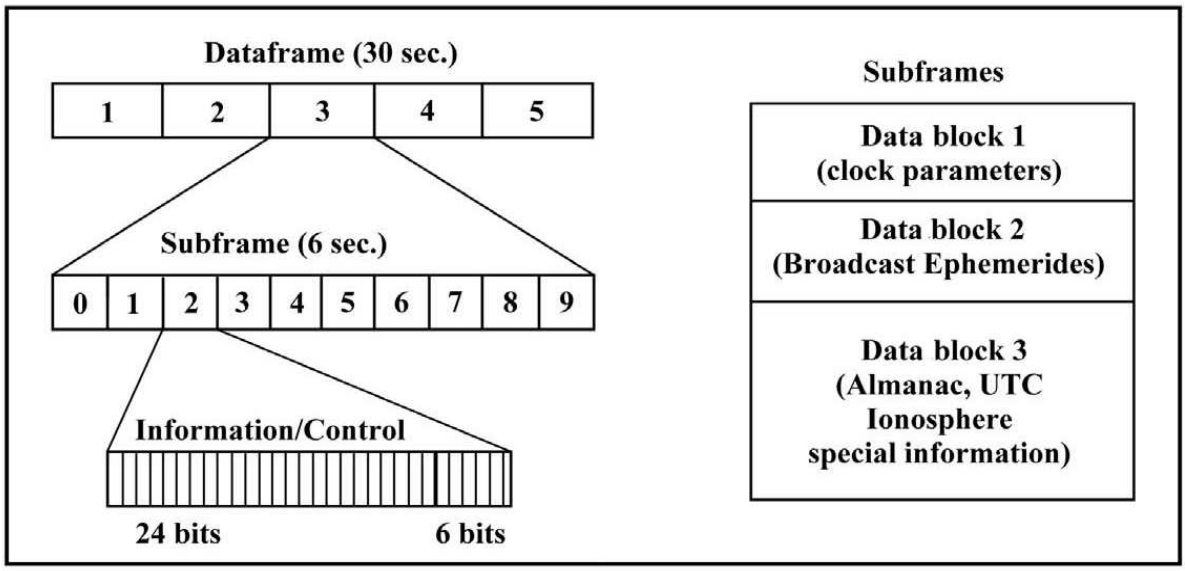

Figure 2.8: GPS navigation data structure.

The records in the navigation data are divided into three blocks known as Data Block I, Data Block II and Data Block III. Information contained in Data Block I which appears in the first subframe include GPS week number, satellite correction terms and the satellite vehicle (SV) accuracy and health while Data Block II which appears in second and third subframes contains all necessary ephemeris parameters for computing satellite coordinates. The information in Data Block III which appears in the fourth and fifth subframes includes the almanac data with clock and ephemeris parameters for all available satellites of GPS system, ionospheric correction parameters, universal time data and particular alphanumeric information for authorized users. The fourth and fifth subframes which have total information content available every 12.5 minutes consist of 25 pages that appear subsequently, where each page covers the almanac data of one satellite from the total constellation. The almanac data includes the parameters which represent the ephemeris of a particular space vehicle,

corrections to the satellite clock, identification number, and satellite health status. However, almanac and satellite health status are included in subframe five for satellite 1-24 while those in subframe four are for satellites numbered 25 and higher. The less accurate almanac data are useful since they can be used for satellite prediction computation (alerts) and for faster lock-on to satellite navigation signals. For more details on GPS navigation data refer Seeber [2003] § 7.1.5.4.

Currently the signal broadcast on two L-band frequencies by GPS satellites has three components namely: a carrier signal at the centre frequency, a bi-phase shift key (BPSK: phase modulation with $\varphi \pm \pi$) modulated PRN code(s), and binary navigation data (Zhang, 2007). In order to determine position in real-time using GPS signal, carriers are modulated with sequences of binary values (zeros and ones or +1 and -1) which appear to have random character called pseudorandom noise (PRN) codes. Two PRN codes used to derive pseudorange are the P-code and the C/A-code which means precision or protected code and clear/acquisition code respectively. The P-code and C/A-code are modulated on the two carrier frequencies known as L1 and L2 signals. Each satellite transmits signals on the two carrier frequencies also known as the navigation signals (codes), and on the navigation and system data (message) (Seeber, 2003). Both P-code and C/A-code are contained in L1 signal while the P-code is contained only in L2 signal.

The generation of the three carrier frequencies (L1, L2 and L5) are coherently derived from the fundamental 10.23 MHz frequency generated by the onboard atomic oscillators in such a way that: L1 = 154 x 10.23 MHz = 1575.42 MHz (~ 19.05 cm) and L2 = 120 x 10.23 MHz =1227.60 MHz (~ 24.45 cm) (Seeber, 2003) and the third one being L5 = 115 x 10.23 MHz = 1176.45 MHz (~25.48 cm).

Being present on both L1 and L2 frequencies, the P-code which is the principle code for navigation has 10.23 MHz frequency which corresponds to about 30m wavelength. Its sequence of 10.23 million binary digits or chips per second known as chipping rate is extremely long since it repeats after 266 days (38 weeks). When implemented and activated with Anti-spoofing (AS), the P-code can only be accessed by authorized users (mainly military) when encrypted with the protected code named Y-code through the service called Precise Positioning Service (PPS) (Seeber, 2003). The aim of AS was to prevent an adversary from generating a copy of GPS signal and to spoof or mislead a receiver. This was aimed so to prevent unauthorized users to access L2 carrier signal which carried the encrypted P-code.

However, receiver manufacturers developed a technique to gain access to L2 signals under AS though with decreased accuracy (Seeber, 2003).

The C/A-code which is transmitted on L1 carrier is generated at a chipping rate of 1.023 MHz that corresponds to about 300m wavelength (Seeber, 2003). The C/A-code which has phase lag of 90º on L1 to the P-code known as phase quadrature is designed only for civilian access through the service available to the civil community called Standard Positioning service (SPS) (Seeber, 2003).

Additionally, GPS signal accuracy was limited internationally through the technique called Selective Availability (SA). This is the degradation of the GPS signal by adding controlled errors in the measurement data (Seeber, 2003). Two effects involved in this technique are ephemeris data manipulation and dithering, or systematic destabilization of the satellite clock which results in corrupted measured pseudorange. However, dithering technique was mainly used which resulted in a roughly five-fold increase in positioning error (Seeber, 2003). SA was implemented first on March 23, 1990 which later was disabled on August 2, 1990 due to Gulf crisis. However, it was implemented to SPS users in November 1991 after being effective again in July 1991. After long discussions, the former U.S. President Bill Clinton directed the DoD to turn off the SA feature in May 2, 2000. Later in 2007, the U.S. government announced plans of permanent elimination of the SA by building the GPS III satellites without it under the ongoing GPS modernization program in order to benefit the civil and commercial users worldwide. Until 2001, the global position accuracy achieved was $\leq$ 13 meters horizontal error and $\leq$ 22 meters vertical error with 95% confidence interval (Seeber, 2003). However, through SPS performance under ongoing modernization program, GPS will provide to the civilian community a “worst case” pseudorange accuracy of 7.8 meters at a 95% confidence level. By combining GPS with augmentation systems like Wide Area Augmentation System (WAAS), the Nationwide Differential GPS System (NDPS), Continuous Operating Reference Stations (CORS), Global Differential GPS (GDGPS), the IGS itself, and other augmentation systems, higher accuracy has been achieved enabling the real-time positioning to a few centimeters and post-mission measurements at the millimeter level. GPS augmentation system is any system which aids GPS in providing accuracy, integrity, availability or any other improvement to positioning, navigation, and timing (PNT) that is not inherently part of GPS itself. Safety of life applications will be supported by combining GPS Space-Based Augmentation System (SBAS) receivers using the European

Geostationary Navigation Overlay Service (EGNOS) and GPS Wide Area Augmentation System (WAAS) by reaching obscured environments where buildings, trees or terrain block large portion of the sky. Additionally, using the combination of 31 GNSS satellites (Beutler, 2011; Miller, 2013), 30 GLONASS satellites and 30 Galileo satellites (Clore, 2012), GPS accuracy, integrity, availability and flexibility will be met in real-time applications. However, higher civilian accuracy will be enabled by the U.S. government without these augmentations under GPS constellation modernization program. For more information on augmentation systems, refer http://www.gps.gov/systems/augmentations/.

2.1.7 GPS observables

Satellite navigation observables are one-way range measurements deduced from measured time or phase differences based on a comparison between received signals and receiver-generated signals (Hoffman et al., 2008). One-way range measurement is the one in which, clock reading at the transmitter antenna is compared with a clock reading at the receiver antenna. Since the observed signal travel time contains a systematic synchronization error, the ranges are biased by satellite and receiver clock errors and thus denoted as pseudoranges. Three basic types of GPS observables are pseudoranges from code measurements, pseudoranges from carrier phase measurements, and the Doppler frequency shift (Hofmann-Wellenhof et al., 2008; Seeber, 2003; Zhang, 2007). However, code pseudorange and carrier phase measurements are generally considered as two basic range observables (Zhang, 2007) and will be explained in details in the next sections.

2.1.7.1 Code pseudorange measurements

Code range measurement is obtained when the time shift necessary to correlate the incoming code sequence from satellite with a code sequence generated in the GPS receiver is multiplied by the velocity of light (Seeber, 2003). The time shift which is known as the signal propagation time between GPS satellite and the receiver is the difference between clock readings which aligns the satellite and reference signal during code correlation procedure in the receiver (Hofmann-Wellenhof et al., 2008; Zhang, 2007). Due to lack of synchronization between satellite and receiver clocks to GPS time, the time shift is affected by clock errors resulting in the code pseudorange. However, the satellite clock bias can be modelled if the respective information is transmitted accordingly in the navigation message (Hofmann-Wellenhof et al., 2008). The equation for code pseudorange is obtained by Hofmann-

Wellenhof et al, [2008], Seeber, [2003], and Zhang, [2007] as:

$$R_r^s = (t_r - t^s) * c \tag{2.15}$$

Where R_r^s is the code pseudorange between the receiver r and the satellite s; t_r is the receiver clock time, t^s is the satellite transmit time and c is the velocity of light. Expression 2.15 can be related to true range by including satellite and receiver clock corrections.

$$t_r = t_r + \delta t_r \,,\; t^s = t^s + \delta t^s \tag{2.16}$$

Where t_r and t^s are the receiver and satellite true times respectively, δt_r and δt^s are receiver and satellite clock corrections respectively. Generally, expression 2.15 for a single pseudorange can be re-written as:

$$R_{r,i}^s(t) = \rho_r^s + (\Delta t_r - \Delta t^s) * c + dI_r^s + dA_r^s + dT_r^s + dM_r^s - dR_r^s + \varepsilon_r^s \tag{2.17}$$

Where the true or geometrical range ρ_r^s between satellite and receiver is given by:

$$\rho_r^s(t_r^s) = (t_r - t^s) * c = \sqrt{\left(X^s(t^s) - X_r(t_r)\right)^2 + \left(Y^s(t^s) - Y_r(t_r)\right)^2 + \left(Z^s(t^s) - Z_r(t_r)\right)^2} \tag{2.18}$$

Where:

- $R_r^s(t)$ is the code pseudorange between satellite s and receiver r at GPS time t;
- $\rho_r^s(t_r^s)$ is the true range between satellite s and receiver r;
- The subscript i represent the frequency band of the observation. i.e. $i = 1$ for L1, and $i = 2$ for L2;
- Superscript s represents the satellite being observed;
- Subscript r represent the receiver;
- d represent the error term;
- dI_r^s is the ionospheric delay;
- dA_r^s is the atmospheric delay;

- dT_r^s is the tropospheric delay
- dM_r^s is the multipath effect;
- dR_r^s is the relativistic effects due to the satellite motion and the Earth gravitation field;
- ε_r^s is the associated error with the observation;
- X^s, Y^s, Z^s is the satellite position;
- X_r, Y_r, Z_r is the receiver position;
- δt_r is the receiver clock correction;
- δt^s is the satellite clock correction.

The biased code pseudorange measurement with respect to the satellite-to-receiver is due to above listed errors in their absolute values in units of meters. The ionospheric correction term is assigned positive since the ionosphere delays the GPS code signal resulting in an increase in range measurement. The same positive sign is assigned to tropospheric correction which delays the signal travel time. Similar positive sign is assigned to the receiver clock which contributes to an extra signal travel distance compared to satellite clock which decrease the measured distance assigned by a negative sign. Another positive sign is assigned to multipath which causes the measured distance to be longer than the direct distance. The multipath effect occurs due to multiple reflections of the indirect signal(s) coming into the receiver (Zhang, 2007).

The derived code pseudorange from code measurements has a precision of about 1% of the chip length which indicate that, for a C/A-code of 300m chip length would yield a precision of about 3m, and for a P-code of 30m chip length would yield a precision of about 0.3m. However, the precision of about 0.1% is possible due to more recent developments (Hofmann-Wellenhof et al., 2008).

However, one of the complications that arise in code pseudorange measurements is that, if the satellite position is not calculated at transmission time, satellite range can change as much as 60 meters from the time the signal was transmitted, to the time the signal was received, which

is approximately 0.07 seconds later (Blewitt, 1997).

2.1.7.2 Calculation of user position with code pseudorange

To calculate the receiver position using code pseudorange measurement, the following expression is used.

$$R_i^j(t) = \rho_i^j(t) + c(\delta t_i - \delta t^j) \tag{2.19}$$

Where $R_i^j(t)$ is the measured code pseudorange between the user receiver i at site and the satellite j , $\rho_i^j(t)$ is the geometrical distance between the satellite and the observing point, and c is the speed of light (in a vacuum). User point coordinates which are implicitly in $\rho_i^j(t)$ and in 2.19 are defined by the following expression:

$$\rho_i^j(t) = \sqrt{\left(X^j(t) - X_i\right)^2 + \left(Y^j(t) - Y_i\right)^2 + \left(Z^j(t) - Z_i\right)^2} \tag{2.20}$$

Where $X^j(t), Y^j(t), Z^j(t)$ represent the geometric position vectors of the satellite at epoch t , and X_i, Y_i, Z_i are unknown coordinates of the user position in Earth Centered Earth Fixed (ECEF) coordinate system. The known satellite clock bias can be calculated at every epoch using information provided in the broadcast navigation message using expression 2.2 in §2.5 in the form of polynomial coefficients. In this case equation 2.19 can be written as:

$$R_i^j(t) + c\delta t^j = \rho_i^j(t) + c\delta t_i \tag{2.21}$$

The left hand side of equation 2.21 contains the observed or known quantities while the right hand side contains the unknowns. After putting $\rho_i^j(t)$ in linear form using Taylor theorem with approximate coordinates (X_{0i}, Y_{0i}, Z_{0i}) of the user receiver yield the following expression:

$$\rho_i^j(t) = \rho_{i0}^j(t) - \frac{X^j(t) - X_{0i}}{\rho_{i0}^j(t)}\Delta X_i - \frac{Y^j(t) - Y_{0i}}{\rho_{i0}^j(t)}\Delta Y_i - \frac{Z^j(t) - Z_{0i}}{\rho_{i0}^j(t)}\Delta Z_i \tag{2.22}$$

Where:

$$\rho_{0i}^j(t) = \sqrt{\left(X^j(t) - X_{0i}\right)^2 + \left(Y^j(t) - Y_{0i}\right)^2 + \left(Z^j(t) - Z_{0i}\right)^2} \tag{2.23}$$

Substituting 2.22 and 2.23 into 2.21 and rearranging it we get the final expression as follows:

$$R_i^j - \rho_{i0}^j(t) + c\delta t^j = -\frac{X^j(t) - X_{0i}}{\rho_{i0}^j(t)}\Delta X_i - \frac{Y^j(t) - Y_{0i}}{\rho_{i0}^j(t)}\Delta Y_i - \frac{Z^j(t) - Z_{0i}}{\rho_{i0}^j(t)}\Delta Z_i + c\delta t_i \qquad (2.24)$$

Equation 2.24 contains four unknowns named $\Delta X_i, \Delta Y_i, \Delta Z_i, \delta t_i$ and to solve it, at least four satellites are needed. Arranging 2.24 in matrix-vector form and solving it using least-squares, the user coordinates X_i, Y_i, Z_i can be calculated using equations 2.25 to 2.27.

$$X_i = X_{0i} + \Delta X_i \qquad (2.25)$$

$$Y_i = Y_{0i} + \Delta Y_i \qquad (2.26)$$

$$Z_i = Z_{0i} + \Delta Z_i \qquad (2.27)$$

The accuracy of the user coordinates depend on the accuracy of the displacements $\Delta X_i, \Delta Y_i, \Delta Z_i$ which also depend on the user's accuracy requirements. That is, the displacements are acceptable if the user's accuracy requirements are met. If the values of displacements exceed the required value, the process is reiterated by replacing ρ by a new estimates of pseudorange based on calculated point coordinates (Hofmann-Wellenhof et al., 2008).

However, care must be taken in order to achieve high quality results especially relative positioning, point positioning and kinematic surveying (Hofmann-Wellenhof et al., 2008). The important factor that guide to high accurate results is the geometry of the visible satellites during observations called dilution of precision (DOP). The important DOP values are vertical dilution of precision (VDOP), positional dilution of precision (PDOP), horizontal dilution of precision (HDOP), geometric dilution of precision (GDOP), and time dilution of precision (TDOP) which may be computed in advance using almanac data or other orbital information without considering observations (Hofmann-Wellenhof et al., 2008). DOP values also can be computed from the cofactor matrix of the local topocentric coordinates with its axes along the local north, east , and up by law of covariance propagation. Refer Hofmann-Wellenhof et al. [2008] for more information on the DOP values computations. Usually VDOP values are higher compared to HDOP which makes vertical positions to be less precise than horizontal positions. Since DOP values are purely function of satellite geometry, a good geometry gives low DOP values while a bad geometry of constellation gives very high DOP

values (Blewitt, 1997). In order to have a good geometry and better satellite constellation, PDOP values should be less than 3 and HDOP values should be less than 2 (Hofmann-Wellenhof et al., 2008). For example if VDOP has value of 5, the expected code pseudorange error of 1 meter maps into vertical position errors of 5 meters and again if PDOP values are larger than 5, they are considered as poor. Moreover, if there is insufficient number of satellites to produce a solution, or if two out of four satellites lie approximately in the same direction in the sky, then the cofactor matrix becomes singular and the DOP values go to infinity (Blewitt, 1997).

2.1.7.3 Carrier phase measurements

Carrier phase measurement which is another way of measuring the distance from satellite to the receiver by multiplying the phase and wavelength requires phase comparison between the received doppler-shifted carrier signal and the constant receiver generated carrier signal when there is a lock of a receiver onto a GPS satellite (Zhang, 2007; Seeber, 2003). The proper observable in carrier phase measurements is the phase difference which is obtained by subtracting the incoming or received GPS carrier phase from satellite from receiver-generated reference phase. However, the phase difference which is also known as carrier phase or carrier beat phase is ambiguous by an integer number of cycles called integer ambiguity. The expression of carrier phase in unit of cycles is given by Hofmann-Wellenhof et al. [2008] as:

$$\varphi_r^s(t) = \varphi^s(t) - \varphi_r(t) \tag{2.28}$$

where $\varphi_r^s(t)$ is the carrier beat phase or simply carrier phase, $\varphi^s(t)$ is the phase of the received and reconstructed carrier with frequency f^s, $\varphi_r(t)$ is the phase of reference carrier generated in the receiver with frequency f_r, and t is an epoch in a common time system reckoned from an initial epoch $t_0 = 0$. By including satellite and receiver clock errors, and an integer ambiguity, the general carrier phase expression is given by (Hofmann-Wellenhof et al. 2008) as:

$$\varphi_r^s(T_r) = f^s \frac{\rho}{c} + f^s\delta^s - f_r\delta_r + (f^s - f_r)t - N_r^s \tag{2.29}$$

Where:

δ^s is the satellite clock error, δ_r is the receiver clock error, ρ is the phase pseudorange, c is the speed of light, and N_r^s is an integer number of cycles between satellite and the receiver. Considering the nominal carrier frequency $f \approx 1.5GHz$ we find that, frequencies f^s and f_r may deviate only in some fractional parts of hertz of $df \approx 1.5 * 10^{-3} Hz$ if we take a consideration of short-time stability in frequencies of $\frac{df}{f} \approx 10^{-12} GHz$. During signal propagation with $t = 0.07s$, the resulting frequency error may generate a maximum error of 10^{-4} cycles in the carrier phase which may be neglected since it is below the noise level (Hofmann-Wellenhof et al., 2008).

Scaling equation 2.29 with wavelength, the carrier phase measurement relating receiver and satellite position is given by Zhang, [2007] as:

$$\lambda_i \varphi_{r,i}^s(t) = \rho_r^s(t_r, t^s) - dI_{r,i}^s + dT_r^s + c.dt_r(t) - c.dt^s(t - \tau_r^s) - \lambda_i N_{r,i}^s + \lambda_i \varphi_{r,i}^s(0) + dM_r^s - dR_r^s + \varepsilon_r^s \quad (2.30)$$

Where:

- λ_i is the wavelength of the carrier phase whereby, 19.3 cm is for L1 carrier frequency and 24.4 cm is for L2 carrier frequency;
- $\lambda_i \varphi_{r,i}^s(t)$ Is the carrier phase observable of the i-th frequency for the receiver r and satellite s;
- $\varphi_{r,i}^s(t)$ is the carrier phase measured on L1 and L2 frequencies;
- $N_{r,i}^s$ is the integer ambiguity of the carrier phase measurement of the i-th frequency;
- $\lambda_i \varphi_{r,i}^s(0)$ is the initial fraction of the carrier phase on the i-th frequency for receiver r and satellite s when the receiver achieves the initial lock;
- ε is the noise of the carrier phase measurement;
- $\rho_r^s(t_r, t^s)$ is the true or geometrical range between satellite s and receiver r;

- The subscript i represent the frequency band of the observation. i.e. $i = 1$ for L1, and $i = 2$ for L2;
- Superscript s and r represent the satellite and receiver respectively;
- dI_r^s is the ionospheric delay;
- dT_r^s is the tropospheric delay;
- dM_r^s is the multipath effect;
- dR_r^s is the relativistic effects due to the satellite motion and the Earth gravitation field;
- $dt_r(t)$ and $dt^s(t-\tau_r^s)$ are the receiver and satellite clock corrections respectively;
- $\lambda_i \varphi_{r,i}^s(0) - \lambda_i N_{r,i}^s$ is called the bias term.

The carrier phase model in equation 2.30 looks similar to code pseudorange model except that, the bias term doesn't appear in code pseudorange and the ionospheric delay is equal but in opposite negative sign due to phase advancing (Zhang, 2007). Other terms like geometrical range, clock, and tropospheric errors are similar comparing to code pseudorange. However, multipath errors and the noise terms are much smaller in phase compared to those in pseudorange (noise term being 100 times smaller in phase data).

Although the instantaneous fractional part of carrier phase on a receiver at epoch t_0 can be measured, the initial number N of cycles between satellite and receiver called integer ambiguity is unknown. However, if no loss of lock, the integer ambiguity remains constant over an orbit arc. If loss of lock occurs between satellite and receiver, the integer number of a receiver-satellite pair changes resulting in cycle slip. When a cycle slip occurs, it is necessary to introduce a new integer ambiguity (Zhang, 2007).

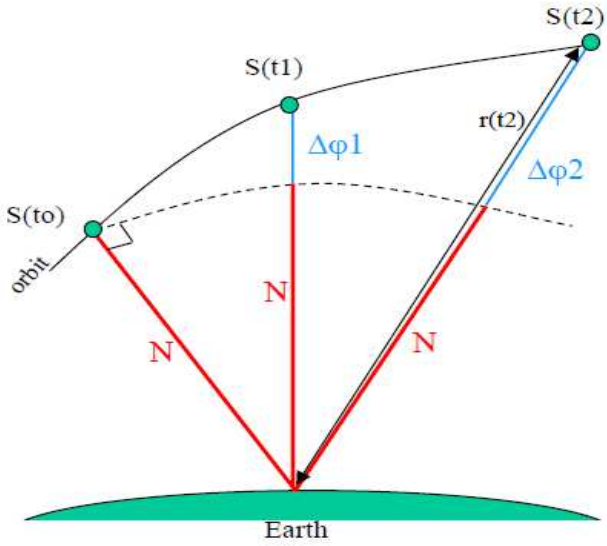

Figure 2.9: Integer ambiguity on phase measurements (Calais, 2010).

Since the wavelength of the carrier waves are very short about 19cm for L1 and 24 cm for L2 approximately compared to the C/A-code (~300m) and P-code (~30m), the phase measurements can be made to better than 0.01 cycles which corresponds 1% of wavelength resulting in millimeter precision of ~2 mm for L1, ~2.4 mm for L2, and ~2.6 mm for L5 compared to a few meters precision for C/A-code and several decimeters for P-code for a frequency in the gigahertz range (Hofmann-Wellenhof et al., 2008). This makes phase measurements to be very precise and accurate but ambiguous compared to code pseudorange measurements which are less precise but absolute. The accuracy of 0.2 mm is theoretically possible for accurate phase measurements in GPS receivers if ~0.005 cycles are used (Calais, E., 2010). Note that, one missing wavelength for phase measurements can causes an error of 19 cm or 24cm if ambiguity term which is the most demanding problem in the geodetic technique of evaluating GPS observations is not determined with appropriate techniques (Seeber, 2003). The appropriate and simplest method to determine this integer nature as it guarantees the high accuracy of relative GPS positioning particularly on short observation time is to use additional frequencies or signals in the carrier phase measurements (Seeber, 2003). However, since GPS doesn't use more than two frequencies for the time being, other techniques which can be used instead include ambiguity search in the measurement domain, search technique in the coordinate domain, and search technique in the ambiguity domain (Hofmann-Wellenhof et al, 2008). Fortunately, ambiguity domain search is the most effective and powerful approach which is currently considered especially for fast solutions (Seeber,

2003). All these basic approaches on ambiguity resolution are demonstrated in detail in the Hofmann-Wellenhof et al., [2008] in §7.2.

2.1.7.4 Calculation of user position with carrier phase measurements

The procedure is the same as in code pseudorange whereby, the linearization is performed for $\rho_i^j(t)$ in 2.31 and known terms are shifted to the left hand side and the whole equation multiplied by λ which yield equation 2.32 (Hofmann-Wellenhof et al., 2008).

$$\varphi_i^j(t)+\frac{c}{\lambda}\delta t^j=\frac{1}{\lambda}\rho_i^j(t)+\frac{1}{\lambda}\delta t_i+N_i^j \tag{2.31}$$

Where $\varphi_i^j(t)$ is the measured carrier phase expressed in cycles, λ is the wavelength, $\rho_i^j(t)$ is the geometrical range from satellite to user receiver, N_i^j is the unknown integer ambiguity, and c denotes the speed of light. The terms δt^j and δt_i are the satellite and receiver clock biases respectively.

$$\lambda\varphi_i^j(t)-\rho_{i0}^j(t)+c\delta t^j=-\frac{X^j(t)-X_{0i}}{\rho_{i0}^j(t)}\Delta X_i-\frac{Y^j(t)-Y_{0i}}{\rho_{i0}^j(t)}\Delta Y_i-\frac{Z^j(t)-Z_{0i}}{\rho_{i0}^j(t)}\Delta Z_i+c\delta t_i+\lambda N_i^j \tag{2.32}$$

Comparing to code pseudorange measurements, the number of unknowns is increased due to increase in ambiguity term N_i^j. Considering four satellites and re-arranging equation 2.32 in matrix-vector form, four observation equations are obtained which are inadequate to solve for the eight unknowns. This makes impossible to solve for kinematic point positioning with phase measurements in this form which require single epoch unless phase ambiguities are known from some initialization which makes phase range model to convert to code range model (Hofmann-Wellenhof et al., 2008). To solve the above equation using phase measurements, at least three epochs (i.e. 12 satellites) containing 12 equations and 10 unknowns should be taken into account. This solution is performed using least-squares adjustment (Hofmann-Wellenhof et al., 2008) where the final receiver coordinates are calculated using equation 2.25 to 2.27.

2.1.7.5 Doppler shift measurements

Doppler shift is a result of relative motion between receiver and a transmitter which cause frequency difference between the received signal and the source signal in the receiver

(Zhang, 2007). Using the received carrier frequency f_r from satellite and the reference frequency f_g within the receiver, pseudorange differences can be derived from Doppler shift observations yielding an integrated Doppler count N_{jk} as:

$$N_{jk} = \int_{t_j}^{t_k} (f_g - f_r)\, dt \,. \tag{2.33}$$

Where N_{jk} is the measure of range difference between receiver antenna and the two consecutive orbital positions of the same satellite at two different epochs t_j and t_k (Seeber, 2003).

Carrier phase measurement of a GPS receiver relates to integrated Doppler shift measurements by taking first derivative of Doppler shift with respect to time (Zhang, 2007). The Doppler shift observation is given by first derivative of phase equation 2.30 as given by Zhang, [2003] as:

$$\lambda_j D^s_{r,j}(t) = \lambda_i \dot{\varphi}^s_{r,i}(t) = \dot{\rho}^s_r(t_r, t^s) - d\dot{I}^s_{r,i} + d\dot{T}^s_r + c.d\dot{t}_r(t) - c.d\dot{t}^s(t-\tau^s_r) + d\dot{M}^s_r - d\dot{R}^s_r + \dot{\varepsilon}^s_r \tag{2.34}$$

Whereby, a dot over a variable denotes its first derivative with respect to time, and all other terms being defined in §2.1.7.1 and 2.1.7.3. Equation 2.34 shows that, the initial fraction part of phase measurement and integer ambiguity have vanished. This makes Doppler shift measurements to be free from integer ambiguity problem compared to carrier phase observations (Zhang, 2003). Doppler shift observables are also cleaner than carrier phase observables since the errors and biases are the time derivatives of error sources in carrier phase measurements (Zhang, 2007).

The achievable accuracy of integrated Doppler shift is estimated to be 0.001 Hz which correspond to $3*10^{-4} ms^{-1}$ if the raw Doppler shift which is less accurate is based on an emitted frequency of 1GHz. Regardless its low accuracy, and apart from being used in navigation purposes, Doppler shift observations are applied in determining the integer ambiguities in a kinematic surveying and for point positioning as an additional independent observable (Hofmann-Wellenhof et al., 2008).

Doppler shift can also be measured using codes but the resolution of the code frequency is very poor compared to carrier phase frequency (Seeber, 2003).

2.2 GRACE measurements

2.2.1 Introduction

GRACE is a satellite mission which consists of two identical space-crafts flying in the same orbit about 220 kilometres apart in a polar orbit of 89º mean inclination and at a height of approximately 500 kilometres above the Earth. It is a pair nicknamed "Tom and Jerry" orbiting the Earth about 95 minutes. GRACE was launched on March 17, 2002 from the Russian Plesetsk cosmodrome with its primary objectives being determination of the global high-resolution gravity field of the Earth and temporal gravity variations. Additionally, it is aimed at determining total electron content by GPS measurements in order to get knowledge on the refractivity in the ionosphere and troposphere. It is a joint project of the U.S National Aero-nautics and Space Administration (NASA) and the Deutches Zentrum For Luft- und Raumfahrt (DLR), the University of Texas Center for Space Research (CSR), GeoForschungsZentrum Potsdam (GFZ) and the Jet Propulsion Laboratory (JPL). The uniqueness of GRACE is that, the quality measurements of mass flux (movement of materials around and within the Earth) are global, consistent and uniform. GRACE can also monitor the movement of water over the Earth's surface (runoff).

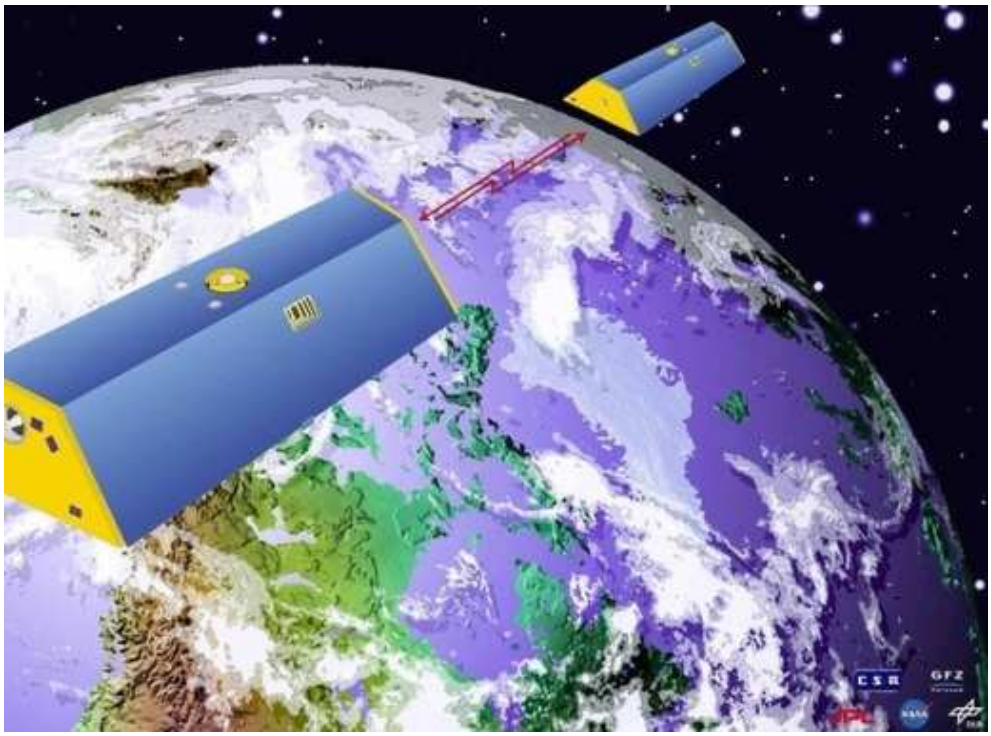

Figure 2.10: GRACE twin satellites nicknamed "TOM and JERRY" (Source: http://arstechnica.com/science/2012/03/earth-celebrates-ten-years-of-grace/).

2.2.2 Theory and principles of GARCE measurements

The theory on how GRACE works is based on the use of K-band ranging system equipped to satellites to measure inter-satellite distance related to gravity change and the change in satellite speed which is measured continuously with micrometer accuracy. The K-band ranging system as the key instrument of GRACE uses dual band microwave signals (i.e. two one-way ranges) with $1\mu ms^{-1}$ to measure the range changes obtained at a sampling rate of 10Hz between both satellites (Avsar et al., 2012). The on-board GPS receivers operate to determine satellite position and synchronizing the time tags of these range measurements of the two satellites. In order to measure high non-gravity accelerations, high accurate accelerometers are used together with two star cameras which provide the satellites' altitude. Mean while, the laser retro-reflectors are used to track the satellites from the ground stations (Avsar et al., 2012; Dunn et al., 2003).

Grace satellites use the principle of satellite-to-satellite tracking (SST) in high-low mode (SST-hl) and low-low mode (SST-ll) which improves the accuracy of the gravity field after processing the data (Avsar et al., 2012).

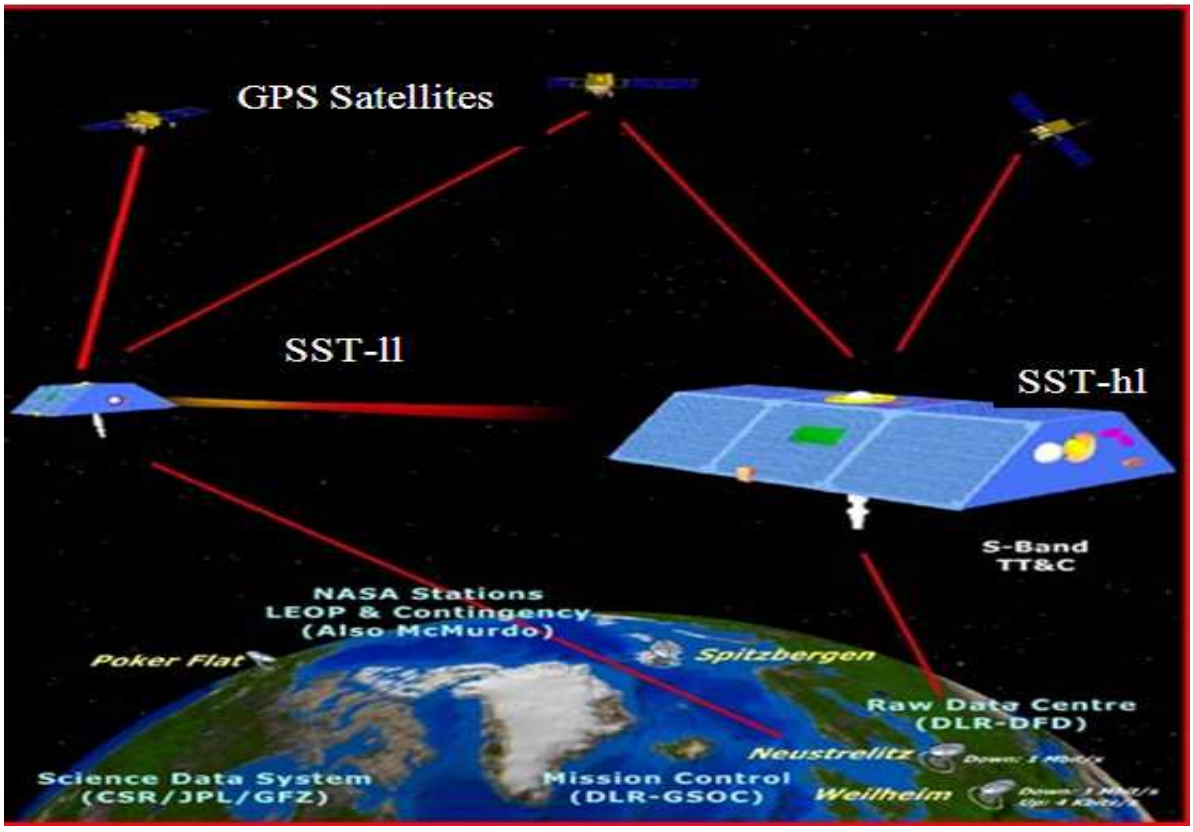

Figure 2.11: Satellite to satellite tracking (Source: http://www.csr.utexas.edu/grace/).

Basically as the two satellites travel in space, both at 500 kilometers above the earth (Figure 2.12A), the precise speed of each satellite and the distance between them are constantly communicated via a microwave K-band ranging instrument. As the front satellite approaches the area of high-gravity, its speed increases since it is pulled towards the area of higher gravity (Figure 2.12B-D). The increase in distance between the two satellites disturbs the orbit slightly. As the front satellite passes over the area of high gravity, it slows down while the speed of the trailing satellite increases at that moment towards the front satellite (Figure 2.12E). Again when the trailing satellite passes over the area of high gravity, it slows down leaving the front satellite's speed unaffected (Figure 2.12F). The procedure starts over from Figure 2.12G-K. This change in distance as the two satellites move around the Earth, is measured uniquely and precisely by GRACE microwave ranging system to an accuracy of smaller than micrometer per second in relative velocity. Hence the scientists can create a map of the Earth's gravity field every 30 days from the measured relative motion of the satellites. At the same time, the satellites use the GPS system to determine precisely where and when the measurements were taken. Figure 2.12L shows the two satellites at the moment of taking measurements. For more information refer http://www.csr.utexas.edu/grace.

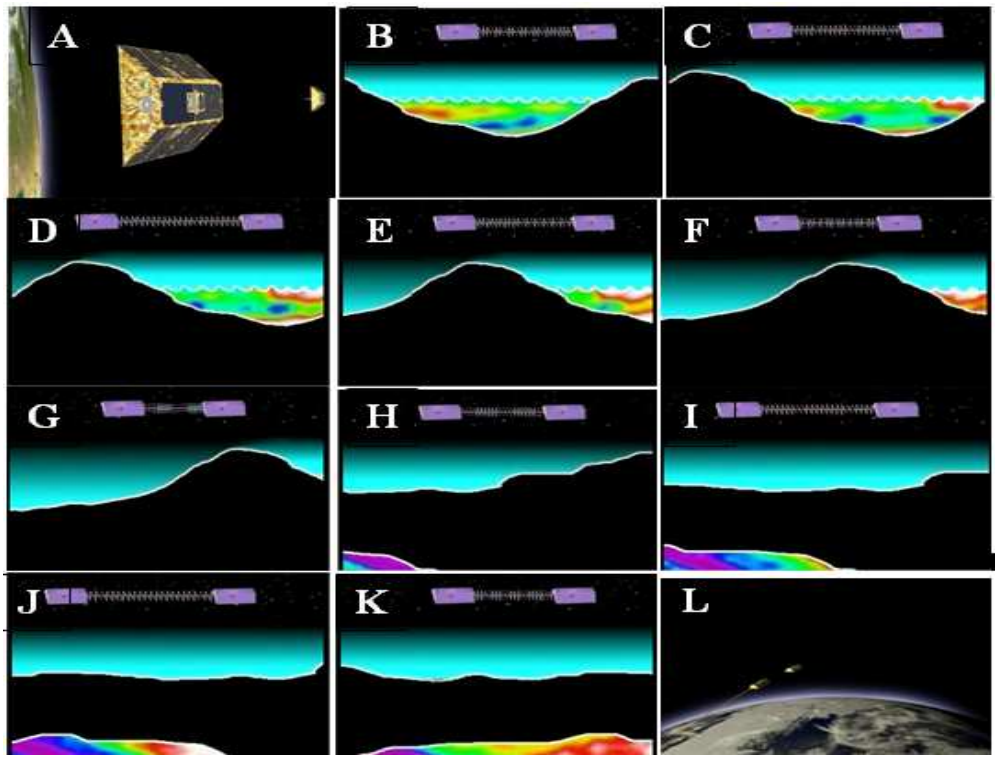

Figure 2.12: Theory and principles of GRACE measurements (Source: http://www.csr.utexas.edu/grace/ and http://www.astrium.eads.net/en/programme/grace.html).

GRACE data extraction and processing is done by a shared system called GRACE Science Data System (SDS) distributed between Jet Propulsion Laboratory (JPL), University of Texas Center for Space Research (UTCSR) and Deutches GeoForschungsZentrum (GFZ). GRACE data is categorized in three levels known as Level-1A, Level-1B, and Level-2 data. The Level-1A data which is a raw data is collected from satellite, calibrated and time-tagged in a non-destructive sense before undergoing extensive and irreversible processing. These Level-1A data are converted to editable and cleaned products but not distributed to the public. The level-1B data which are calibrated instrument data includes among others, the inter-satellite range, range-rate, range-acceleration, the non-gravitational accelerations from each satellite, the pointing estimates, the orbits, etc. These data are processed to generate Earth's gravity field estimates called Level-2 data in form of truncated sets of spherical harmonic coefficients at approximately monthly intervals (or shorter). The time variations in these spherical harmonic coefficients can then be used in estimating the changes in mass distribution in the Earth's system. After that, SDS delivers and distribute the Level-2 data in accompany with Level-1B to the public after validation via two portals named the Physical Oceanography Distributed Active Archive Center (PO.DAAC) at the Jet Propulsion Laboratory, Pasadena, USA, and the Information System & Data Center (ISDC) at GeoForschungsZentrum Potsdam in Germany (see Chapter three §3.1) (Avsar et al., 2012). For more information refer http://www.csr.utexas.edu/grace/asdp.html.

GRACE data processing is done using the satellite-only and combined models recently released depending on the improvements of the processing methods, updated softwares and increasing data (Avsar et al., 2012; ICGEM, 2012). These models have been developed by a number of scientific teams worldwide since the launch of GRACE twin satellites (Newton's Bulletin, 2009). The GRACE-only models include GGM02S (Tapley et al., 2005), EIGEN-GL04C (Förste et al., 2008), GGM03S and GGM03C (Tapley et al., 2007) and the most recent being EGM2008 (Pavlis et al., 2008). However, the Gravity Observation Combination (GOCO) has the aim of computing high-accuracy and high-resolution static global gravity models based on data from satellite gravity missions CHAMP, GRACE, and GOCE, terrestrial gravity field, satellite altimetry, and Satellite Laser Ranging (SLR) data (Pail et al., 2011). The Gravity field and steady-state Ocean Circulation Explorer (GOCE) is a satellite mission which was launched on March 17, 2009 with the objective of providing high-accuracy and high-resolution global model of the Earth's static gravity field and the geoid

(Farahani and Ditmar, 2011). These satellite-only models will be complemented in the future by combined global gravity models also incorporating terrestrial gravity and satellite altimetry data (Pail et al., 2011). Figure 2.13 shows the improvement of global gravity models derived from GRACE. The images show that, the global model from GRACE and surface gravity (right) data has better resolution compared to global model from GRACE only of 2004 and 2010.

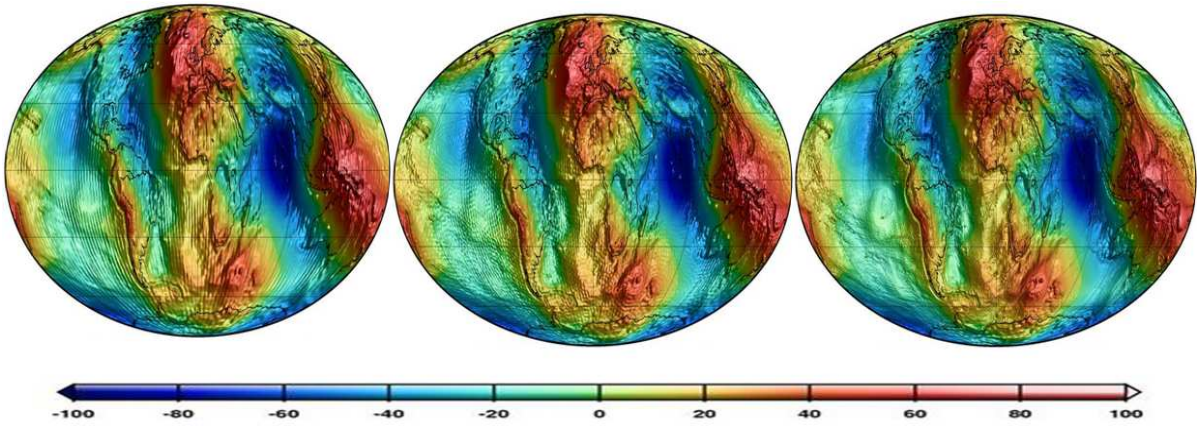

Figure 2.13: Global gravity models from GRACE for years 2004 (left), 2010 (middle), and GRACE with surface data (right) (Barthelmes and KÖhler, 2010).

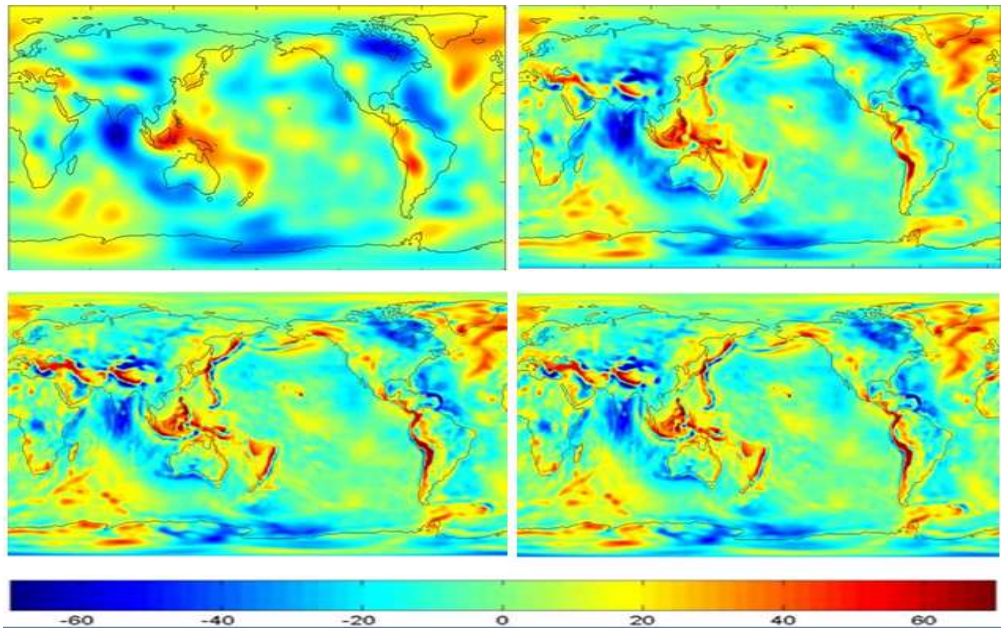

Figure 2.14: Global Gravity maps showing gravity anomalies from decades of tracking Earth-orbiting satellites (top left), from 111 days of GRACE data (GGM01S) (top right), from 363 days of GRACE data (GGM02S) (bottom left), and from four years (2003-2006) of GRACE data (GGM03S) (bottom right). (Source: http://www.csr.utexas.edu/grace/gravity/).

Figure 2.14 shows global gravity anomaly maps using different global gravity models. The maps show clearly the increase in resolution of satellite-determined gravity field from decades of tracking Earth-orbiting satellites as compared to new improved gravity models. For example the Figure shows that, GGM03S gravity model which was derived from globally distributed, precise inter-satellite range rate measurements derived by GRACE mission, and which was developed from older GGM02S model, has improved GRACE data, processing methods, and accuracy as compared to the previous released models. In this case it is clear that, the new generated models are more accurate than previous models at all wavelengths. Hence the models help in providing dramatically improved map of mean Earth gravity field which helps to refine the knowledge of the composition and structure of the Earth by providing the accurate reference surface relative to which deep ocean currents can be determined. For more detail on the context, refer http://www.csr.utexas.edu/grace/gravity/.

The interpretation of static gravity field and shape of the Earth is based on the surface geoid which is the level surface that approximates sea level in the absence of disturbing forces. The increase in Geoid caused by spatio-temporal variability in hydrological signal indicates an increase in mass and the decrease indicates mass loss. The mass redistribution and time variable gravity are explained in the following section.

2.2.3 Time-variable gravity and mass distribution

The mass distribution of the earth is irregular (not constant) and bumpy which makes gravity to vary since its variation depends on mass and shape of the earth. The changes and bumpy of the Earth is caused by molten rocks which flow in the mantle of the Earth. The changes in the earth's mass in time are occurred due to dynamic processes taking place in the earth's interior or on or above its surface. These dynamic processes refer to the mass transportation of continental water storages, oceans, atmosphere, ice sheets and glaciers and post-glacial rebound, tectonic motions and mantle dynamics within the Earth. The temporal variations of the earth's gravity field caused by these physical processes range from 10 to 100 parts per million (variation from the mean) and they occur on a variety of time scales from minute to secular. The signals which are varying with time mostly come from Earth's fluid envelope (Avsar et al., 2012).

2.2.4 Mass change and Gaussian smoothing

The errors affecting GRACE measurements include large errors along satellites' orbits (Wahr et al., 1998; Avsar et al., 2012). Other system noise errors in the inter-satellite range-rate include accelerometer error, error in the ultra stable oscillator and measurement errors. The GRACE satellites are featured mainly with nearly polar orbits which make their along-track direction mostly parallel to North-South directions. In this case, there is an East-West variations of accuracy of GARCE derived gravitational field sensed more badly than North-South directions which results in North-South stripping effects strongly in higher degrees. The presence of these stripping effects means the correlations in the gravity field coefficients. Hence the noise degrades GRACE solutions especially the short wavelength component. This error can be suppressed by filtering GRACE data. Gaussian filter is the best preferred method which is proposed by Wahr et al, [1998]. The filter to remove correlated errors in the spherical harmonic coefficients has been designed by Swenson and Wahr, [2006] whereby, a modified filter is given by Chen et al, [2008]. Swenson et al, [2003] developed a filter called the optimal regional filter to minimize both GRACE measurement and leakage errors. The latter being undesired signals since they cause temporal aliasing (Avsar et al., 2012).

The reliability of spherical harmonic coefficients C_n^m and S_n^m in GARCE models decreases rapidly with large degree n, with some additional increase for large order m. It is better to apply filter which suppress the noise making it decrease smoothly to zero as n increases rather than truncating the spherical harmonic series at some particular degree. A suitable filter is the one that convolves the space domain gravity signal with a Gaussian curve. As Gaussian half width increases, smoothing increases and vice versa (Bedada, 2007).

From Avsar and Ustun, [2012], the static part of the Earth's gravitational potential V on a reference sphere expressed as a series of spherical harmonics is given by Hofmann-Wellenhof and Moritz [2005] as:

$$V(r,\theta,\lambda)=\frac{GM}{R}\sum_{n=0}^{\infty}\left(\frac{R}{r}\right)^{n+1}\sum_{m=0}^{n}(C_{nm}\cos m\lambda+S_{nm}\sin m\lambda)\overline{P}_{nm}(\cos\theta) \tag{2.35}$$

Where r, θ and λ are the spherical geocentric radial distance, co-latitude and longitude coordinates respectively of the computation point; GM is the geocentric gravitational

constant; R is the semi-major axis of a reference ellipsoid; C_{nm} and S_{nm} are spherical harmonic coefficients where n, m are the degree and order respectively. $\overline{P}_{nm}(\cos\theta)$ are the fully normalized associated Legendre functions. However, due to the condition of the available data such as the precision, the measurement altitude of the gravity field cannot be estimated with unlimited spatial resolution which makes it necessary to truncate GRACE data to a certain maximum degree ($n_{\max}$) and set to equation 2.35 (Avsar et al., 2012).

The residual gravitational potential ΔV which is associated with the residual signal is given by

$$\Delta V(r,\theta,\lambda) = \frac{GM}{R}\sum_{n=0}^{n_{\max}}\left(\frac{R}{r}\right)^{n+1}\sum_{m=0}^{n}(\Delta C_{nm}\cos m\lambda + \Delta S_{nm}\sin m\lambda)\overline{P}_{nm}(\cos\theta) \qquad (2.36)$$

Where ΔC_{nm} and ΔS_{nm} represent the time variable dimensionless stokes coefficients.

The spatiotemporal changes in observations of the geoid height N which is the distance from geoid to reference ellipsoid are quantified by the changes in the distribution of mass in the Earth (Swenson et al., 2003). Geoid height can be derived from disturbing potential using Bruns formula. The disturbing potential is the difference between real gravitational potential V and normal gravitational potential U .

$$N(\theta,\lambda) = \frac{V(r,\theta,\lambda) - U(r,\theta)}{\gamma(\theta,\lambda)} \qquad (2.37)$$

Where, γ is the normal gravity on ellipsoid. The normal gravitational potential U is constant (i.e. does not change) since it is connected to reference ellipsoid. In this case, the differences in the geoid heights are completely determined by the residuals or changes of the gravitational potential. Hence, the shape of geoid is expressed as the sum of normalized associated Legendre functions and spherical harmonics.

$$\Delta N(\theta,\lambda) = R\sum_{n=0}^{n_{\max}}\sum_{m=0}^{n}(\Delta C_{nm}\cos m\lambda + \Delta S_{nm}\sin m\lambda)\overline{P}_{nm}(\cos\theta) \qquad (2.38)$$

Where, R is the mean radius of the Earth, θ is co-latitude and λ is the longitude. ΔC_{nm} and ΔS_{nm} represent the time variable dimensionless stokes coefficients. The spatial scale which is half-wavelength of the Legendre function is roughly (20000/n) km (Swenson et al., 2003). Swenson and Wahr, [2002] showed that, the Stokes coefficients ΔC_{nm} and ΔS_{nm} can be used to estimate water storage anomaly as:

$$\Delta\sigma(\theta,\lambda)=\frac{R\rho_{earh}}{3}\sum_{n=0}^{n_{\max}}\sum_{m=0}^{n}\frac{2n+1}{1+k_n}(\Delta C_{nm}\cos m\lambda+\Delta S_{nm}\sin m\lambda)\overline{P}_{nm}(\cos\theta) \tag{2.39}$$

For a region, water storage anomaly is given as:

$$\Delta\sigma(\theta,\lambda)=\sum_{n=0}^{n_{\max}}\sum_{m=0}^{n}\frac{1}{\Omega_{region}}\frac{R\rho_{earh}}{3}\frac{2n+1}{1+k_n}(\Delta C_{nm}\cos m\lambda+\Delta S_{nm}\sin m\lambda)\overline{P}_{nm}(\cos\theta) \tag{2.40}$$

Where ρ_{earh} is the average density of the Earth, Ω_{region} is the angular area of the region (i.e. area divided by R^2), $N_{\max}=120$ is the largest angular degree in GRACE gravity solution. k_n are the load Love numbers representing the effect of the Earth's response to surface loads. Importantly, the ratio of $\Delta\sigma/\rho_{earth}$ is the ratio which represent the variation in equivalent water thickness often used to interpret the seasonal variations of global land water from GRACE solutions (Avsar et al., 2012).

Avsar and Ustun, [2012] indicated that, level-2 GARCE datasets contains some errors which makes equation 2.40 triggering to misinterpret surface mass variability. The method suitable for reducing the error is the low pass filtering which is a kind of spatial average. That is, smaller weights are given to higher degree coefficients. By putting weight value W_n for degree n, equation 2.40 can be modified as;

$$\Delta\sigma(\theta,\lambda)=\frac{R\rho_{earh}}{3}\sum_{n=0}^{n_{\max}}W_n\sum_{m=0}^{n}\frac{2n+1}{1+k_n}(\Delta C_{nm}\cos m\lambda+\Delta S_{nm}\sin m\lambda)\overline{P}_{nm}(\cos\theta) \tag{2.41}$$

The most used Gaussian filter from Jekel (1981) and Wahr et al. (1998) is given as;

$$W(\psi) = \frac{b}{2\pi} \frac{\exp[-b(1-\cos\psi)]}{1-\exp(-2b)}, \tag{2.42}$$

Where ψ is any angle between 0 and π, and

$$b = \frac{In2}{1-\cos(r_{1/2}/R)} \tag{2.43}$$

R is the radius of the Earth and $r_{1/2}$ is the half width radius of the Gaussian averaging function.

That means when $\psi = r_{1/2}/R$, $w(\psi)$ has decreased to half its value at ψ = 0.

The values in equations 2.42 and 2.43 can be calculated from recursive formula from Jekel [1981] and Wahr et al. [1998] as:

$$W_0 = \frac{1}{2\pi},\ W_1 = \frac{1}{2\pi}\left[\frac{1+e^{-2b}}{1-e^{-2b})} - \frac{1}{b}\right],\ W_{n+1} = -\frac{2n+1}{b}W_n + W_{n-1} \tag{2.44}$$

2.2.5 Changing gravity anomalies to water layer thickness

The spherical harmonic coefficients δC_n^m and δS_n^m describing gravity potential can be related to spherical harmonic coefficients describing the varying water thickness h_n^m. This relation is different for each term of degree n and can be shown as:

$$V_n^m = \frac{GM}{R}\delta C_n^m = \frac{4\pi G(1+k_n)\rho_w R}{2n+1} h_n^m \tag{2.45}$$

Where k_n is the load Love number of degree n accounting for extra potential created when the Earth is distorted elastically under the load of water; ρ_w is the density of water usually 1000 kgm^{-3}. The relationship between free air anomaly and the coefficients of potential can be given from Heiskanen & Moritz, [1967] as:

$$\Delta g_n^m = \frac{GM}{R}\frac{n-1}{R}\delta C_n^m \tag{2.46}$$

Relating to water thickness it can be written as:

$$\Delta g_n^m = 4\pi G\rho_w \frac{n-1}{2n+1} h_n^m \tag{2.47}$$

However, since the ratio $(n-1)/(2n+1)$ tends to 0.5 for large value of n, the approach is estimating average water thickness which is independent of wavelength and is given by:

$$\Delta g = 2\pi G\rho_w h \tag{2.48}$$

In this case the thickness of an equivalent layer of water in mm is given by:

$$\delta h = 23.8\Delta g(mm) \tag{2.49}$$

The equation 2.49 is describing an equivalent water layer thickness and has been used in this thesis in interpreting hydrology of free-air gravity anomaly patterns due to hydrology.

CHAPTER 3: METHODOLOGY

3.1 GRACE data acquisition

The data used in this thesis are level-2 data products version RL05 of the temporal gravity field estimates from four data processing centers; Centre for Space Research (CSR), Geoforschungszentrum (GFZ), Jet Propulsion Laboratory (JPL), and the fourth data being time-variable gravity field (RL02) of Centre National d' Etudes Spatiales (CNES). RL05 time series and release 02 of CNES data are available at the two GRACE archives GFZ/ISDC (Information System and Data Centre) and JPL/PO.DAAC (Physical Oceanography Distributed Active Archive Centre) for the period of February 2004 to present. CSR, GFZ and JPL data can be downloaded from ftp://podaac-ftp.jpl.nasa.gov/allData/grace/L2/ or ftp://podaac-ftp.jpl.nasa.gov/GeodeticsGravity/grace/L2/ portals and GRGS/CNES can be downloaded from http://grgs.obs-mip.fr/grace/variable-models-grace-lageos/grace-solutions-release-02 site in official GRACE format. On contrary to release-04 (RL04), RL05 data products are more consistent among themselves. For example, Chambers and Bonin, [2012] showed that, the variance of residuals with the output of ocean model was 50-60% lower for RL05 data than for RL04 data. Also they found that, the standard error was about 1cm (equivalent water thickness) in low- and mid-latitudes, and 1.5 and 2cm in polar and sub-polar oceans which is comparable to estimated uncertainty for the output from the ocean models.

3.2 GRACE data processing

Data processing was done using Schmidt Fortran program under Linux environment which synthesize global grids of gravity anomalies from spherical harmonic coefficients. This program was used to extract statistical information (mean, standard deviations and root mean squares) by first converting raw (full normalized) data format into semi-Schmidt normalized data that contains degrees n , order m and spherical harmonic coefficients (C_n^m **and** S_n^m**)**. Secondly, the program uses the parameters of Geodetic Reference System 1980 (GRS80) to evaluate the arrays of the free air anomalies and geoid from global model of the gravity potential described by spherical harmonic coefficients given with Schmidt semi-normalization. The program convolves the Stokes coefficients with the Gaussian filter in the space domain providing a smoothed version of free-air gravity anomalies on a regular grid of latitude and longitude. The spherical harmonics are generated by a recursive procedure where

the height above reference ellipsoid is set to zero. Lastly, the program extracts statistical information (mean monthly gravity solutions, standard deviations and root mean squares) in units of mGals from global grids of gravity anomalies using Generic Mapping Tools (GMT) script developed by Wessel & Smith, [1998]. The study area (East Africa) was masked by extracting the latitudes and longitudes along the boundary enclosing the study area. This file was used by GMT to project the area of interest by performing coordinate transformation and map projections. The mask had the value of unity inside and on the polygon and Not-a-Number (NaN) outside the polygon. The four different GRACE data sets used in this study spanning from 2008 to 2012 were truncated to n_max=60 for CSR and GFZ RL05 data products, n_max=50 for 10-day CNES-GRGS solutions RL02 and n_max=60 for RL05 JPL.

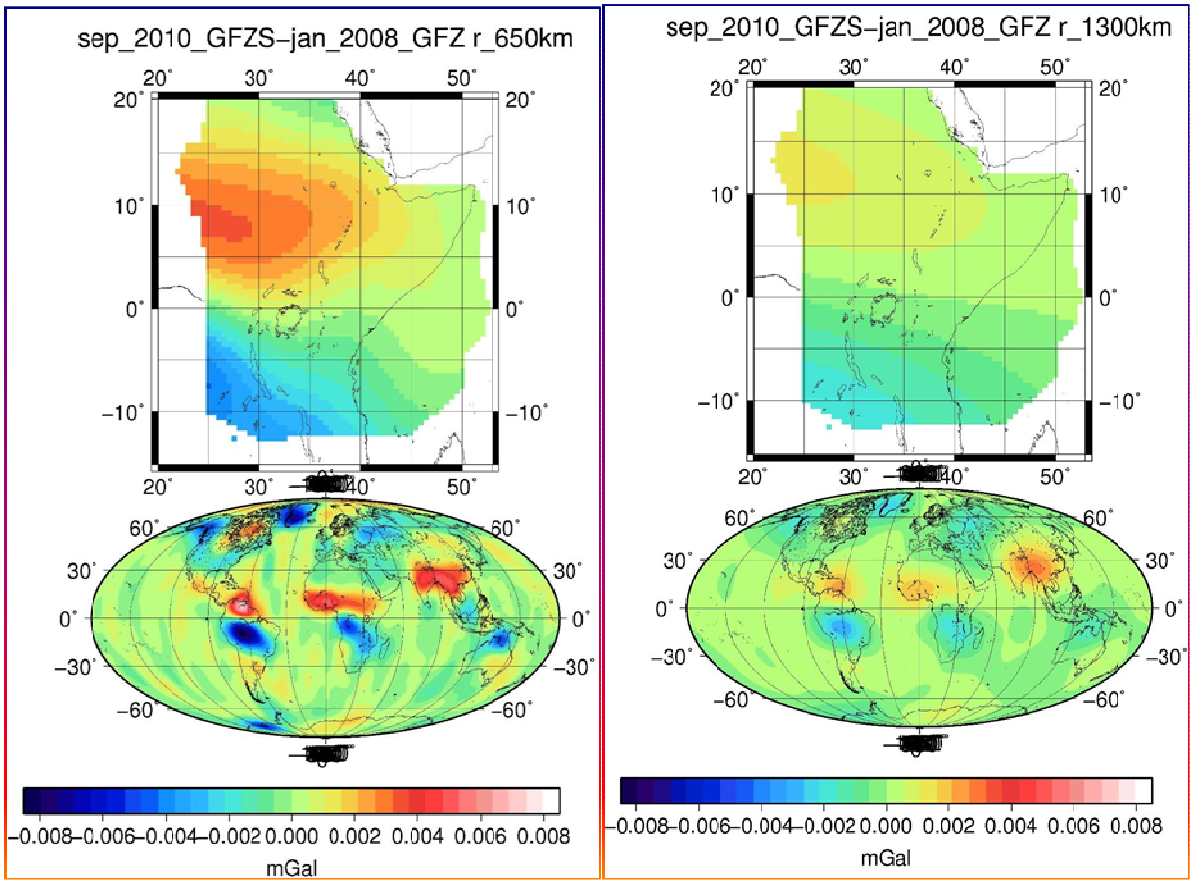

Figure 3.1: Effect of applying Gaussian filter for 650 km half Gaussian radius (left) and 1300 km (right) for GFZ data products for the difference between September 2010 and January 2008.

The GRACE data were processed using Gaussian smoothing filter of 650 km half radius to suppress the ripple errors. This is a better approach rather than truncating the spherical harmonic series at particular degree (Bedada, 2007). However smoothing is not necessary for CNES/GRGS solutions since they are much less affected by the stripping effects because they are much stabilized during their generation process (Avsar et al., 2012). For example Bedada, [2007] stated that, an effect of large degree is suppressed for large value of half radius. Gaussian smoothing is explained more on section 2.2.4.

3.3 GPS data acquisition

The GPS data used in this thesis involved 5 permanent IGS stations which are ADIS (Addis Ababa, Ethiopia), MAL2 (Malindi Kenya), MBAR (Mbarara Uganda), RCMN (Nairobi Kenya), and NURK (Kigali Rwanda), in addition to six stabilization IGS site which are NKLG (Libreville Gabon), BAN2 (Bangalore), MAS1 (Maspalomas), SEY1 (Republic of Seyc), WTZR (Wettzell in German), and RAMO (Mitzpe_Ramon) for a period of 5 years from June 2008 to March 2012. All the GPS data were downloaded from ftp://garner.ucsd.edu site.

3.4 GPS data processing

Data processing was done using GAMIT (version 10.4) software and GLOBK (version 5.2) to generate daily estimates of network station coordinates and velocities for the 5 IGS stations operating in East Africa. The software was developed at Massachusetts Institute of Technology (**MIT),** the Harvard-Smithsonian Center for Astrophysics (**CfA**), and the Scripps Institution of Oceanography (**SIO**) to estimate station coordinates and velocities, stochastic or functional representations of post-seismic deformation, atmospheric delays, satellite orbits, and Earth orientation parameters (Herring et al., 2010). The IGS stations were tied to the global International Terrestrial Reference Frame ITRF2008. To improve the repeatability of baseline lengths and significant changes in the terrestrial reference frame (Boehm et al., 2004), the Vienna mapping functions (VMF1) were used in data processing. The VMF1 functions were used to model the tropospheric effect which is one of the major sources of errors in the analysis of Global Positioning System and Very Long Baseline Interferometry (VBLI) observations (Boehm et al., 2005). Boehm et al. [2005] showed that, VMF improves the precision of geodetic results and reveals seasonal signals in the station height time series more clearly. VMF1 were also used to adjust atmospheric gradients (estimated twice per day for N-S and E-W directions) and zenith tropospheric delays (ZTDs) (Nahmani et al., 2012).

The elevation cut-off angle was set to 15 degrees. This is the maximum value recommended whereby, the minimum is 10 degrees. Setting at least 10 degrees elevation angle, helps to eliminate the noisiest data, and therefore improves the baseline statistics, while setting above 15 degrees may eliminate usable data (Henning, 2011; Yahya and Kamarudin, 2008). The model FES2004 was used during data processing for correcting ocean tide loading effects. During data processing, non-tidal atmospheric pressure loading was used since it affects the vertical component of GPS stations at 1 to 2 mm level [Nahmani et al, 2012; Tregoning and Watson , 2009; Dach et al., 2011]. Second and third order ionospheric corrections which affect the station positions at sub-mm level near the equator with a quasi-annual oscillation in north component of less than 1 mm (Nahmani et al., 2012) were also used. GPS position time series from GPS station position residuals were averaged to 30 days epochs to comply with GRACE solutions which were also averaged to 30 days solutions for comparisons.

3.5 Quality of GPS solution

The quality of obtained GPS positions and velocities is based on standard deviations, the weighted root mean squares (wrms) and repeatability of estimated coordinates (Saria, 2007). Assessing the quality of GPS positions and velocities was necessary due to dominant errors in GPS observations which have correlation times ranging from a few minutes (multipath, water vapor) to days or months (station motions) due to monument instability and atmospheric, hydrological, and ocean loading together with non-gravitational forces on the satellites (Herring et al., 2010). Past studies show that, on studying long-term GPS coordinate time series, the white noise over few days' period increases steadily over long periods. The weighted root mean square was obtained by combining the binary h-files on generation of GPS time series and velocity solutions from GAMIT processes. By generating time series for multiyear analysis, statistics of the data can be evaluated and determined if there is any outlier that can distort the velocity solutions. To get the statistics, a Linux "grep" command was used to get position status that gives the summery of status on wrms and nrms which are used to assess the quality of the obtained positions and velocities. For better results, the wrms in horizontal components should be 1 to 2 mm and 3 to 10 mm in vertical component. Additionally, the histograms of nrms and wrms should approximate the Gaussian curve with median nrms ~1. After averaging the coordinates using GLOBK, the obtained position estimates and velocities are accompanied with standard deviations. For results on repeatability, standard deviations, wrms and nrms, see next chapter. The equation used to

measure precision of station coordinates by measuring the position scatter from the mean is given by equation 3.1 while the standard deviation and correlation equations are given by equation 3.2 and equation 3.3 respectively.

$$wrms = \sqrt{\frac{N}{N-1}\frac{\sum_{i=1}^{N}\frac{(y_i - \bar{y})i}{\sigma_i^2}}{\sum_{i=1}^{N}\sigma_i^2}} \tag{3.1}$$

$$Stdev = \sqrt{\frac{1}{N-1}\sum_{i}^{N}(y_i - \bar{y})^2} \tag{3.2}$$

Where:

- $wrms$ is the weighted root mean square;
- $Stdev$ is the standard deviation;
- $Correl$ is the correlation;
- N is the number of occupation days;
- y_i are the estimated coordinates of the station;
- $\sum_{i}^{N}\sigma_i^2$ is the error of the coordinates for day i;
- $\bar{y}$ is the weighted mean of the coordinates of the station.

The correlation ($Correl$) between two sets of data given by the following equation:

$$Correl = \frac{\sum_{i}^{N} (y_i - \overline{y})(x_i - \overline{x})}{\sqrt{\sum_{i}^{N} (y_i - \overline{y})^2 \sum_{i}^{N} (x_i - \overline{x})^2}} \quad (3.3)$$

Where:

- N is the number of days;
- x_i are the estimated data of first dataset;
- y_i are the estimated data of second dataset;
- $\overline{x}$ is the weighted mean of the estimated data of the first dataset;
- $\overline{y}$ is the weighted mean of the estimated data of the second dataset.

CHAPTER 4: RESULTS AND ANALYSIS

4.1 Overview

This chapter looks at the results obtained from both GRACE monthly solutions from the four data processing institutes, GPS coordinate estimates and velocity solutions. The chapter will also show GRACE monthly solution time series to indicate the hydrological signal pattern, GPS time series, and finally combining the two time series to see their correlation on a different time scale.

4.2 GRACE hydrological mass estimates

In this section, the monthly average estimates of the changes in equivalent water thickness over the whole East African region will be looked at. The hydrological mass estimates were processed using the four processing groups which are CSR, GFZ, JPL and CNES and equation 2.49 was used to estimate the corresponding height changes (hydrological mass estimates) from GRACE monthly gravity solutions. With 650km Gaussian smoothing, the signal pattern for all groups looks almost similar for the mean monthly water thickness. The computed mean standard deviation between the four estimates which indicates the mismatch between the four products is 2.88 cm. The mean signal amplitude of equivalent water thickness ranges from ~5 mm to ~7 mm maximum and from ~10 mm to 17 mm minimum. The signal pattern shows little decrease in mass storage from August 2008 to March 2009 by 8 mm of equivalent water thickness which later increased to 4.5 mm in April 2009. From April 2009, the mass storage decreased by 11.5 mm and reached 10 mm in October 2009 which later increased again to 7.3 mm maximum peak in May 2010. The great mass loss occurred between November 2010 and October 2011 which reached to a maximum loss of ~17 mm in July 2011. The mass storage then increased to 4.2 mm peak in November 2011 but decreased from there to ~10 mm in March 2012. This signal pattern shows that, the maximum mass storage which is 7.3 mm occurred in May 2010 while the greatest mass loss which is 17 mm occurred in July 2011.

Table 4. 1: Mean of equivalent water thickness, mean standard deviations, and the mean of RMS of the four GRACE processing groups averaged over five years from 2008 to 2012.

GRACE data processing institutes	**CSR**	**GFZ**	**JPL**	**CNES**	**MEAN**
Mean equivalent water thickness (mm)	**1.0**	**-0.1**	**0.9**	**-1.13**	**-2.4**
Standard deviation (cm)	**2.84**	**2.76**	**2.80**	**3.10**	**2.88**
RMS (cm)	**2.89**	**2.85**	**2.87**	**3.38**	**3.00**

Although the variations are small in standard error and root mean square, they may have been caused by processing errors during transforming GRACE data from level-1 to level-2 products or may have been caused by GRACE instrumental errors (Bedada, 2007). However, the mismatch between the three data groups CSR, GFZ and JPL is very small (0.2 mm) compared to the mismatch between the three groups and CNES which is 3 mm for standard deviation and 5 mm for RMS which makes the four data to be almost equal in accuracy.

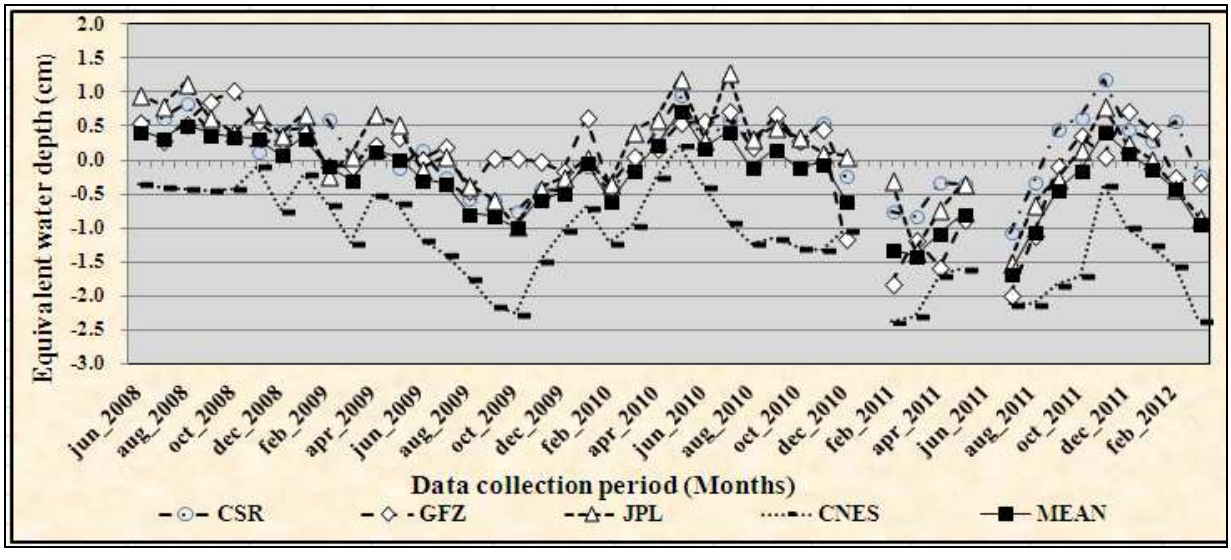

Figure 4.1: The pattern of the mean monthly equivalent water thickness of GRACE gravity solutions for the four data processing institutes smoothed with 650 km half radius Gaussian filter.

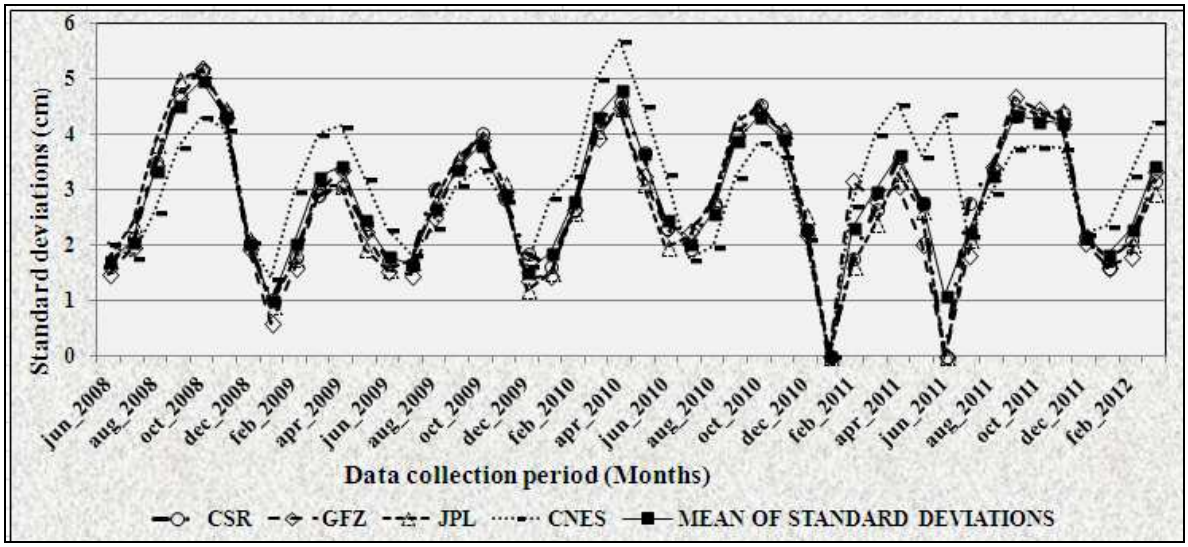

Figure 4.2: The signal pattern of the standard deviations with their mean for the four GRACE data processing institutes smoothed with 650 km half radius Gaussian filter.

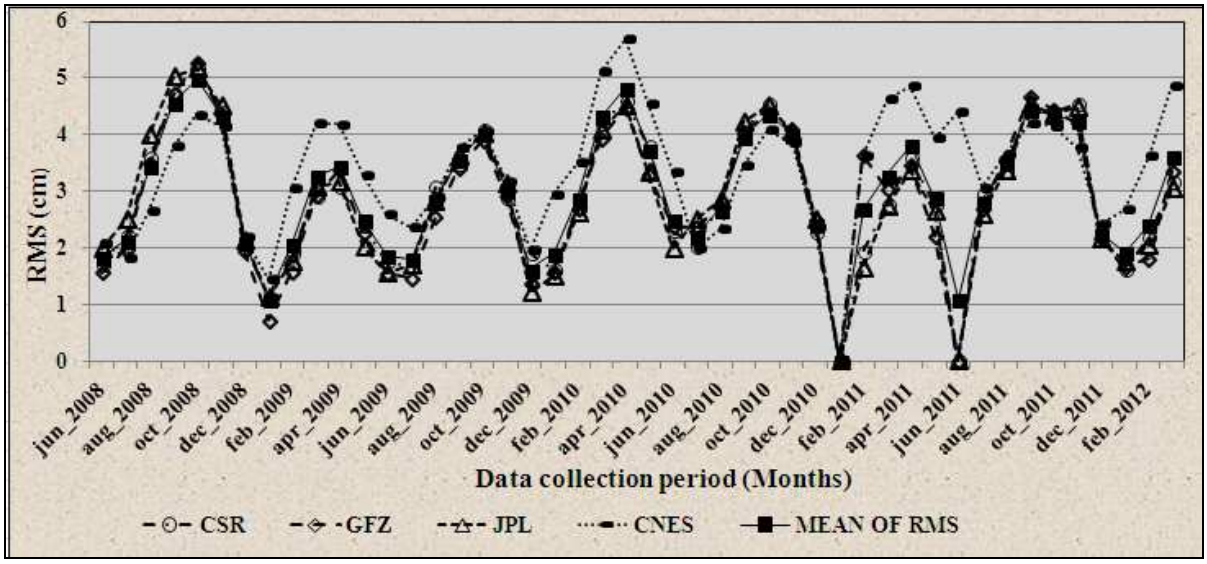

Figure 4.3: The signal pattern of the root mean squares (RMS) with their mean for the four GRACE data processing institutes smoothed with 650 km half radius Gaussian filter.

More results are the maps which show the pattern of equivalent water thickness (in mGals) for the four groups of data (Figure 4.4). 1μGal corresponds to ~23.8 mm of equivalent water thickness (see equation 2.49) and one milligal (or mGal) is equivalent to 0.00001 m/s^2 which can be compared to the total gravity on the Earth's surface of approximately 9.8 m/s^2.

Figure 4.4 shows that, the gravity anomaly maps of the four GRACE data processing institutes have similar patterns for January 2010. The datum chosen to find the change in gravity anomalies was arbitrary (Bedada, 2007) and all the data were subtracted from this. The chosen date also was arbitrary but it is the average dry month for the whole East African region. However, the patterns shown are sensitive to the choice of datum month (Bedada, 2007) which gives time changes of gravity within GRACE data to be identified.

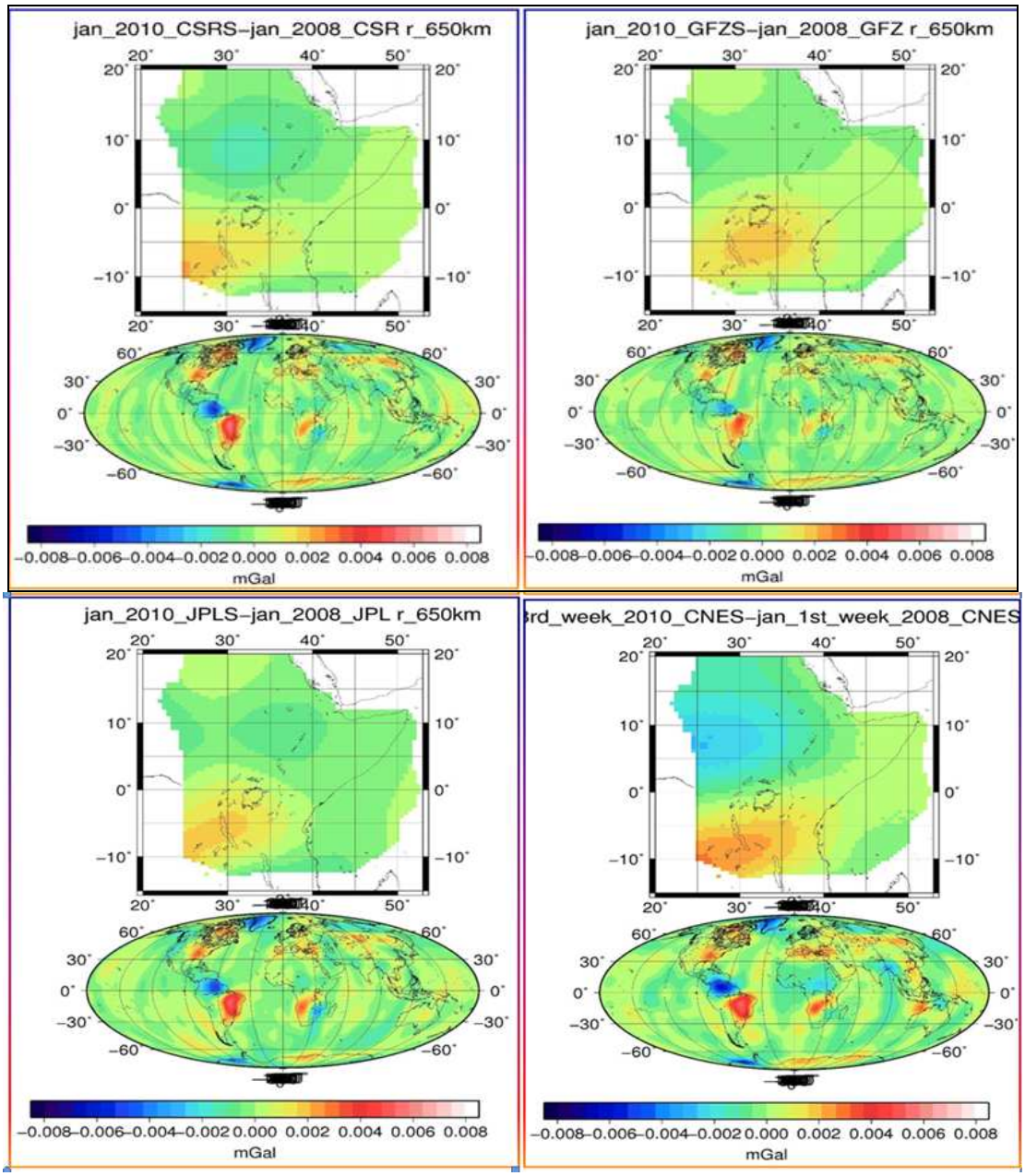

Figure 4.4: Water induced anomaly maps for January 2010 from CSR (top left), GFZ (top right), JPL (bottom left), and CNES (bottom right) gravity models with 650 km Gaussian smoothing radius.

4.3 GRACE results with hydrological data of previous studies

Figure 4.5 to Figure 4.8 show the comparison between patterns shown by the four GRACE data and the rainfall pattern shown by Bedada, [2007] for August, September, and October. Although the years of study are different for GRACE and rainfall data, but the seasonal patterns between the two studies look almost similar for the three months which seems to be the rainfall seasons for most of East African countries. GRACE has been interpreted as change in terrestrial water storage mass and the later as observed hydrological data of monthly rainfall. However, much of monthly change in water storage shown by GRACE results reflects seasonal storage of water in soil moisture, ground water recharge, and surface water in lakes and reservoirs while only very small portion of the rainfall water becomes stored in the rivers (Bonsor et al., 2010). Bonsor et al., [2010] showed that, large amount of rainfall which reaches ground surface in the Nile Basin is lost through evapotranspiration. This comparison was taken between smoothed rainfall and the four smoothed GRACE data using half radius of 650 km of Gaussian filter. It should be noted however that, the level-2 GRACE data used in this thesis is corrected to indicate monthly change in terrestrial water storage in East African region (excluding atmospheric water). This is different from previous GRACE release (RL04) which indicated monthly change in total water mass including atmosphere (Bonsor et al., 2010). The comparison also shows that, much of the rainfall is stored within terrestrial water bodies which are important since along with other geophysical processes, continental or regional water storage causes crustal deformation which results in variations of station positions (Rajner et al., 2011).

The comparison in Figure 4.5 to Figure 4.8 shows that, the pattern of rainfall seems to be maximum in August indicating large amount of water storage but seems to decrease in September and October indicating that there is less water stored in September and the least in October.

Figure 4.5 to Figure 4.8 show that, the rainfall was high in August when there was more concentration of terrestrial water stored in the ground. The rainfall pattern seems to decrease in September and October indicating decrease in terrestrial water mass especially over Ethiopian highlands. The trend shown by the four GRACE data products indicates westward movement of main storage water flux accompanied by local evaporation and movement of moist air into Chad and Central Republic (Bedada, 2007).

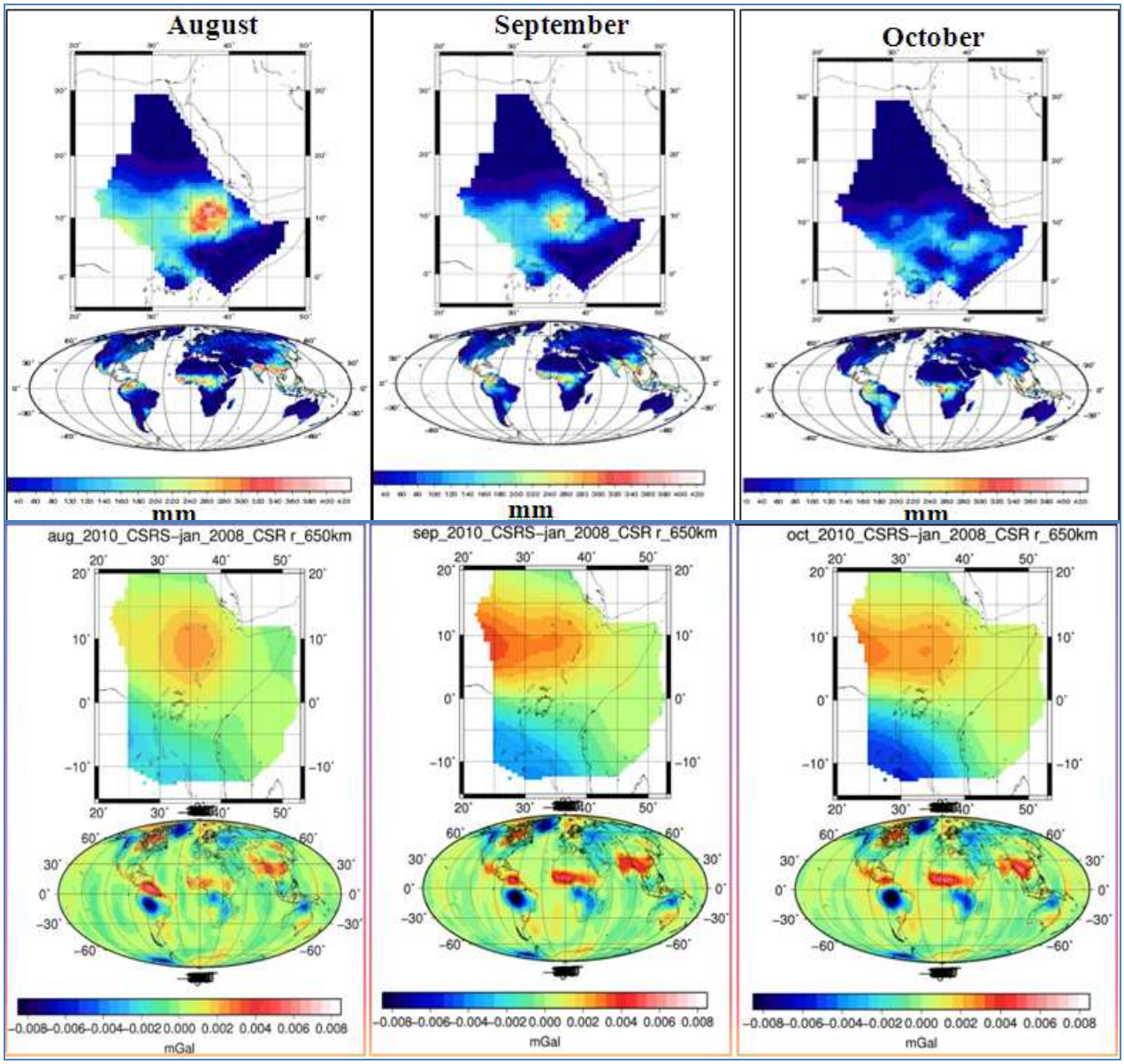

Figure 4.5: Comparison of (climatological) rainfall maps (top) (Bedada, 2007) with CSR gravity anomaly maps for August, September and October 2010.

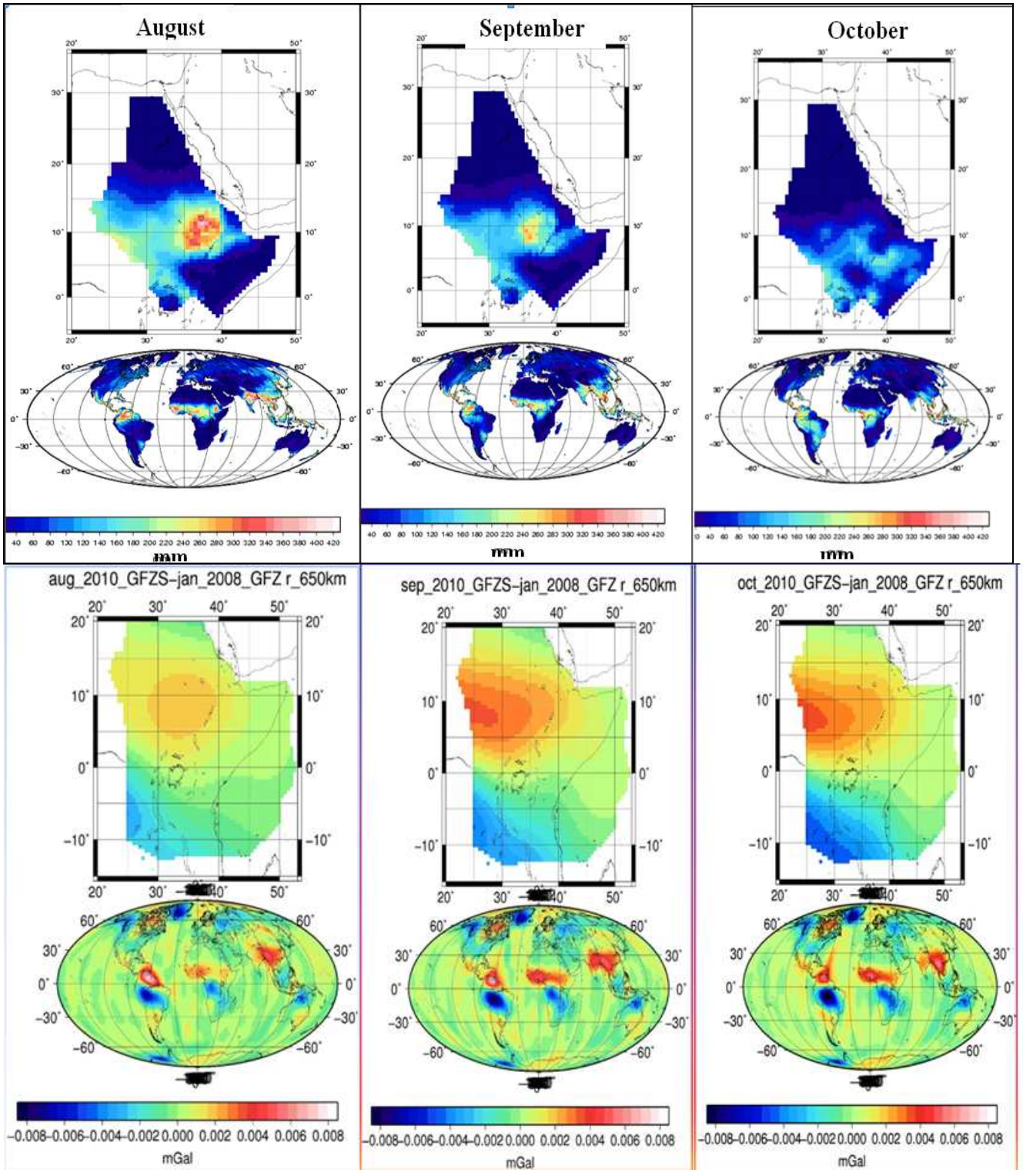

Figure 4.6: Comparing (climatological) rainfall pattern (top) (Bedada, 2007) with GFZ gravity anomaly maps for August, September and October 2010.

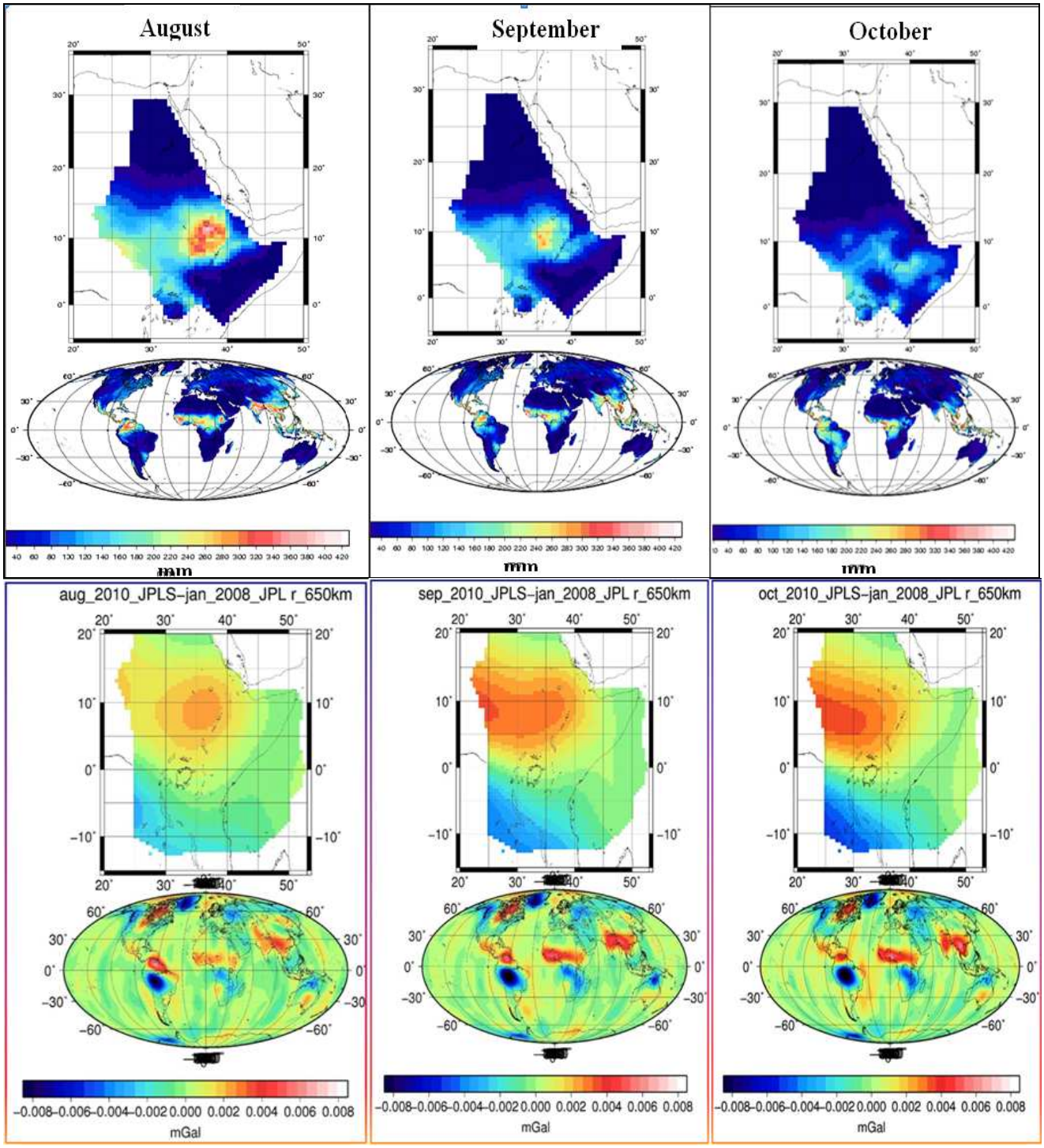

Figure 4.7: Comparing (climatological) rainfall pattern (top) (Bedada, 2007) with JPL gravity anomaly maps for August, September and October 2010.

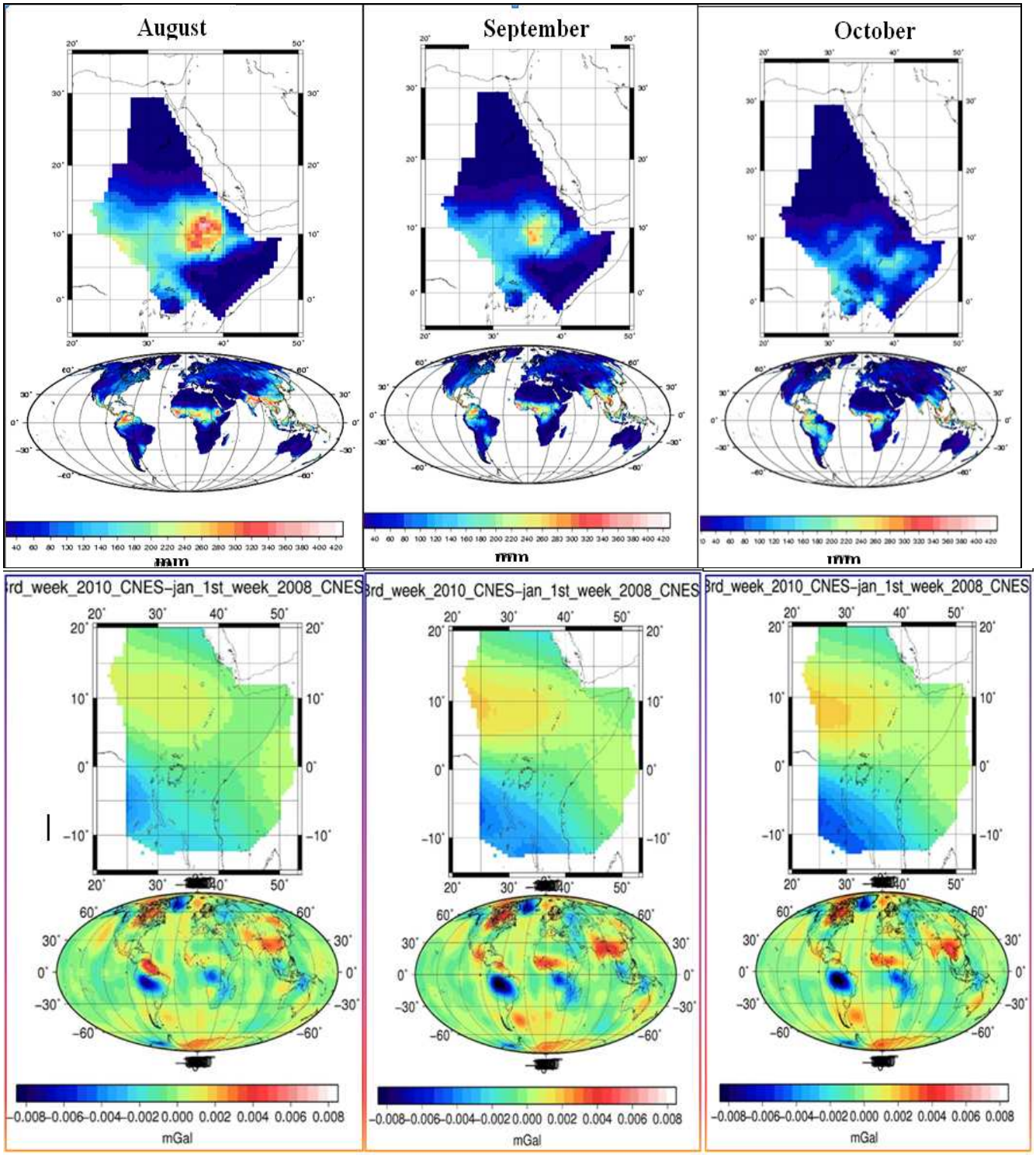

Figure 4.8: Comparing (climatological) rainfall pattern (top) (Bedada, 2007) with CNES gravity anomaly maps for August, September and October 2010.

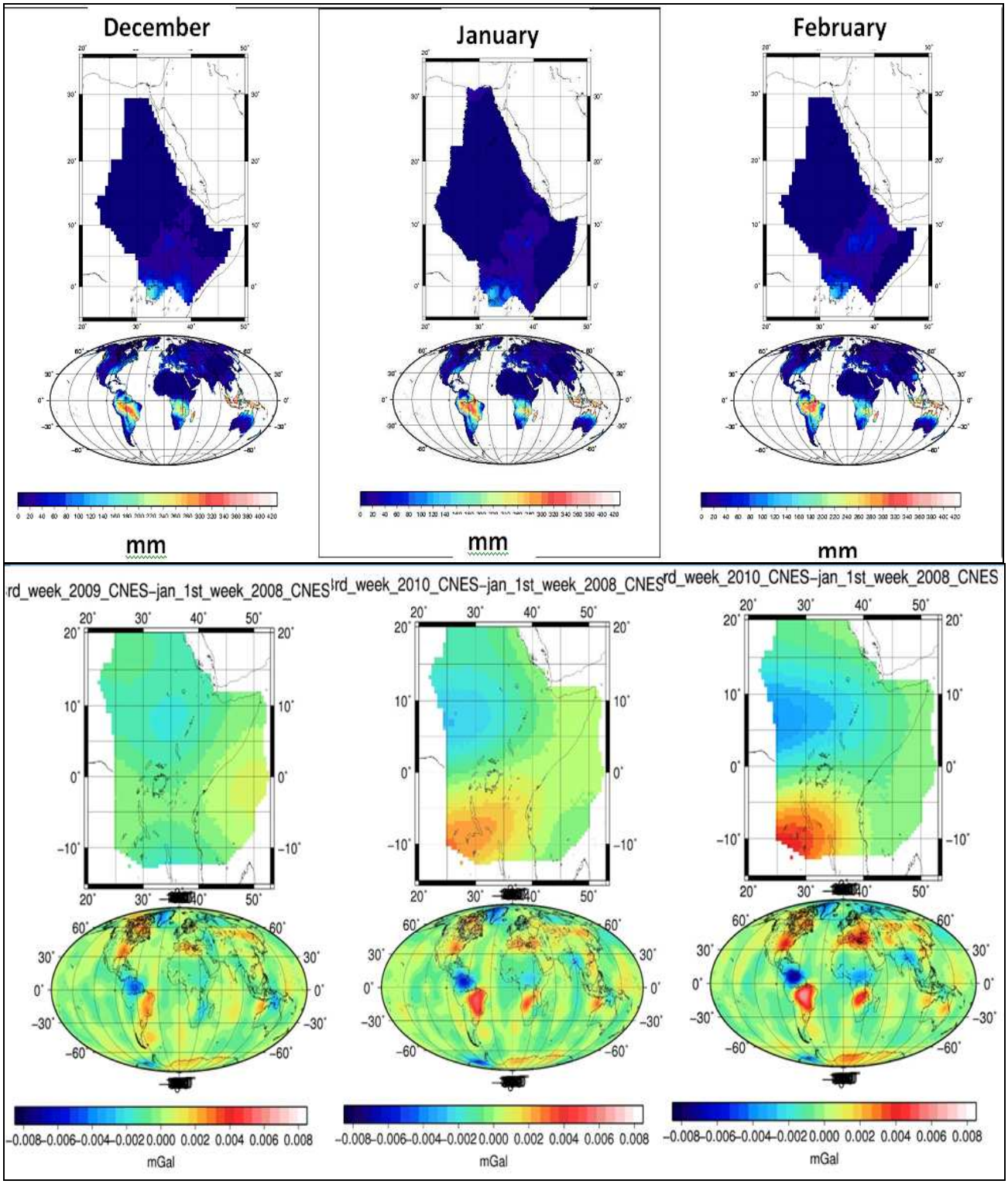

Figure 4.9: Comparison of precipitation map results (Bedada, 2007) and accumulated water storage mass (this study) using CNES GRACE data for December 2009, January 2010 and February 2010.

Figure 4.9 shows the comparison between precipitation maps (Bedada, 2007) and CNES maps (this study) for December, January and February in which, rainfall seems to have stopped in December. The mass seems to drain away in January to February creating a flux to the Southern part of Tanzania through Lake Victoria which is the same trend when compared with precipitation maps from Bedada, [2007] and water storage anomaly maps in this study.

4.4 GPS results and analysis

The daily GPS position estimates were averaged to 30 days solution to comply with GRACE mass solutions after being transformed to ITRF 2008 using coordinates of 12 sites. Five sites in the study area were used in the analysis, which are ADIS, MAL2, MBAR, RCMN, and NURK. The quality of obtained GPS results were based on formal standard deviations of obtained coordinates and repeatability of the estimated coordinates. The horizontal velocity accuracy results ranged from 0.1 to 0.27 mm/year and 0.7 to 0.79 mm/year for vertical velocities. The monthly position repeatability computed as weighted root mean square (WRMS) of daily station position residuals were found to be between 1 mm and 3 mm in horizontal component and 4 mm to 6.7 mm in vertical component (Figure 4.10). Table 4.2 shows the results in position, accuracy, repeatability and correlation in northing, easting and up coordinates while Figure 4.11 (b) illustrates the repeatability in the form of histogram.

Table 4. 2: Obtained positions, accuracy and repeatability

SITE	**Positions (Deg)**		**Position Accuracy (mm)**			**Repeatability (wrms)(mm)**			**Correlation**		
Name	**Lat**	**Lon**	**σN**	**σE**	**σU**	**N**	**E**	**U**	**NE**	**NU**	**EU**
MAL2	**-2.9961**	**40.1941**	**0.39**	**1.01**	**0.51**	**1.1**	**1.6**	**6.0**	**0.961**	**0.186**	**0.086**
ADIS	**9.0351**	**38.7663**	**0.22**	**0.45**	**0.44**	**2.2**	**1.9**	**6.5**	**-0.87**	**-0.01**	**-0.05**
RCMN	**-1.2208**	**36.8935**	**0.09**	**0.80**	**0.46**	**1.0**	**1.7**	**4.5**	**-0.26**	**0.23**	**0.02**
MBAR	**-0.6015**	**30.7379**	**0.78**	**0.73**	**0.54**	**1.4**	**2.8**	**5.9**	**-0.97**	**0.15**	**-0.09**
NURK	**-1.9446**	**30.0897**	**0.86**	**0.88**	**0.54**	**1.2**	**1.7**	**6.7**	**-0.98**	**0.17**	**-0.11**

Table 4.3 shows the obtained ITRF 2008 positions, velocities, and their accuracies while Table 4.4 displays the final ITRF2008 positions with their accuracies. The accuracy in velocities is shown in Figure 4.11 (c) and it is illustrated as sigma in northing, sigma in easting, and sigma in up for each station. Figure 4.11 (a) illustrate the precision in station position estimates which range from 0 to 1 mm for both horizontal and vertical components.

Table 4. 3: Obtained ITRF 2008 positions, velocities and velocity accuracies.

Site	Lat(Deg)	Long (Deg)	Vel N (mm/yr)	Vel E (mm/yr)	Vel U (mm/yr)	σVN (mm/yr)	σVE (mm/yr)	σVU (mm/yr)
MAL2	-2.9961	40.1941	14.42	24.52	2.37	0.19	0.27	0.72
ADIS	9.0351	38.7663	17.54	23.42	1.02	0.2	0.26	0.72
RCMN	-1.2208	36.8935	14.7	25.03	-3.03	0.18	0.24	0.72
MBAR	-0.6015	30.7379	16.59	22.34	-1.52	0.18	0.22	0.79
NURK	-1.9446	30.0897	15.74	21.78	-9.9	0.19	0.22	0.77

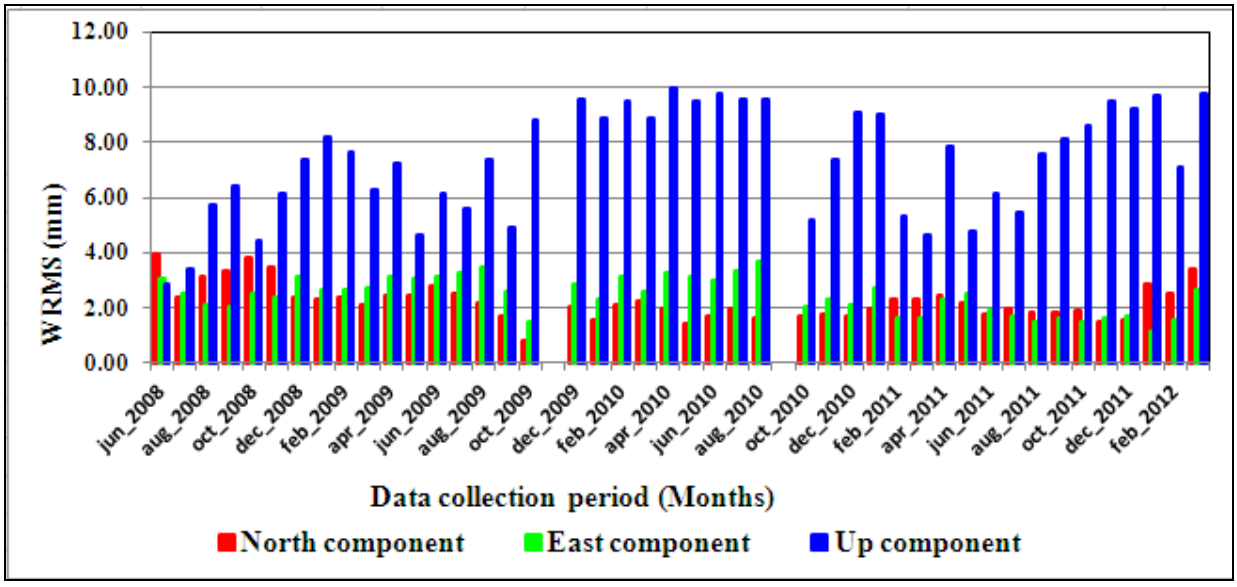

Figure 4. 10: The weighted root mean square (WRMS) for GPS components.

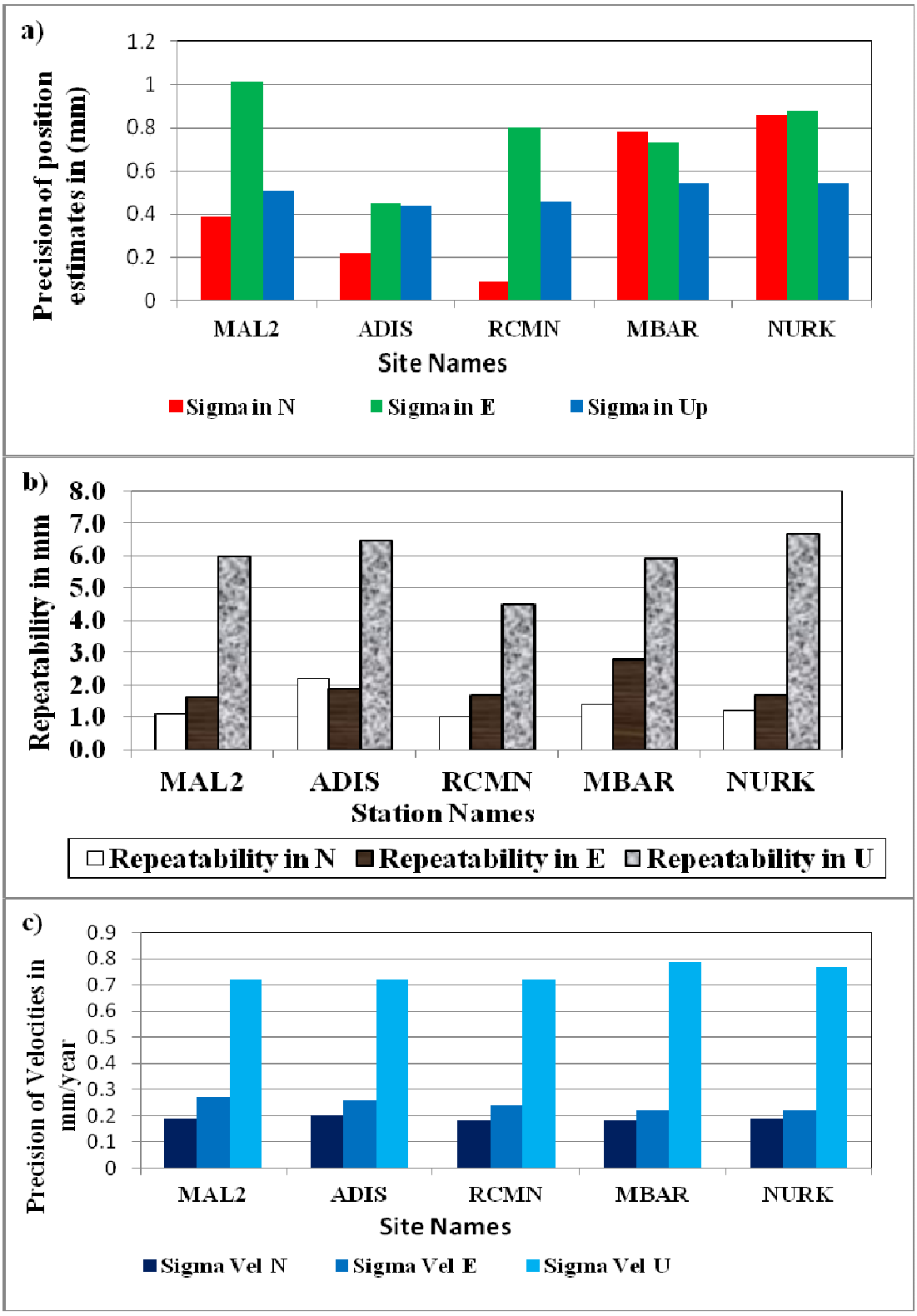

Figure 4. 11: Precision of position estimates (a), repeatability histogram (b), and precision of velocities (c).

Table 4.4: The obtained final ITRF2008 positions with their accuracies.

SITE NAME	X (m)	Y (m)	Z (m)	σX (m)	σY (m)	σZ (m)
MAL2	4865385.5829	4110717.3020	-331137.5311	0.0007	0.0009	0.0004
ADIS	4913652.7352	3945922.6844	995383.3514	0.0004	0.0005	0.0002
RCMN	5101056.7025	3829074.3161	-135016.2377	0.0006	0.0007	0.0001
MBAR	5482951.1800	3260442.7174	-66519.7153	0.0006	0.0007	0.0008
NURK	5516756.5632	3196624.8616	-215027.2071	0.0007	0.0008	0.0009
NKLG	6287385.7176	1071574.6890	39133.0864	0.0008	0.0005	0.0032
BAN2	1344087.3269	6068610.2902	1429292.1808	0.0009	0.0016	0.0044
MAS1	5439192.1907	1522055.3097	2953455.0353	0.0018	0.0022	0.0049
SEY1	3602870.4280	5238174.5553	-516275.3402	0.0016	0.0022	0.0022
WTZR	4075580.4258	931853.9808	4801568.2319	0.0029	0.0037	0.0019
RAMO	4514721.6990	3133507.9757	3228024.8433	0.0019	0.0023	0.0004
	Lat (°)	**Lon (°)**	**H (m)**	**σ Lat(°)**	**σLon (°)**	**σH (°)**
MAL2	-2.9961	40.1941	-20.9244	3.5000	9.1000	0.0005
ADIS	9.0351	38.7663	2439.1411	2.0000	4.1000	0.0004
RCMN	-1.2208	36.8935	1591.9763	0.8000	7.2000	0.0005
MBAR	-0.6015	30.7379	1337.5116	7.0000	6.6000	0.0005
NURK	-1.9446	30.0897	1483.8134	7.7000	7.9000	0.0005
NKLG	0.3539	9.6721	31.4828	28.8000	5.0000	0.0007
BAN2	13.0343	77.5116	831.8731	39.9000	8.2000	0.0016
MAS1	27.7637	344.3667	197.1715	47.7000	17.2000	0.0010
SEY1	-4.6737	55.4794	537.1893	20.2000	11.1000	0.0024
WTZR	49.1442	12.8789	666.0462	24.0000	58.0000	0.0011
RAMO	30.5976	34.7631	886.8554	3.2000	30.1000	0.0008
	N (m)	**E (m)**	**U (m)**	**σ N(m)**	**σE (m)**	**σU (m)**
MAL2	-333519.2563	4468272.8208	-20.9244	0.0004	0.0010	0.0005
ADIS	1005786.7286	4261897.8235	2439.1411	0.0002	0.0005	0.0004
RCMN	-135902.1089	4106031.6695	1591.9763	0.0001	0.0008	0.0005
MBAR	-66955.0948	3421536.1442	1337.5116	0.0008	0.0007	0.0005
NURK	-216466.4131	3347637.5797	1483.8134	0.0009	0.0009	0.0005
NKLG	39396.8734	1076675.5172	31.4828	0.0032	0.0006	0.0007
BAN2	1450973.949	8406231.809	831.87311	0.00444	0.00089	0.00158
MAS1	3090645.744	33921878.6	197.17152	0.00531	0.0017	0.00103
SEY1	-520275.9509	6155412.513	537.18934	0.00225	0.00123	0.00242
WTZR	5470707.274	937828.8666	666.04624	0.00267	0.00423	0.00107
RAMO	3406110.006	3330960.698	886.85536	0.00035	0.00288	0.00082

The velocity map depicting the motion of the five IGS stations within the study area is shown in Figure 4.12. The velocity map was generated using the Generic Mapping tools (GMT) software package which was developed by Smith and Wessel, (1990) to create high-quality postscript maps in different projections. The map shows the rate at which, the IGS stations are moving both horizontally and vertically.

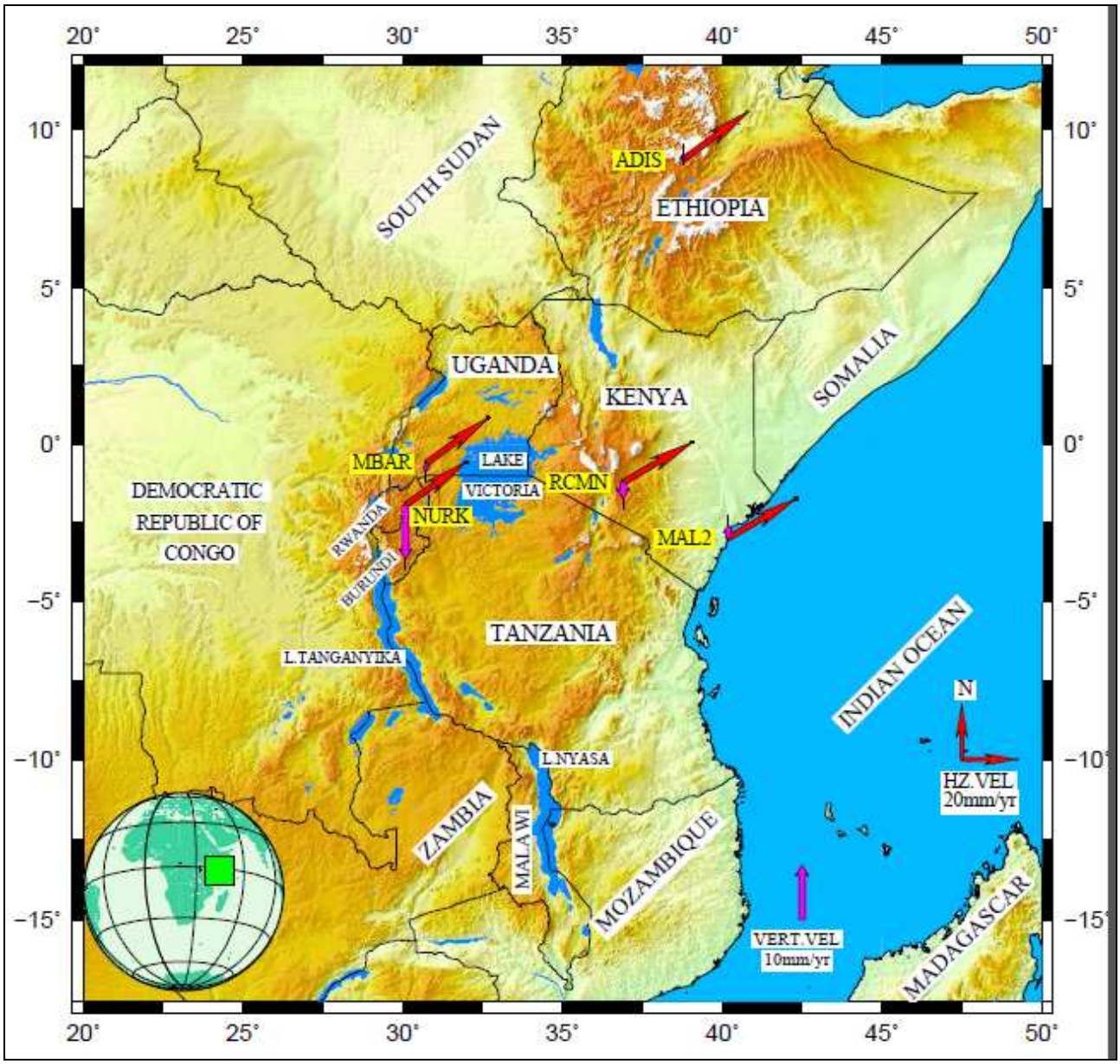

Figure 4.12: Velocity map showing continuous IGS stations' for horizontal velocities (red) and vertical velocities (magenta). The downward magenta arrows represent downward velocities while the upward magenta arrows represent upward velocities.

Figure 4.12 shows that, all stations move approximately North-East in horizontal motion. ADIS shows very small upward vertical displacement of 1.02 mm/year along the ellipsoidal normal in time while MBAR shows vertical downward displacement at also a very small rate of 1.52 mm/year. MAL2 and RCMN show very little upward and downward displacements of 2.37 mm/year and 3.03 mm/year respectively. NURK shows a greater downward displacement of 9.9 mm/year along the ellipsoidal normal compared to other IGS stations. The time series for the five IGS sites are of shown in Appendix I.

4.5 Combined GRACE and GPS results

The 3-D deformations from GRACE at every GPS station caused by surface density anomaly can be computed using load love numbers which can be deduced from Preliminary Reference Earth Model (PREM). The love numbers account for the Earth's sphericity and radial heterogeneity (Nahmani et al., 2012). To be consistent with GPS estimates, the potential love numbers are included in GRACE estimates before processing (Nahmani et al., 2012) while the station velocities for GRACE observations are realized in International Terrestrial Frame (ITRF2008). Additionally, ocean tidal loading is corrected using FES2004 model. The hydrological mass estimates from GRACE monthly spherical coefficients which were computed using equation 2.49 were compared with the three component displacements (north, east and up) obtained from GPS time series and plotted to see their consistence and correlation. The two GRACE and GPS signals showed high level of correlation when GRACE and the three GPS (North, East and up) components were plotted and correlated. Note however that, although neither rainfall nor precipitation data were used in this study, but both show high level of agreement with monthly water storage change indicated by GRACE data in other studies. Nahmani et al, [2012] who used hydrological loading model estimated from Global Land Data Assimilation System (GLDAS) merged with precipitation data from Tropical Rainfall Measuring Mission (TRMM) found good agreement with GRACE estimates both in terms of spatial distribution and seasonal variations which showed high level of agreement with GPS estimates. Bonsor et al, [2010] who compared the change in terrestrial water storage mass from GRACE with observed monthly rainfall over Nile delta found that, much of the monthly change in water storage indicated by GRACE data reflected the seasonal storage of water in the soil moisture, ground water recharge, and surface lakes and reservoirs.

Further results show that, the weighted root mean squares (WRMS) range from 0 to 4 mm for GPS horizontal components and 2 mm to 10 mm for vertical component while the normalized root mean squares (RMS) range from 0 to ~4 mm for both horizontal and vertical components. The GPS WRMS obtained are close to the range of values stated by Herring et al, [2010] which are 1-2 mm for horizontal components and 3-10 mm for vertical component while Saria, [2007] reported the range of 0.25 mm to 5.0 mm for normalized root mean square (RMS) for a good solution. On the other hand, the average RMS for GRACE was 30.0 mm for 650 km Gaussian smoothing radius while the root mean square difference (RMS) between GRACE and GPS was 2.85 cm.

.

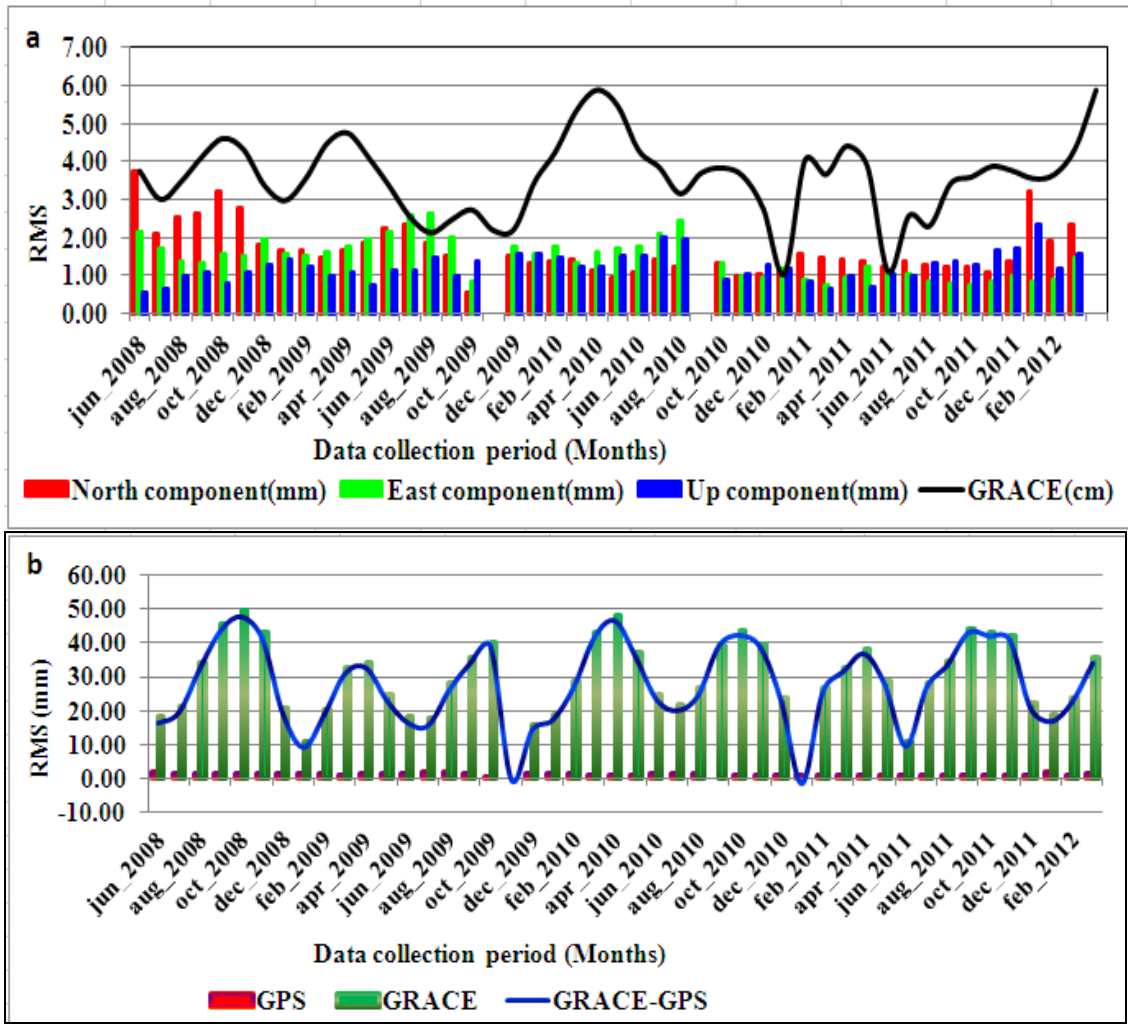

Figure 4.13: The root mean squares (RMS) for GPS and GRACE (black) (a) and the root mean square difference (blue) between GRACE (green) and GPS (red) signals (b).

The errors in RMS in GRACE are nearly longitude-independent and are smaller near the poles (8 mm) than at low latitudes (25 to 27 mm) due to presumably denser ground track coverage near the poles (Wahr et al., 2006). The RMS value of 30mm obtained in this research conforms with the range stated by Wahr et al, [2006] who showed that, the variation of errors in GRACE from one month to another to depend on the size of the region and they decreased as smoothing radius increased falling from 38 mm to 15 mm at 500 km and 1000 km Gaussian smoothing radius respectively.

The comparison of the obtained GPS deformations and GRACE load love estimates was done on monthly basis by superimposing the two signals as shown on Figure 4.15, Figure 4.16, and Figure 4.17 for five years. The two GRACE and GPS signals were then correlated on yearly basis between GRACE and GPS north component, GRACE and GPS east component, and GRACE and GPS up component and the average in correlations for each component was calculated as shown on Table 4.4 and Figure 4.14. The percentages of correlation results on yearly basis show that, positive correlations are 29%, 32% and 56% for GRACE and north component, GRACE and east, and GRACE and up component respectively. The negative correlations are 50%, 56% and 28% while zero correlations are 8%, 0%, and 4% for GRACE and north component, GRACE and east, and GRACE and up component respectively. Furthermore, the averaged correlation percentages show that, positive correlations are 20%, 20%, and 80% while negative correlations are 40%, 40%, and 0 for GRACE and north component, GRACE and east, and GRACE and up component respectively. The zero correlations are 40% for GRACE and horizontal components and 20% for GRACE and up component. There was 13% of GPS data missing for correlating with GRACE signal.

ADIS and MBAR stations showed strong negative correlation with GRACE signal in north components while RCMN and MAL2 showed strong negative correlations in east components compared with other IGS stations. This indicates strong anti-correlation or phase difference between the two signals. The correlation analysis for north component in 2008 indicate that, only MAL2 station showed strong positive correlation of 0.8 compared to MBAR station which showed 0 correlation, and RCMN and ADIS which showed negative correlations of 0.1 and 0.6 respectively. The correlation between GRACE and east component in 2008 shows that, MBAR and RCMN stations showed strong positive correlations of 0.6 and 0.7 respectively while ADIS and MAL2 had negative correlations of 0.1 (weak) and 0.5 respectively. North component correlation in 2008 however shows that,

MBAR and ADIS stations showed strong positive correlations of 0.5 and 0.6 respectively while RCMN and MAL2 had zero and -0.3 correlations.

In 2009, only RCMN, ADIS, and MAL2 showed strong positive correlations of 0.8, 0.6, and 0.8 for north, east and up components respectively. NURK and RCMN showed also positive but weak correlations of 0.2 and 0.3 for east and up components respectively. Other stations like ADIS and MBAR showed strong negative for north component, RCMN and MAL2 for east component, and NURK and ADIS for up component. NURK station showed weak negative correlation (0.1) for north component and MBAR for east and up components.

NURK showed 0.5 (north component) while MBAR showed correlations of 0.7 and 0.6 for east and up components respectively in 2010. Other correlations were weak except MBAR and RCMN which showed strong negative correlations for north, east and up components of 0.8, 0.5 and 0.5 respectively.

The correlations in 2011 were very weak between 0.1 and 0.2 for north component except for ADIS station which showed strong negative correlation of 0.9. For the east component, only NURK and ADIS stations showed positive correlations of 0.5 and 0.1 (weak) respectively while the rest of the stations were negatively correlated with GRACE signal. All the stations were positively correlated for up component in which, both MBAR and MAL2 stations had a strong correlation of 0.6.

The correlation in 2012 was faced by missing GPS data for some stations whereby, only three GPS stations were correlated with GRACE signal. RCMN, MAL2 and ADIS stations showed strong negative correlations for both north and east components ranging from 0.7 to 1.0. The three stations showed strong positive correlations of 1.0 (RCMN and ADIS) and 0.6 (MAL2) for up component. The correlation on average basis shows that, many stations showed zero and negative correlations for north and east components except NURK which is the only station with positive correlation of 0.2 and 0.3 for north and east components respectively. All stations were positively correlated with GRACE signal for up component ranging from 0.1 to 0.3 indicating weak correlation between the two signals. Negative correlation in this analysis indicates anti-correlation or phase difference between the two signals (Tregoning et al., 2009).

Table 4.5: Correlation coefficients between GRACE and GPS.

(a)	**GRACE and GPS North component**				
Period(Years)	**NURK**	**MBAR**	**RCMN**	**MAL2**	**ADIS**
2008	NA	0.0	-0.1	0.8	-0.6
2009	-0.1	-0.6	0.8	0.0	-0.5
2010	0.5	-0.8	0.3	0.1	0.0
2011	0.1	-0.2	0.1	-0.2	-0.9
2012	NA	NA	-1.0	-0.9	-0.7
Average	**0.2**	**-0.3**	**-0.1**	**-0.1**	**-0.5**
(b)	**GRACE and GPS East component**				
Period(Years)	**NURK**	**MBAR**	**RCMN**	**MAL2**	**ADIS**
2008	NA	0.6	0.7	-0.5	-0.1
2009	0.2	-0.1	-0.5	-0.7	0.6
2010	0.3	0.7	-0.5	-0.2	-0.3
2011	0.5	-0.1	-0.5	-0.4	0.1
2012	NA	NA	-1.0	-0.8	-0.1
Average	**0.3**	**0.0**	**-0.3**	**-0.5**	**0.0**
(c)	**GRACE and GPS up component**				
Period(Years)	**NURK**	**MBAR**	**RCMN**	**MAL2**	**ADIS**
2008	NA	0.5	0.0	-0.3	0.6
2009	-0.5	-0.1	0.3	0.8	-0.8
2010	-0.1	0.6	-0.5	-0.2	0.3
2011	0.6	0.3	0.1	0.6	0.2
2012	NA	NA	1.0	0.6	1.0
Average	**0.3**	**0.2**	**0.1**	**0.3**	**0.0**

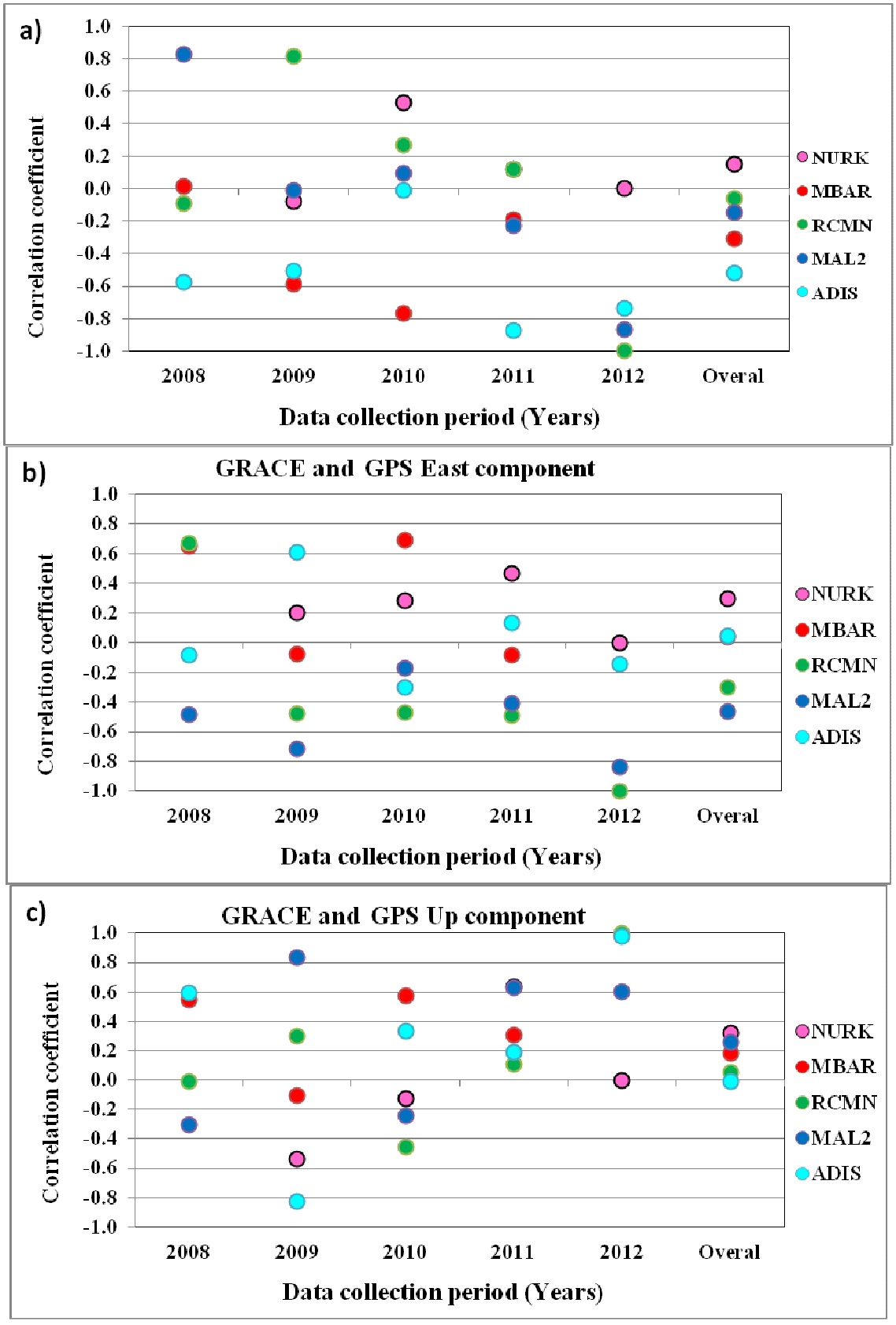

Figure 4.14: The temporal patterns of correlation for each year between GRACE and GPS.

The studied correlations on yearly basis show convincing results compared to the correlations on average basis since they show good agreement with the phase of the anomaly signals between GRACE and individual IGS stations (Figure 4.15, Figure 4.16 and Figure 4.17). GPS up component shows good agreement with large amplitudes of 5 mm to 9 mm peak to peak compared to north and east components which show good agreement but with smaller amplitudes of 1 mm to 4 mm peak to peak.

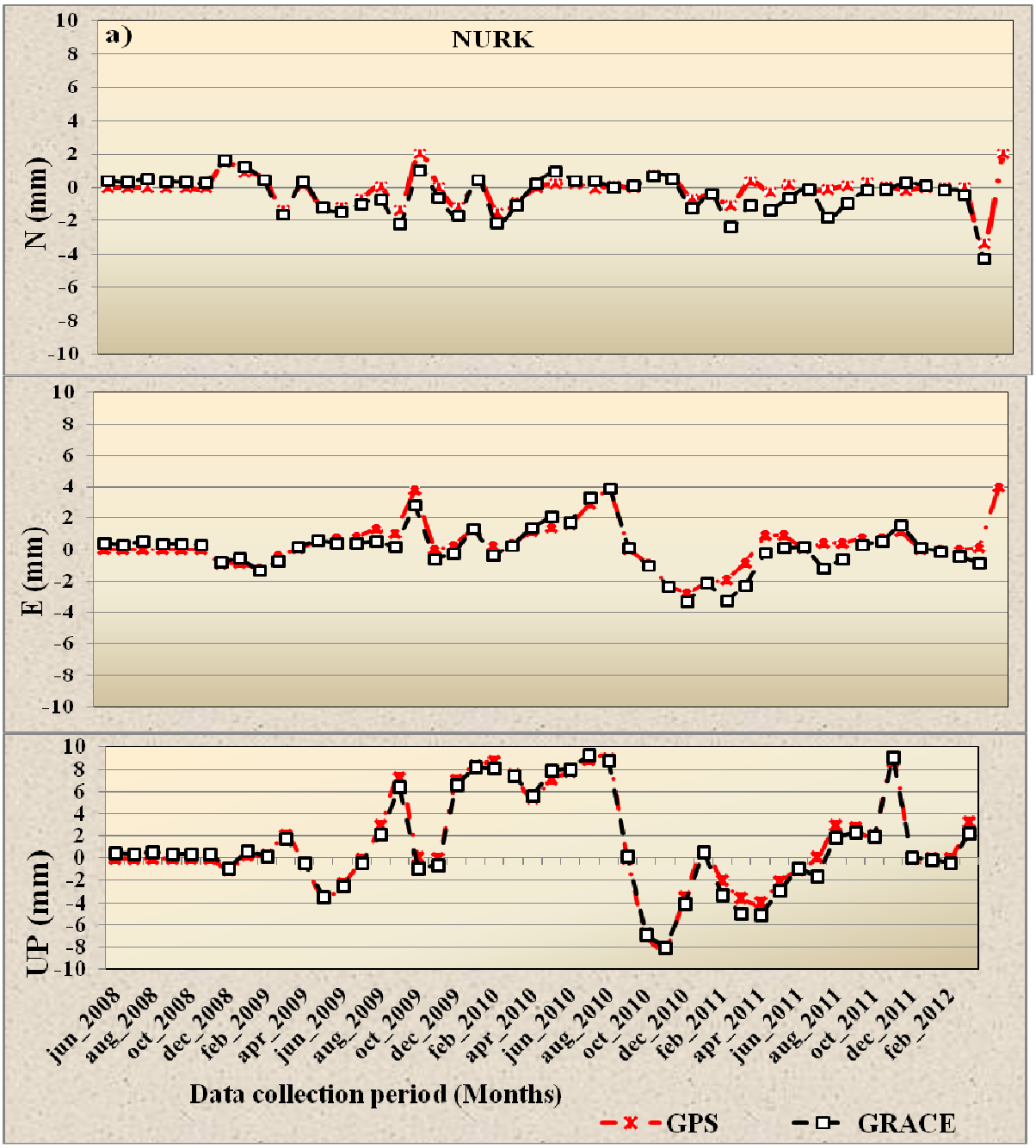

Figure 4.15: Time series for NURK (red) superimposed with GRACE signal (black).

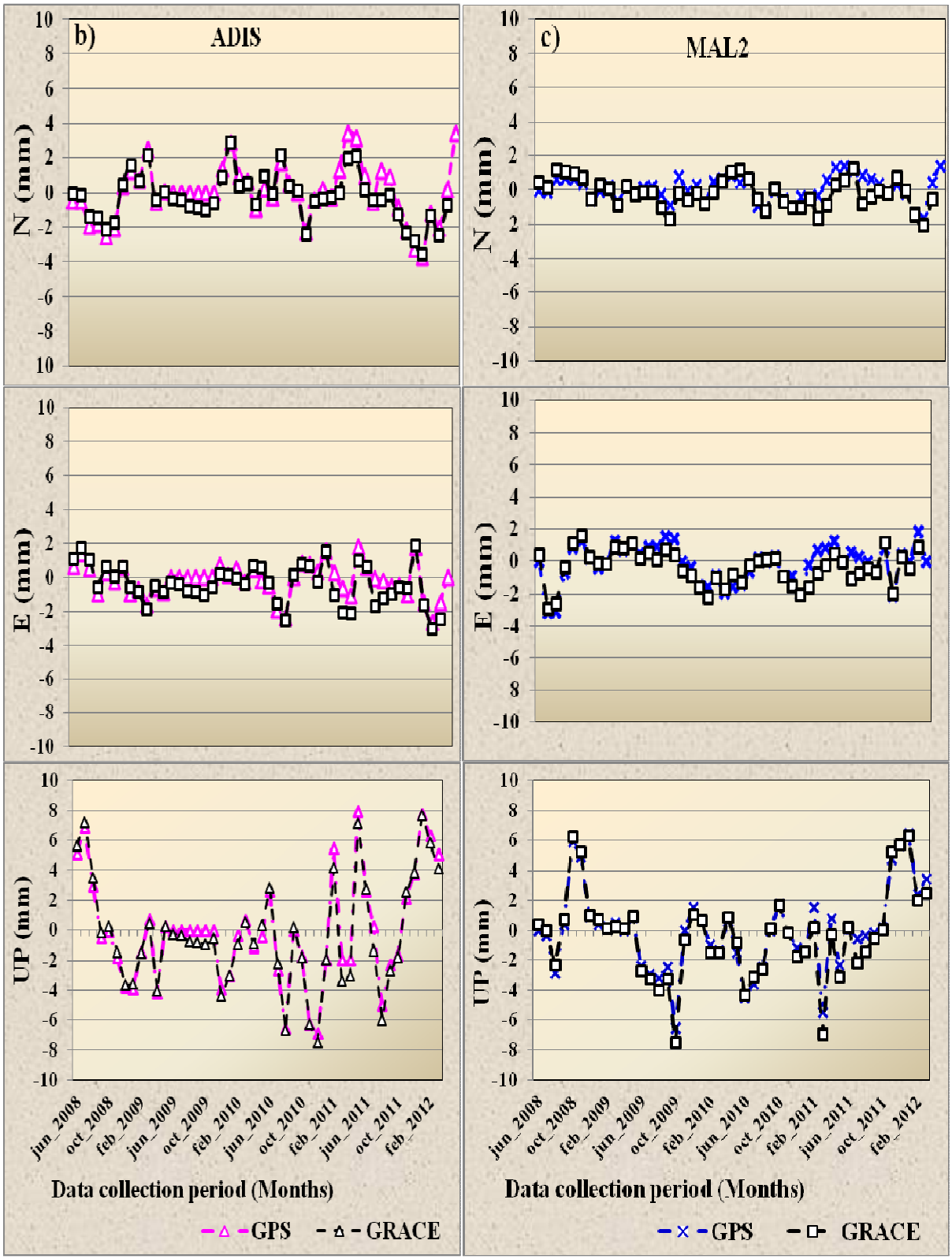

Figure 4.16: Time series for ADIS (a) (pink) and MAL2 (b) (blue) superimposed with GRACE signal (black).

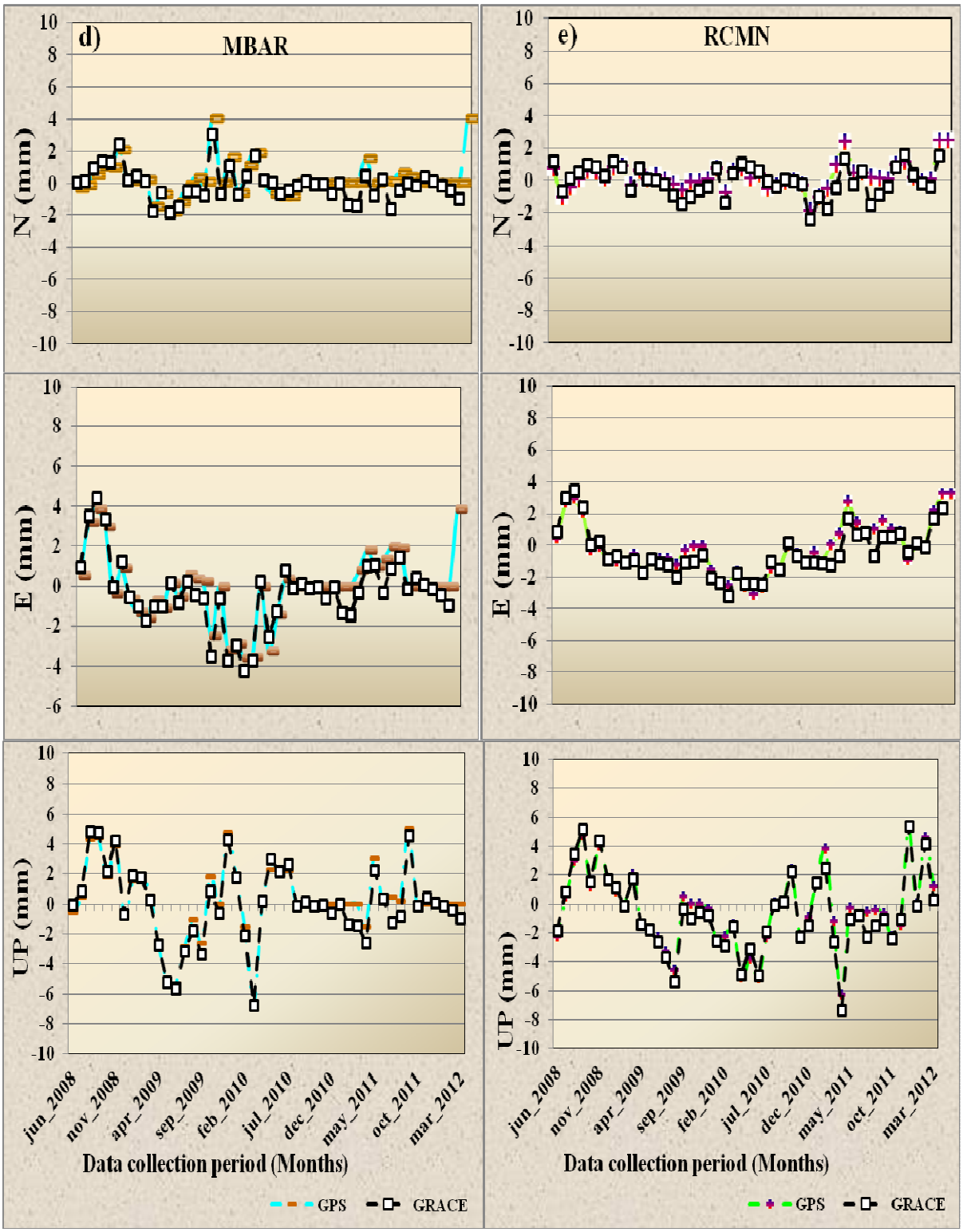

Figure 4.17: Time series for MBAR (d) (brown) and RCMN (e) (green) superimposed with GRACE signal (black).

The displacement time series for north, east and up GPS components for the five IGS sites superimposed with GRACE water anomaly estimates (hydrological water loading signal) for period of five years from June 2008 to Mach 2012 (Figure 4.15 to Figure 4.17) indicates that, all the IGS stations move with horizontal velocities approximately towards North-East (N-E) direction as shown on the velocity map in Figure 4.12.

ADIS station which moves horizontally to north-east direction (Figure 4.12) with upward vertical velocity of 1.02 mm/year has a maximum displacement of < 4 mm from April to May and from August to December 2011 for the North component. The rest of the months for north and east component show little displacements of < 2 mm. However, the trend for vertical component is different since it shows maximum uplifts in July 2008 (~7 mm), June 2010 (~3 mm), February 2011 (5.5 mm), May 2011 (~8 mm), and January 2012 (~8 mm). The trend for GRACE mass storage in this period indicates that, there was increase in mass in August 2008 (5 mm), May 2010 (~7 mm), and November 2011 (~5 mm). Again the station shows maximum subsidence in January, April and December 2009 (~4 mm), August 2010 (6.6 mm), December 2010 (~7 mm), March and April 2011 (~2 mm), and August 2011 (~5 mm) while GARCE signal in this case was 3.4 mm in January, 1.5 mm in April, -4.8 in and December 2009 indicating mass loss for the three months. Other months show low amplitude of -1 mm in August 2010, -5.9 mm in December 2010, -14.1 mm in March 2011, ~ -17 mm in April 2011, and -10.5 mm in August 2011 all indicating hydrological mass loss.

MAL2 station in Malindi Kenya which shows upward vertical velocity of 2.37 mm/year has very little displacements for north and east components (up to 2 mm peak to peak) and 6 to 8 mm peak to peak for up component. It shows maximum uplift of 6 mm in October 2008 when GRACE signal was 3.5 mm, and ~5 mm to 6.5 mm from November 2011 to January 2012 when GRACE signal was maximum (4.2 mm) indicating increase in hydrological mass. On the other hand it shows subsidence of ~3 mm in August 2008 when GRACE signal had 5.2 mm of mass storage, 6.5 mm in October 2009 when GRACE signal was low (-10 mm), 4.5 mm in June 2010 when mass storage was very little (1.8 mm), and 5.48 mm in March 2011 when there was great mass loss of -14.1 mm.

MBAR station at Mbarara Uganda which shows downward displacement of 1.52 mm/year has different trend since it shows 2 mm to 4 mm displacements for north and east components. It also shows uplifts in vertical component of ~4 to 5 mm in August 2008,

September 2008, December 2009, and August 2011 when GRACE signal was 5.2 mm, 3.8 mm, -4.8 mm, and -10.5 mm for the respective months and years. Other months like October 2008, January 2009, May 2010, and May 2011 have very little uplifts of ~2 mm peak to peak.

The months showing maximum subsidence in MBAR station include May and June 2009 (~5.5 mm) and March 2010 (~7 mm) corresponding to ~0 to -3 mm of GRACE signal.

RCMN which has shown a downward velocity of 3.03 mm/year has very little displacements (< 4 mm) for horizontal components. its vertical component shows maximum uplifts of ~5 mm in September 2008 and February 2012, and ~4 mm in November 2008 corresponding to mass storage of 3.8 mm, -4.2 mm (mass loss), and 3.3 mm for the respective months. On the other hand it shows maximum subsidence of ~5 mm and 6.28 mm in August 2009 and April 2011 respectively corresponding to -7.8 mm and -16.9 mm of mass loss in GRACE signal for the respective months and years.

NURK station which shows the greater downward velocity 9.9 mm/year compared to other IGS stations shows little displacements of < 2mm peak to peak for north component and < 4mm peak to peak for east component. The vertical component shows significant uplifts of 7.2 mm in September 2009, ~7 mm to 9 mm from December 2009 to August 2010, and 8.7 mm in November 2011 corresponding to -8.2 mm, -4.8 mm to 7.3 mm maximum, and 4.2 mm of hydrological mass from GRACE signal for the respective months and years. On the other hand it shows subsidence of ~4 mm in May 2009, ~7 and 8 mm in October and November 2010 respectively, and ~4 mm in April 2011 corresponding to 0.3 mm, -1 mm, -0.5 mm, and -16.9 mm of hydrological mass loss from GRACE signal for the respective months and years. The horizontal and vertical displacements are summarized in Table 4.5.

Generally the results show that, the horizontal components show clearly the seasonal variations though with smaller amplitudes of ~2 mm and ~4 mm for North and East components respectively as estimated by GRACE and GPS while vertical component shows 6 mm to 10 mm peak to peak. The obtained results are also comparable to Khan et al, [2011] who studied hydro-climatology of Lake Victoria using hydrologic model. The results showed that, the peak rainfall occurred in April-May similar to great mass storage in April-May 2010 (this study) and July-November similar to great mass storage in July-November 2008 and November 2011 (this study) which is common to parts of immediate equatorial zone especially in East Africa. Similarly, high discharge of Nzoia River which drains water

into Lake Victoria and Nile river basins occurred in May-September indicating high rainfall which is the same incidence when MBAR and NURK stations showed uplifts when there was an increase in mass storage in 2008, 2010 and 2011 as detected by GRACE.

Bedada, [2007] showed that, there was peak precipitation and maximum mass storage from GRACE in August centered on Ethiopian highlands when there was maximum rainfall. The same results were obtained in this study when ADIS station showed uplift in June-August (Figure 4.16(b) when there was an increase in mass storage from GRACE in 2008, 2010 and 2011. Similar results were obtained by Khan et al, [2011] who showed that there was agreement between monthly model runoff estimates and gauge observations for Nzoia River when runoff values responded to precipitation events which occurred across the catchment from March to early June during wet season.

Table 4.6: Summery of horizontal and vertical displacements.

STATION NAME	Upward Displacement (mm)	Subsidence (mm)	Horizontal Displacements (mm)
ADIS	~7mm July 2008 ~3mm June 2010 5.5mm February 2011 ~8mm May 2011 ~8mm Jan 2012	~4mm Jan, April & December 2009 6.6mm August 2010 ~7mm December 2010 ~2mm March & April 2011 ~5mm August 2011	< 4 mm
MAL2	6mm October 2008 ~5-6.5mm Nov 2011 to January 2012	~3mm August 2008 6.5mm October 2009 4.5 mm June 2010 5.48mm March 2011	< 2 mm
MBAR	~4 to 5mm in August & September 2008, December 2009 & August 2011. ~2mm in October 2008, January 2009, May 2010, May 2011.	~5.5mm in May & June 2009 ~7mm in March 2010.	2 to 4mm
RCMN	~5mm in September 2008 & February 2012. ~4mm in November 2008	~5mm in August 2009 6.28mm in April 2011	< 4mm
NURK	7.2mm in September 2009 ~7-9mm in Dec-Aug 2010 8.7mm in November 2011	~4mm in May 2009 ~7mm in October 2010 ~8mm in November 2010 ~4mm in April 2011	<2mm N <4mm E

CHAPTER 5: DISCUSSION, CONCLUSION AND RECOMMENDATIONS

5.1 Discussion

Studying the three dimensional movement of GPS (IGS) stations in East African region due to hydrological water loading using GRACE and GPS data is the aim of this study. The analysis was done by combining GRACE gravity estimates from the four different data processing institutes and the GPS residual estimates for five years starting from June 2008 to March 2012. GRACE gravity estimates have been used to estimate the annual and seasonal variations of hydrological mass (water content) for the whole of East Africa. On the other hand, GPS residual coordinate estimates have been used to estimate the three dimensional displacement variations for the five IGS stations along with velocity estimates to see their movements. The signal pattern shown by the four independent GRACE gravity estimates had a mean standard deviation of 2.88 cm with 650 km Gaussian smoothing half radius.

When GPS coordinate anomalies and GRACE estimates were compared, there was high level of agreement especially when the two signals were correlated. The correlation of the two signals on yearly basis yielded convincing results compared to averaged correlations (see Table 4.4 and Figure 4.10). Taking correlations on yearly basis seems to be necessary when comparing small spatial and temporal scale (GPS) with large spatial and temporal scale (GRACE in this case). However lack of correlation between the two signals for some years in some sites may have been caused by errors in GPS analysis, missing data in GRACE estimates (especially in January and June 2011) and the GPS data or local geophysical processes or site specific analysis errors dominated in GPS deformation estimates (Tregoning et al., 2009).

The results showed the reduction in RMS difference between GRACE and GPS to 2.85 cm and 3.0 cm RMS for GRACE only. The obtained mean annual and seasonal GRACE signal amplitude of ~5 to 7 mm maximum peak and ~10 to 17 mm minimum coincided well with most of GPS stations' displacements. For example MAL2 showed a maximum correlation of 0.8 for north and up components in 2008 and 2009 when it showed maximum uplift of 6 mm in October 2008 and maximum subsidence of 6.5 mm in October 2009. The same incident happened to GRACE signal which showed increase in hydrological mass storage of ~3.5 mm in October 2008 and hydrological mass loss of about 10 mm in October 2009. Other stations

which showed uplifts and subsidence in vertical component corresponding to increase and decrease in hydrological mass and which also showed positive correlation with GRACE signal are ADIS except 2009, MBAR station in 2010, RCMN in 2009, 2011 and 2012, and NURK in 2011. Positive correlation for vertical component is evident since about 56% of IGS stations were positively correlated with GRACE signal on yearly basis and 80% on average basis.

The vertical displacements or velocities of most IGS sites shown on the velocity map may have also been influenced by increase and decrease in GRACE hydrological mass due to positive correlation shown by most of the sites for the vertical component indicating high level of agreement between GPS and GRACE signals. However, this cannot be guaranteed since there was no time series for both horizontal and vertical velocities which could be superimposed and correlated with GRACE signal.

The increase and decrease in hydrological mass from GRACE is evident when compared with previous studies for example Nahmani et al, [2012] who showed consistence between GRACE and hydrological model and precipitation data in West Africa; (Bedada, 2007) who showed consistence between GRACE and rainfall pattern, and GRACE and precipitation data; Bonsor et al, [2010] who compared the change in terrestrial water storage mass from GRACE with observed monthly rainfall over Nile delta and found that, GRACE reflected seasonal storage of soil moisture, ground water and surface lakes and reservoirs. Similar study by Khan et al, [2011] over Nzoia River was consistence with GRACE results in this study due to the fact that high discharge and lowest discharge which occurred during high rainfall in May-September and low rainfall in December-February respectively was highly consistent with great mass storage and less mass storage from GRACE respectively accompanied with uplifts and subsidence of a nearby IGS station (MAL2). Bedada, [2007] showed similar consistence with GRACE results in this study where, the peak precipitation and maximum mass storage with high rainfall in August on Ethiopian highlands, coincided with uplift of ADIS station.

5.2 Conclusion

High level of agreement between GRACE and GPS signals together with high level of correlation when the two signals were combined suggest that, water loading effect is one of the major causes of IGS station movements in East African region. The effect of hydrological water loading has been well detected by GRACE as it has shown large amplitudes ranging from 5 mm to 7 mm peak to peak for hydrological mass increase and 10 to 17 mm minimum for hydrological mass loss. When compared with GRACE signal, the GPS vertical component has shown great correlation with large amplitudes of up to 10 mm peak to peak compared to horizontal position which showed small amplitudes up to 4 mm maximum. However, horizontal movement of GPS sites needs differential technique to be resolved better (Rajner and Liwosz, 2011). Good analysis on horizontal and vertical motion of IGS sites is shown by horizontal and vertical velocities which may have been also influenced by many other geophysical processes taking place within and on the earth's surface. But water loading effect remains to be the most essential factor for most of these geophysical processes such as earth or crustal deformation, glacial rebound, and tectonic movements which may also affect the two observation techniques differently (Tregoning et al., 2009).

Care should however be taken into account on both GRACE and GPS results since they may have been affected by errors during data acquisition, data generation, data transformation and data processing which may have resulted in discrepancies.

5.3 Recommendations

- In order to overcome the missing data in this study, it is suggested in the future study to include more continuous GPS data in the analysis considering long time interval. This is due to the fact that, only 5 IGS stations were used in this study for a period of five years from June 2008 to March 2012. This can be achieved by extending more permanent IGS stations in East African region especially in Tanzania and Burundi where there is no operating IGS station and activate all inactive IGS stations. Currently there are only five operating IGS stations in East Africa.

- Since some stations showed strong negative correlation with GRACE signal in north, east and up components which indicate strong anti-correlation or phase difference between the two signals (Tregoning et al., 2009), there is a possibility that they are effected by other geophysical processes taking place in the respective areas. For

example NURK station which is in the western rift system showed more negative correlation in the up component compared to MBAR which is also in the western rift system and RCMN in the eastern rift system which showed negative correlation in north and east components respectively. Since GRACE has shown its ability to detect hydrological mass component in great efficient, there is a need to incorporate it with more GPS data covering large area, hydrological models and other deformation analysis techniques to study this nature.

APPENDICES

Appendix I: Position time series for ADIS station

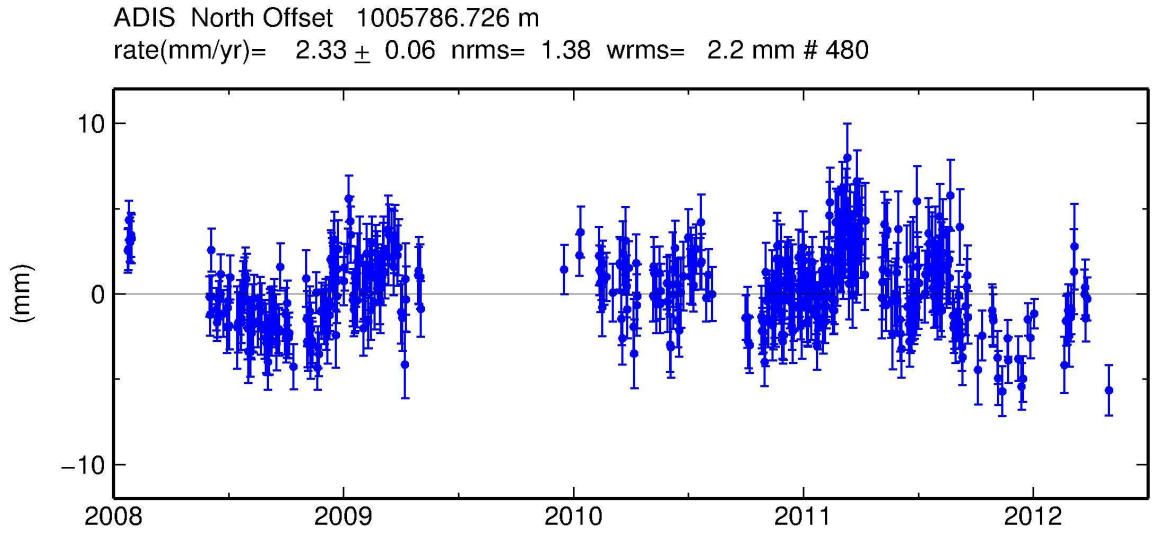

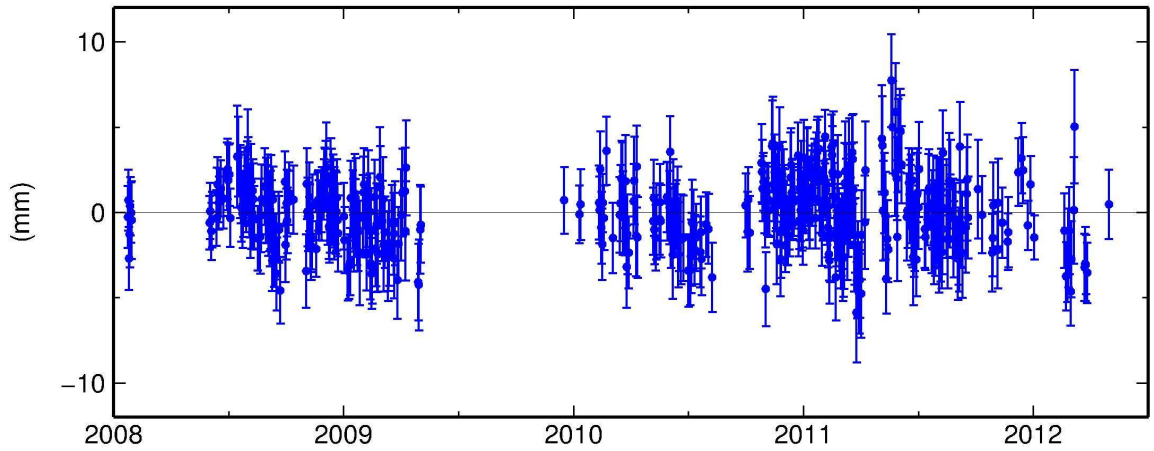

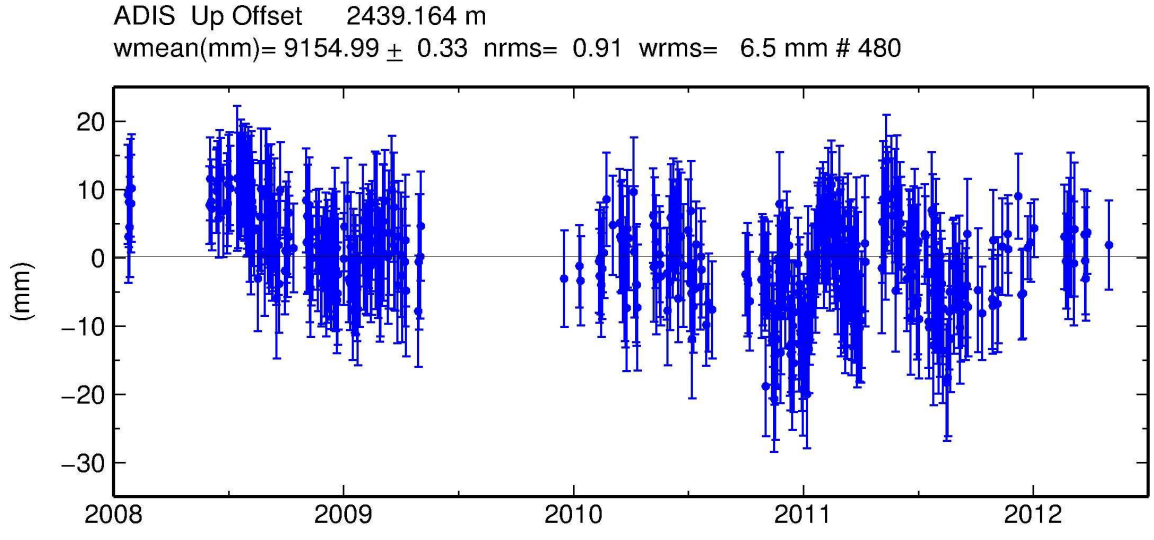

Appendix II: Position time series for MAL2 station

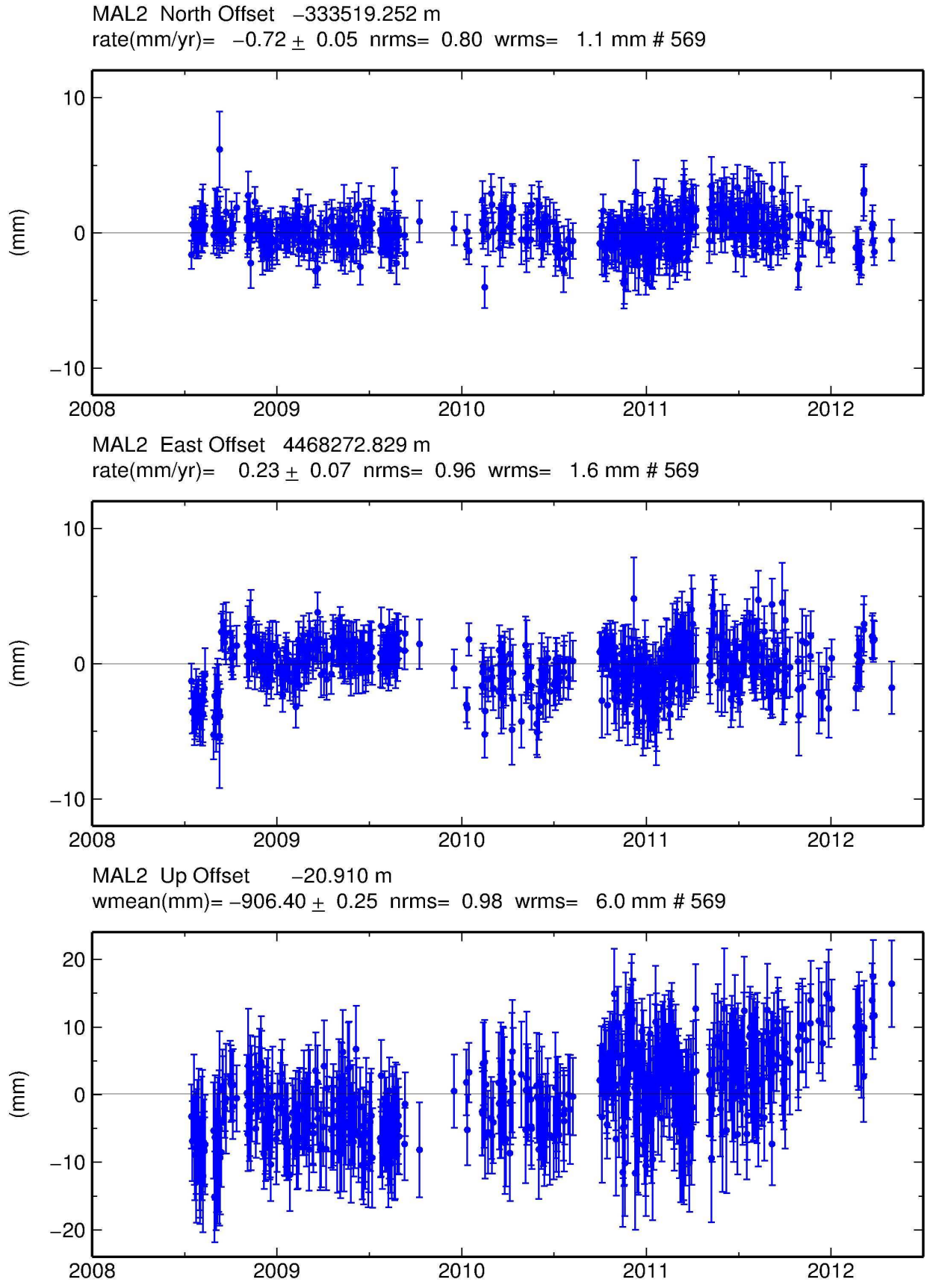

Appendix III: Position time series for NURK station

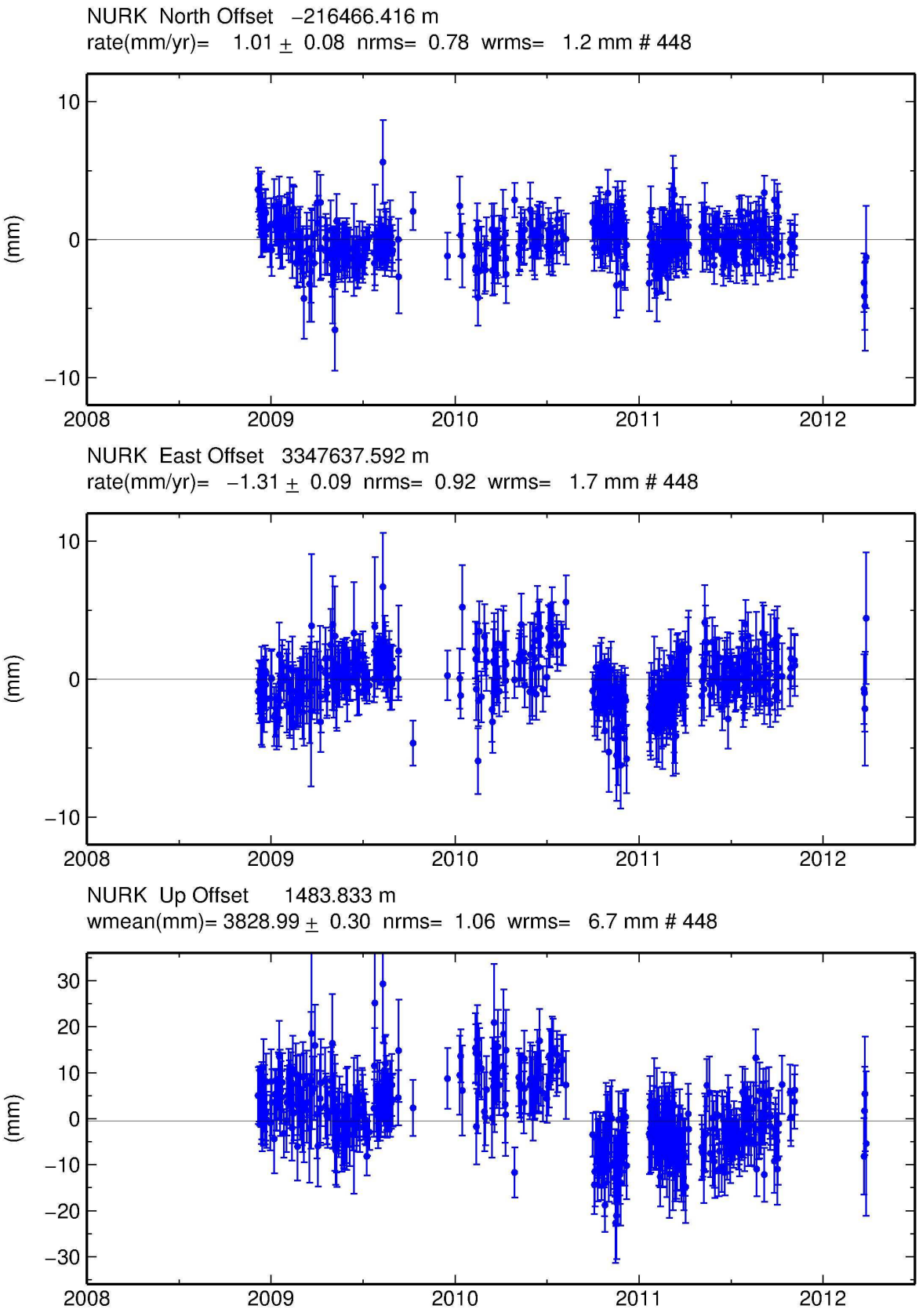

Appendix IV: Position time series for RCMN station

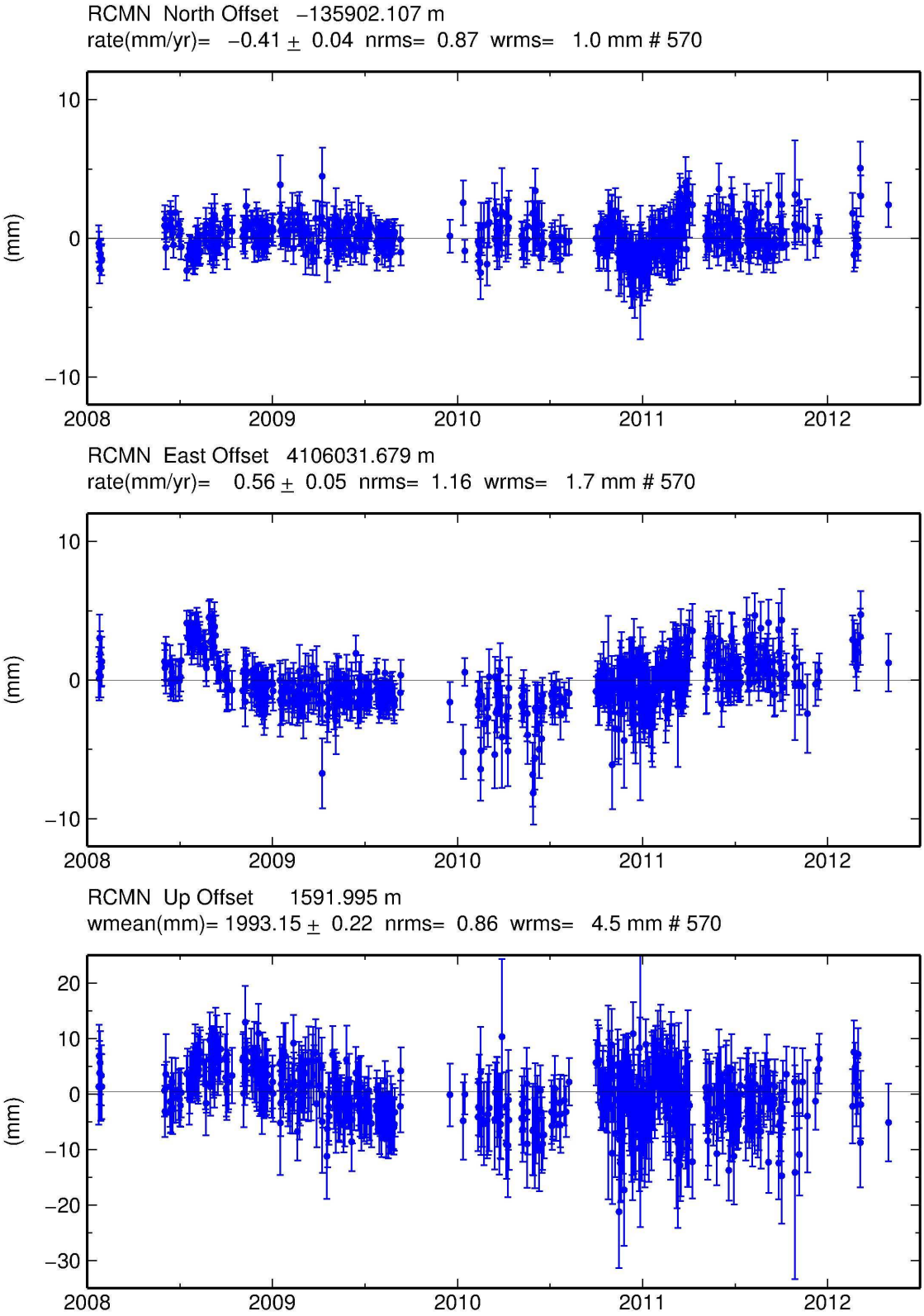

Appendix V: Position time series for MBAR station

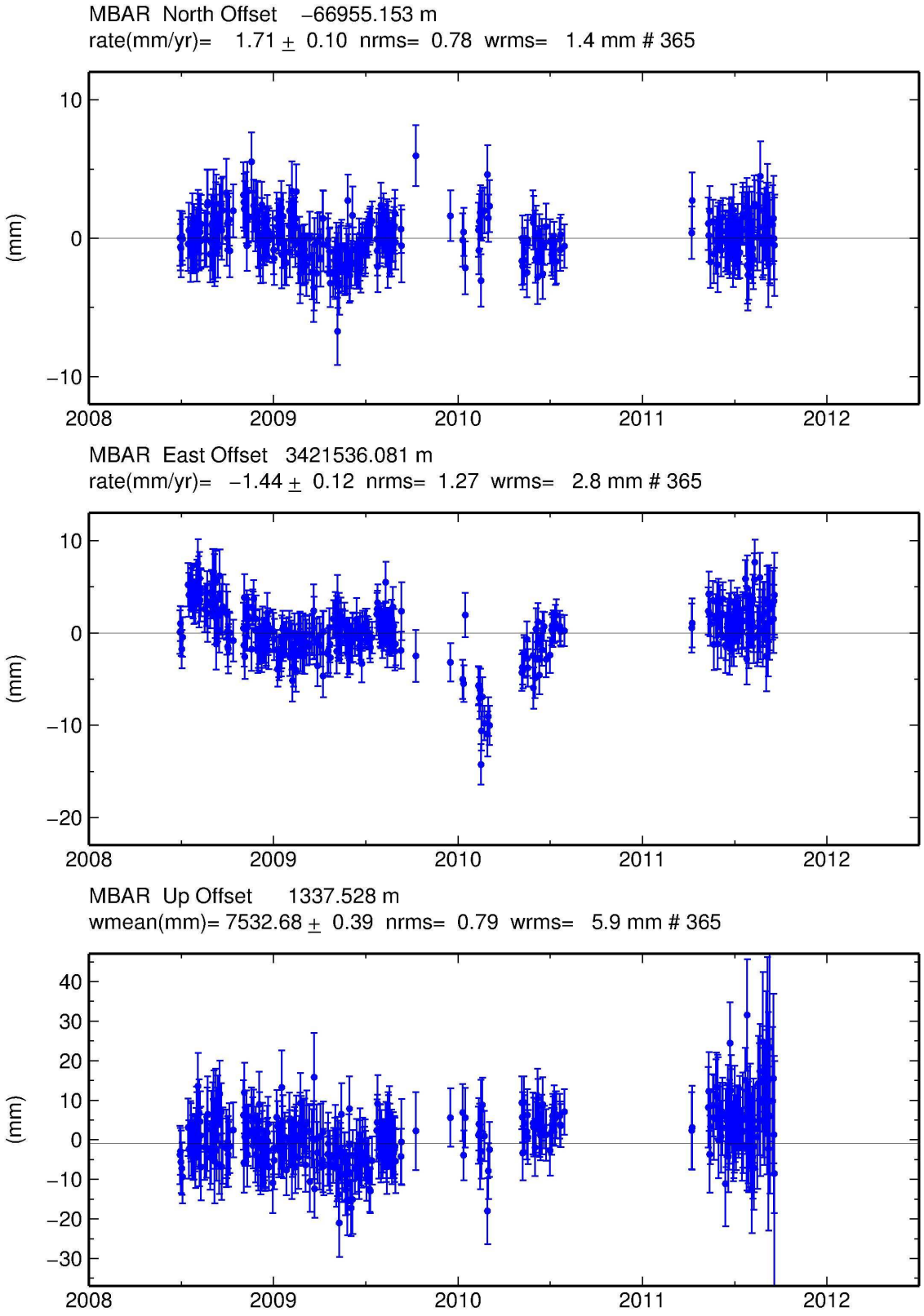

Appendix VI: Anomaly maps for CSR, GFZ, JPL and CNES Models for December 2009

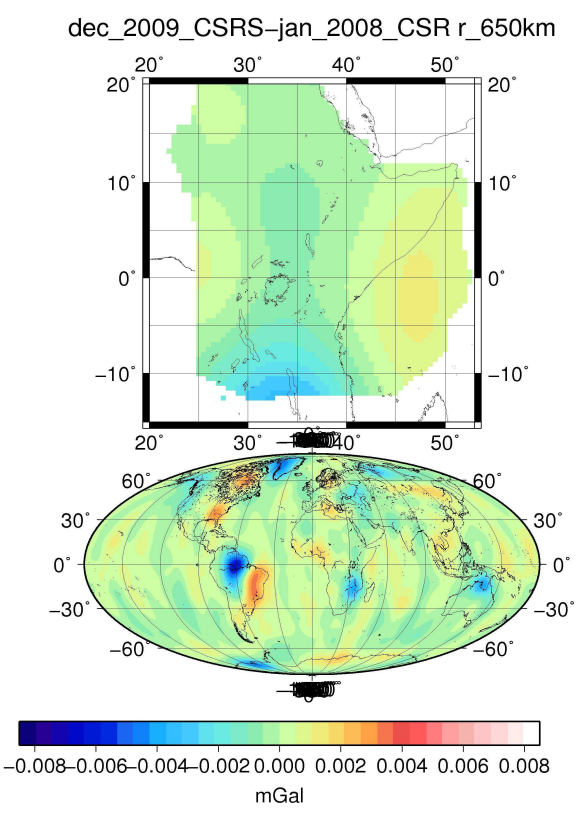

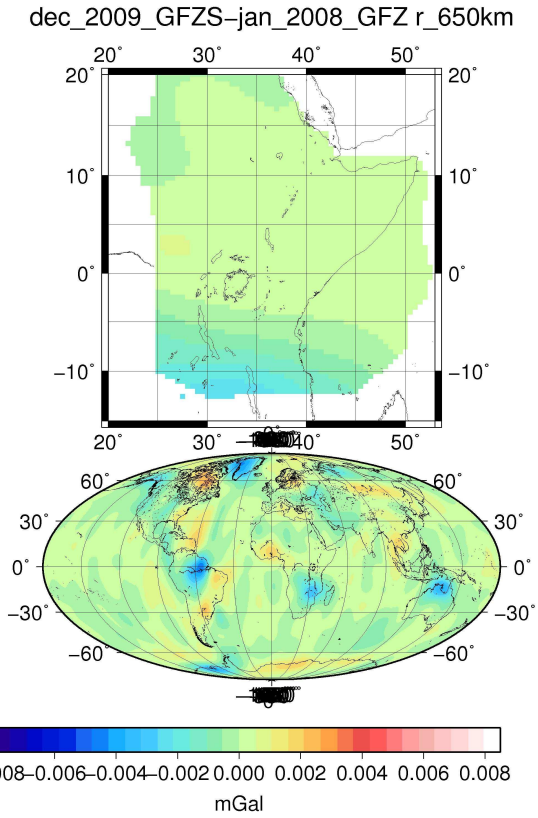

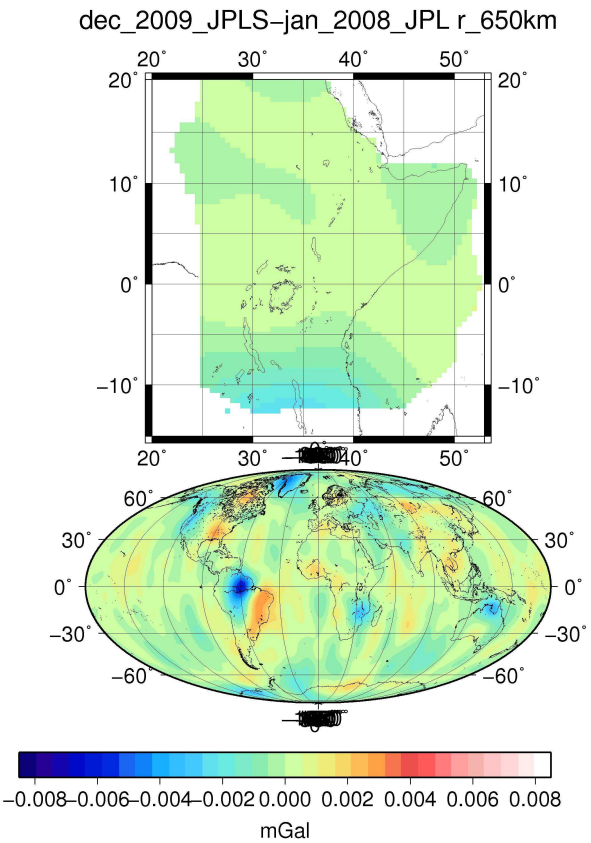

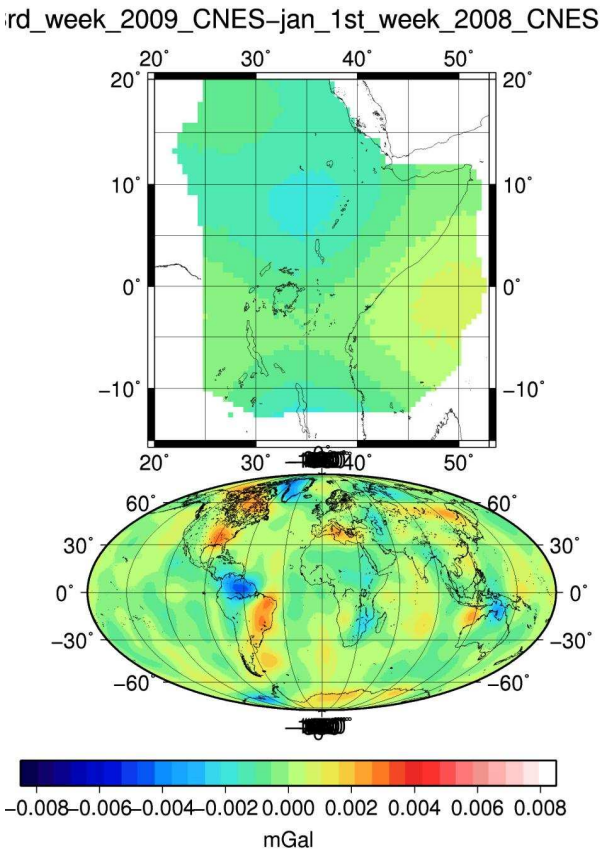

Appendix VII: Anomaly maps for CSR, GFZ, JPL and CNES Models for January 2010

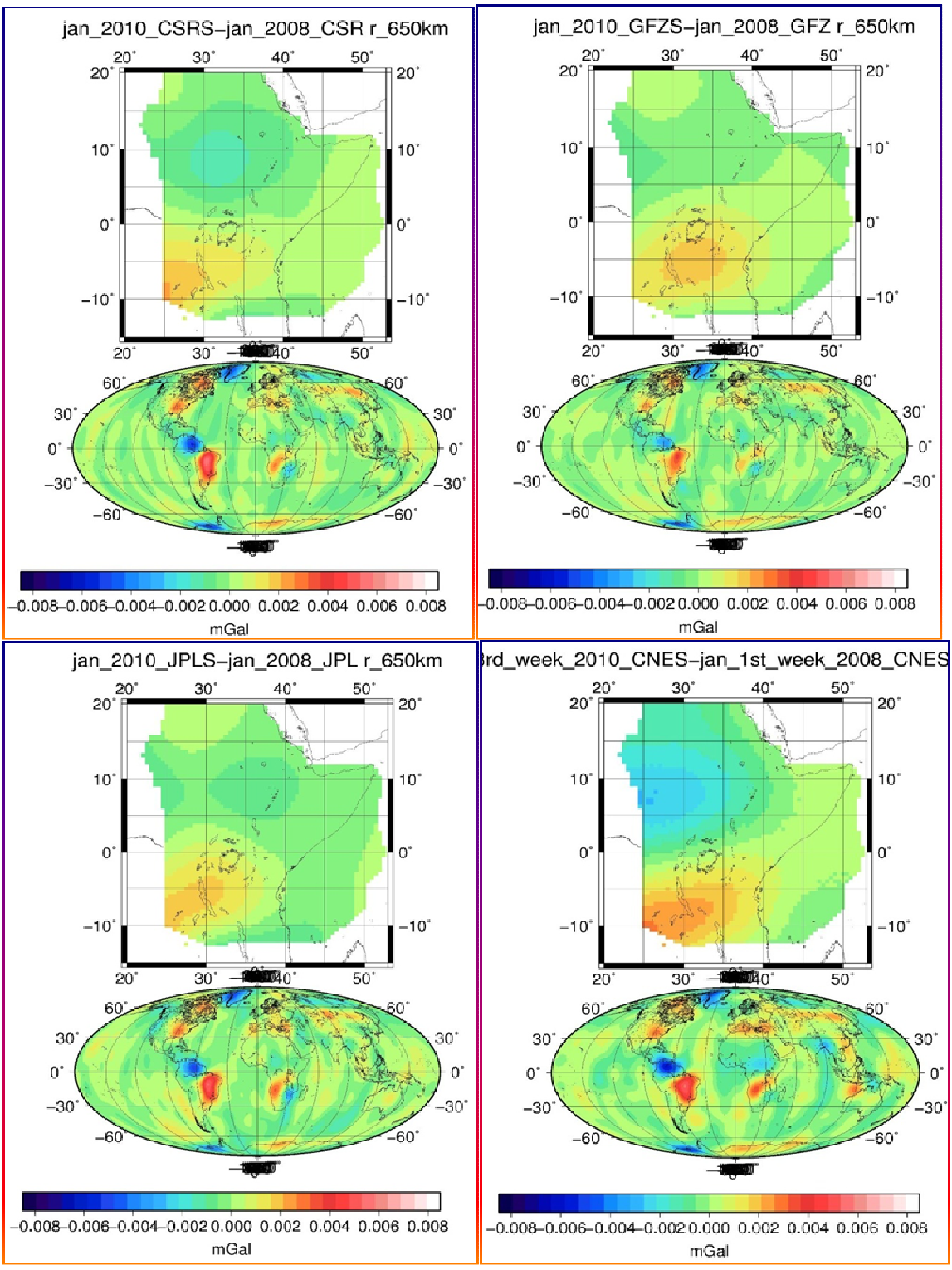

Appendix VIII: Anomaly maps for CSR, GFZ, JPL and CNES Models for Feb 2010

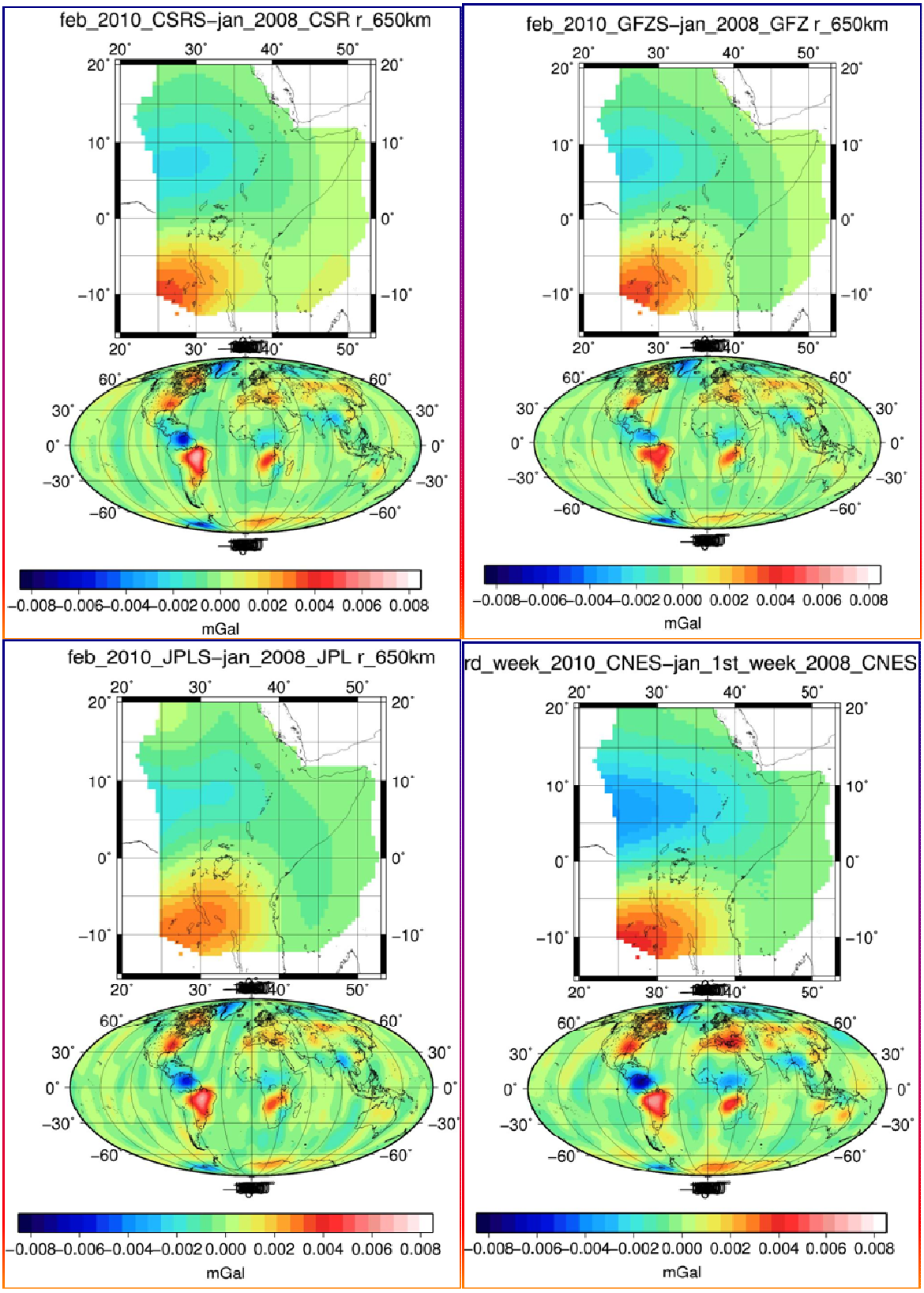

Appendix IX: Anomaly maps for CSR, GFZ, JPL and CNES Models for August 2010

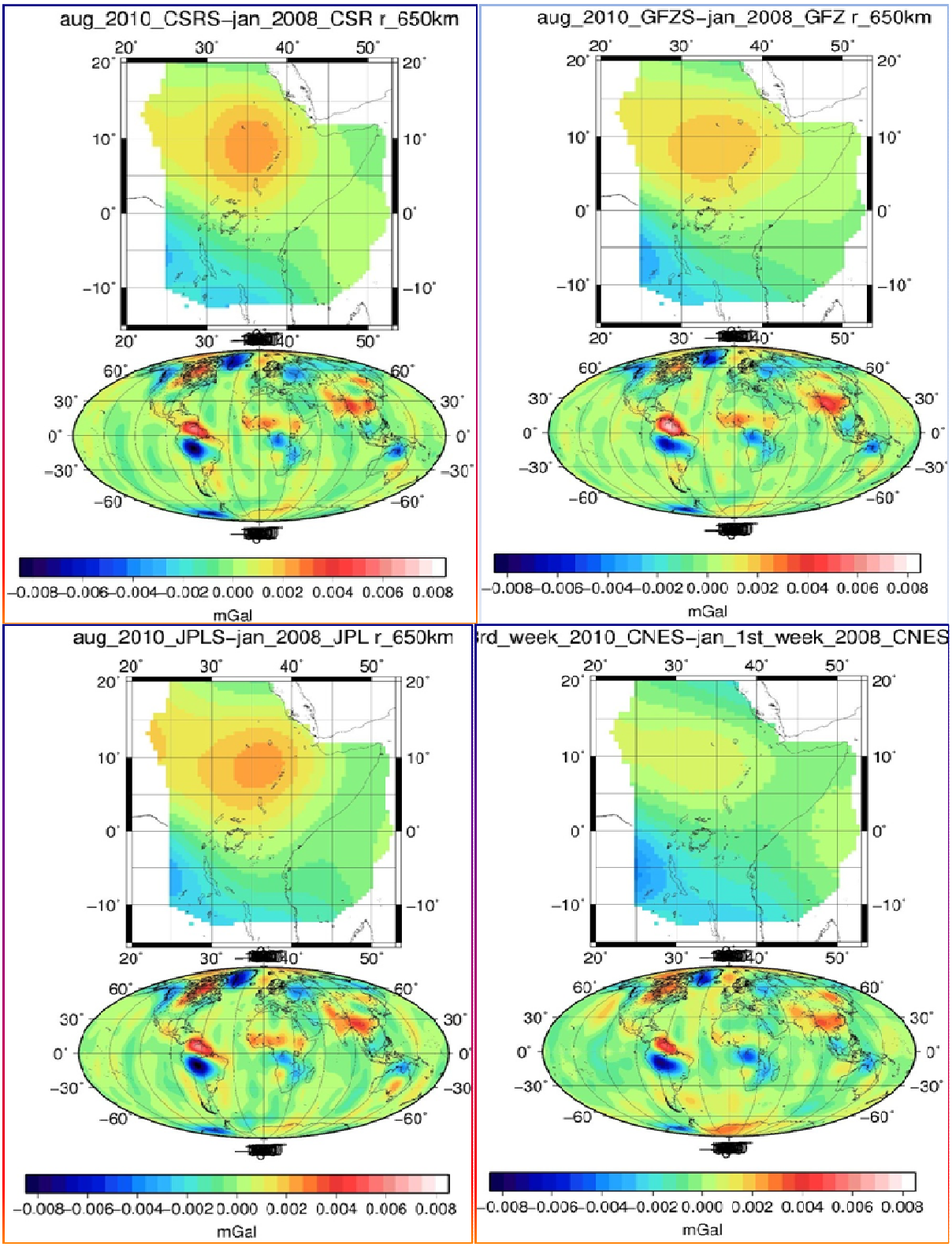

Appendix X: Anomaly maps for CSR, GFZ, JPL and CNES Models for September 2010

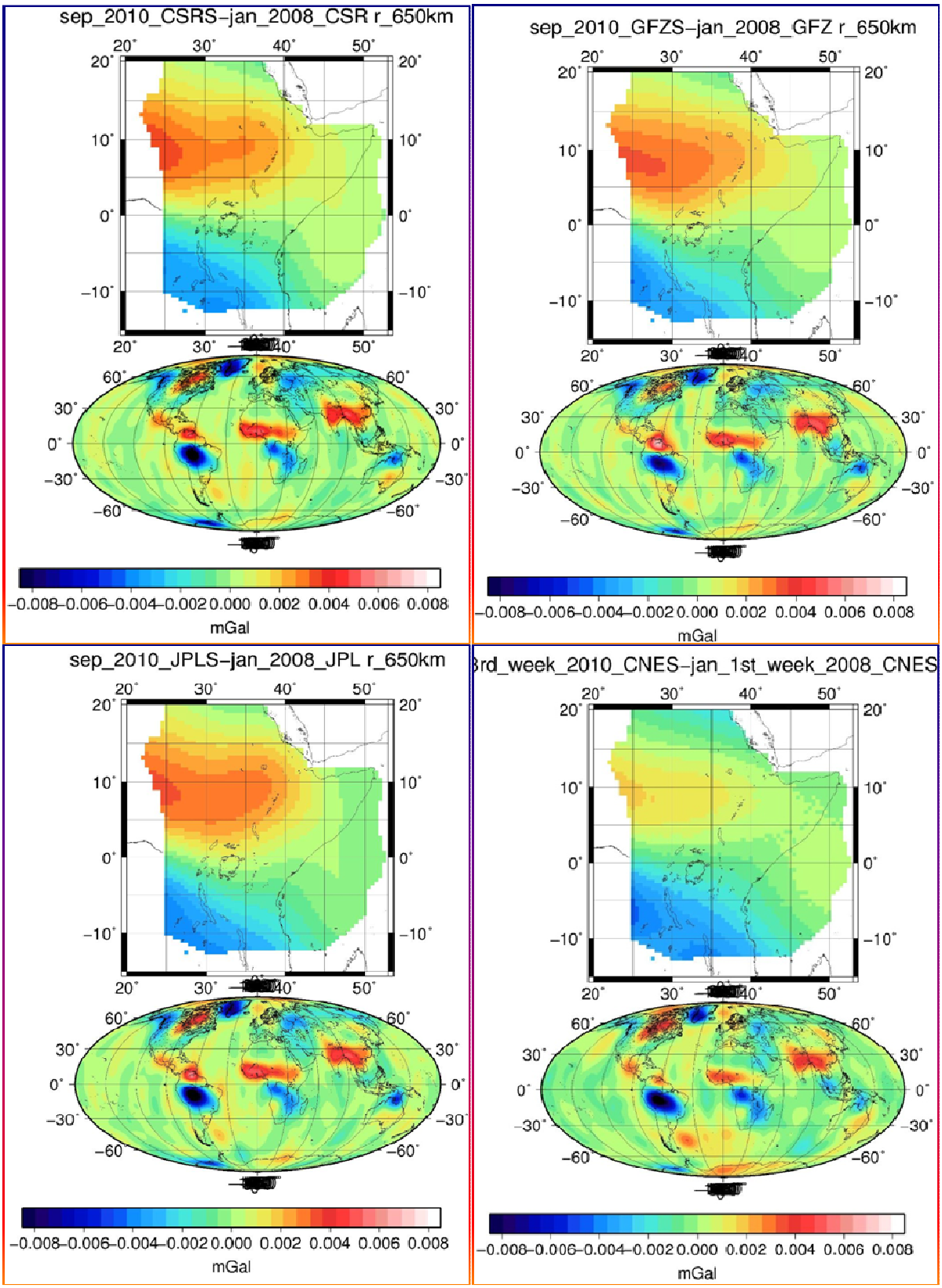

Appendix XI: Anomaly maps for CSR, GFZ, JPL and CNES Models for October 2010

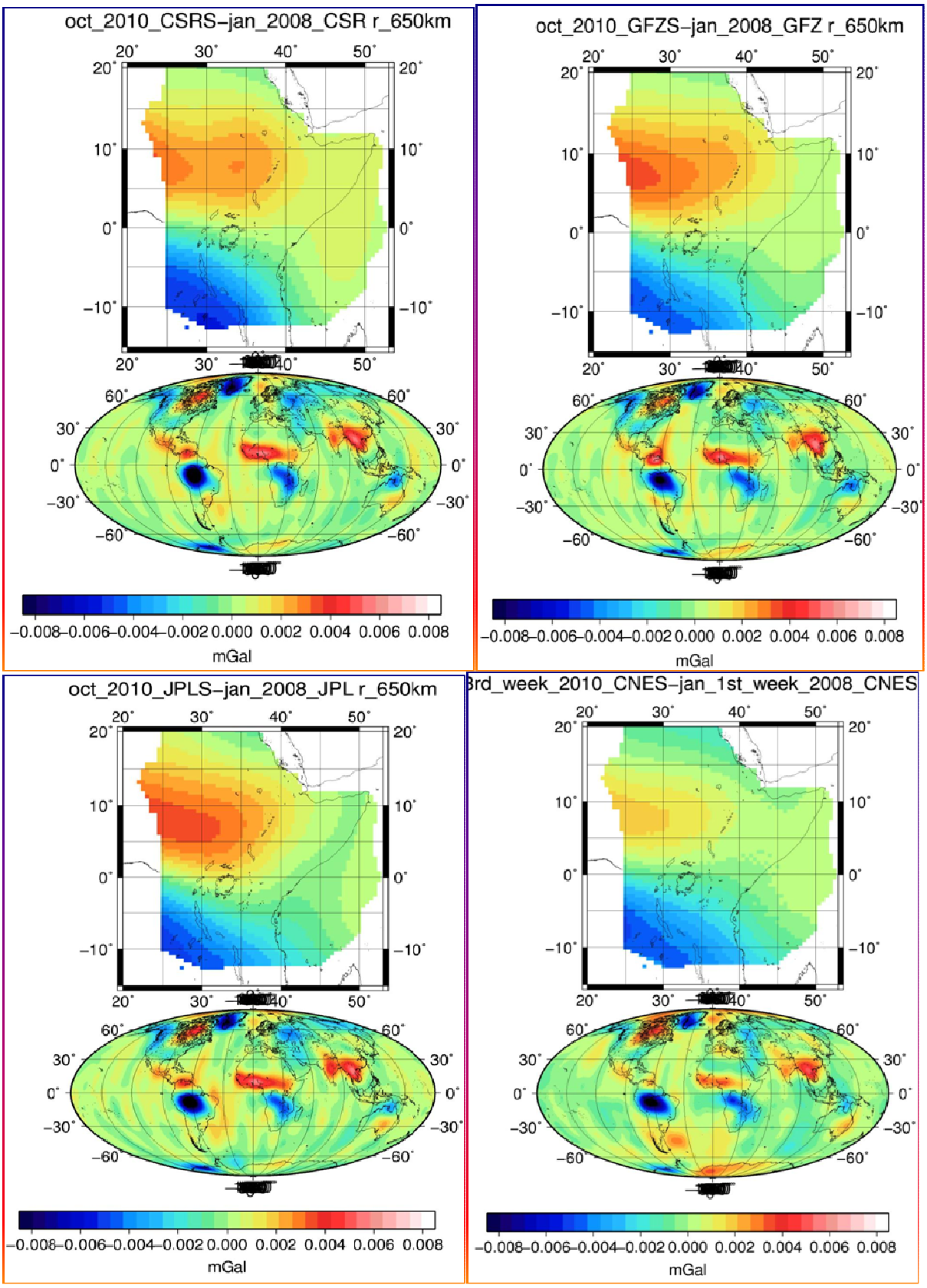

REFERENCES

Altamimi, Z. (2010). Global Terrestrial Reference Systems and Frames. Technical Seminor on Reference Frame in Practice, Rome-Italy.

Altamimi Z, Collilieux X, Métivier L, (2011). ITRF2008: An improved solution of the international terrestrial reference frame. J Geod (2011) 85:457–473 DOI 10.1007/s00190-011-0444-4.

Avsar B. N, and Ustun A, (2012). Analysis of Regional Time-Variable Gravity Using GRACE's 10-day Solutions. Turkey.

Arendt, A. A., K.A. Echelmeyer, W. D. Harrison, C. S. L ingle, and B. Valentine (2002). Rapid wastage of Alaska glaciers and their contribution to rising sea level, Science, 297, 382 -386, 2002.

Barthelmes, F., and Köhler, W., (2010). A web based service for using Global Earth Gravity Field Models. Helmholtz-Centre Potsdam, German.

Bedada, T., (2007). Combining space based GRACE gravity field measurement and Climatologically averaged precipitation data to assess essential features of hydrological mass variations within the Nile Basin. MSc Thesis, Addis Ababa University, Ethiopia.

Beutler, G., (2011). International Association of Geodesy. 1800 Jefferson Davis Highway, Arlington, VA 22202, USA.

Blewitt, G., (1997). Basics of the GPS Technique: Observation Equations. Swedish Land Land Survey, University of Newcastle, Newcastle upon Tyne, NEI 7RU, United Kingdom.

Boehm J, Schuh H (2004). Vienna Mapping Functions in VLBI analyses, Geophys. Res. Lett. 31(1):L01603, DOI:10.1029/2003GL018984

Boehm, J., Cerveira, P.J.M., Schuh, H., and Tregoning, P. (2005). The impact of tropospheric mapping functions based on numerical weather models on the determination of geodetic parameters, IAG Proceedings.

Bonsor H. C, Mansour M. M, MacDonald A. M, Hughes A. G, Hipkin R. G, and Bedada T (2010). Interpretation of GRACE data using a groundwater recharge model, Hydrol. Earth Syst. Sci., 7, 4501–4533.

Calais, E. (2010). The Global Positioning System. Purdue University-EAS Department. Website:http://web.ics.purdue.edu/~ecalais/teaching/geodesy/GPS_observables.pdf).

Chambers, D. P., and Bonin, J. A., (2012). Evaluation of Release-05 GRACE time-variable gravity coefficients over the ocean. Ocean Sci., 8, 859–868, doi:10.5194/os-8-859-2012.

Chen, JL, Wilson, CR, Tapley, BD, Blankenship, D, Young, D, (2008). Antartic regional ice loss from GRACE, Earth Planet Science Letter, 266: 140–148.

Clore, E. R., (2012). International Development in Global Navigation Satellite Systems (GNSS). U.S. Technical Training Institute, George Washington University, Washington, D.C. Website: http://www.gps.gov/multimedia/presentations/2012/

Crowley, J., J. Mitrovica, R. Bailey, M. Tamisiea, and J. Davis (2006). Land water storage within the Congo Basin inferred from GRACE satellite gravity data, Geophys. Res. Lett., 33, L19402, doi:10.1029/ 2006GL027070.

Dach, R., J. Boehm, S. Lutz, P. Steigenberger, and G. Beutler (2011). Evaluation of the impact of atmospheric pressure loading model on GNSS data analysis, J. Geod., 85, 75–91, doi:10.1007/s00190-010-0417-z.

Davis, J. L., P. Elosegui, J. X. Mitrovica, and M. E. Tamisiea (2004). Climate-driven deformation of the solid Earth from GRACE and GPS, Geophys. Res. Lett., 31, L24605, doi:10.1029/2004GL021435.

Dickey, J.O., Bentley, C.R., Bilham, R., Carton, J.A., Eanes, R.J., Herring, T.A., Kaula, W.M., Lagerloef, G.S.E., Rojstaczer, S., Smith, W.H.F., van den Dool, H.M., Wahr, J.M., Zuber, M.T. (1997). Satellite Gravity and the Geosphere, National Research Council Report, National Academy Press, 112 pp.

Dunn, C, et al, 2003. Instrument of GRACE: GPS augments gravity measurements, GPS World, 14(2), 16–28.

Farahani, H. H., and Ditmar, P., (2011). Earth's Gravitational Field Recovery based on an optimal combination of GRACE and GOCE satellite data. Proc. of '4th International GOCE User Workshop' (ESA SP-696, July 2011), Munich, Germany.

Förste, C, Schmidt, R, Stubenvoll, R, Flechtner, F, Meyer, U, König, R, Neumayer, H, Biancale, R, Lemoine, JM, Bruinsma, S, Loyer, S, Barthelmes, F, Esselborn, S, (2008). The GeoForschungsZentrum Potsdam/Groupe de Recherche de Geodesie Spatiale satellite-only and combined gravity field models: EIGEN-GL04S1 and EIGENGL04C. Journal of Geodesy, 82:331–346.

Grippa, M., et al. (2011). Land water storage variability over West Africa estimated by Gravity Recovery and Climate Experiment (GRACE) and land surface models, Water Resour. Res., 47, W05549, doi:10.1029/ 2009WR008856.

Han, S.-C., I.-Y. Yeo, D. Alsdorf, P. Bates, J.-P. Boy, H. Kim, T. Oki, and M. Rodell (2010). Movement of Amazon surface water from timevariable satellite gravity measurements and implications for water cycle parameters in land surface models, Geochem. Geophys. Geosyst., 11, Q09007, doi:10.1029/2010GC003214.

He XF.; Guang Y.; Ding XL.; Chen YQ (2004). Application and evaluation of a GPS-multi-antenna system for dam deformation monitoring. Earth Planets and Space 56 (11): 1035-1039.

Heiskanen, W. & Moritz (1967). H., Physical Geodesy, Freeman, San Francisco, 364 pp.

Herring, T.A., King, R.W., McClusky, S.C., (2010). Introduction to GAMIT/GLOBK. Rel 10.4, Massachusetts Institute of Technology, Australia.

Hofmann-Wellenhof, B., Lichtenegger, H., and Wasle, E (2008). GNSS-Global Navigation Satellite Systems. Springer-Verlag Wien. New York (USA).

Hofmann-Wellenhof, B. and Moritz, H. (2005), Physical Geodesy. Springer-Verlag Wien. Australia.

Hunegnaw, A., (2011). Satellite orbits (lecture notes). Addis Ababa University, Ethiopia. Email: ahunegnaw@gmail.com.

Hu XG, Chen JL, Zhou YH, Huang C, Liao XH (2006). Seasonal water storage changes of the Yangtze River Basin detected by GRACE , Sci China Ser D Earth Sci, 49 (5), 483 – 49, 2006.

ICGEM, (2012). International centre for global earth models (ICGEM), Website. http://icgem.gfz-potsdam.de/ICGEM/ICGEM.html.

IGS Progress Report, (2012). International GNSS service Progress Report. IGS Central Bureau, Pasadena, California, U.S.A. Website: ftp://igs.org/pub/resource/pubs/.

Jekeli, C., (1981). Alternative method to smooth the Earth's gravity field, Dep. Of Geod. Sci.& Surv., Ohio State University, Columbus, Rep.327.

Khan, S. I., Adhikari, P., Hong, Y., Vergara, H., Adler, R. F., Policelli, F., Irwin, D., Korme, T., and Okello, L., (2011). Hydroclimatology of Lake Victoria region using hydrologic model and satellite remote sensing data. Hydrol. Earth Syst. Sci., doi:10.5194/hess-15-107-2011.

King, M., P. Moore, P. Clarke, and D. Lavallée (2006). Choice of optimal averaging radii for temporal GRACE gravity solutions, a comparison with GPS and satellite altimetry, Geophys. J. Int., 166, 1–11, doi:10.1111/ j.1365-246X.2006.03017.x.

King, N. E.; Svarc J. L.; Fogleman E. B.; Gross W. K.; Clark K. W.; Hamilton G. D.; Stiffler C. H.;Sutton J. M. (1995). Continuous GPS observations across the Hayward fault, California, 1991-1994, J. Geophys. Res., 100, 20,271- 20,283, 1995.

Kogan M. G., Steblov G. M., King R. W., Herring T. A., Frolov D. I., Egorov S. G., Levin V. Y., Lerner-Lam A., Jones A. (2000). Geodetic constraints on the rigidity and relative motion of Eurasia and North America, Geophys. Res. Lett., 27, 2041-2044, 2000.

Kusche, J., and Schrama, E. J. O., (2005). Surface mass redistribution inversion from global GPS deformation and GRACE gravity data, J. Geophys. Res., 110, B09409, doi:10.1029/2004JB003556.

Longuevergne, L., B. R. Scanlon, and C. R. Wilson (2010). GRACE Hydrological estimates for small basins: Evaluating processing approaches on the High Plains Aquifer, USA, Water Resour. Res., 46, W11517, doi:10.1029/2009WR008564.

Miller, J., (2013). SATELLITE 2013. (The on-going Modernization of GPS). NASA Headquarters. U.S.A. Website: http://www.gps.gov/multimedia/presentations/2013/03/satellite2013/miller.pdf

Nahmani, S., et al. (2012). Hydrological deformation induced by the West African Monsoon: Comparison of GPS, GRACE and loading models, J. Geophys. Res., 117, B05409, doi:10.1029/2011JB009102.

Neilan, R., Fisher, S., Khachikyan, R., Ceva, J., Craddock, A., Donnelly, N., Maggert, D., and Walia, G (2012). IGS Technical Report 2012 Central Bureau. Website: http://igs.org/organization/orgindex.html.

Newton's Bulletin, (2009). External Quality Evaluation Reports of EGM08, (Issue no. 4); International Association of Geodesy and International Gravity Field Service. ISSN 1810-8555. (http://www.iges.polimi.it/Newton/Newton_4/NEWTON4_TOTAL.pdf)

Pail, R., Goiginger, H., Schuh, W., Eduard Höck, E., Brockmann, J.M., Fecher, T., Mayer- Gürr, T., Kusche, J., Adrian Jäggi, A., Lars Prange, L., Daniel Rieser, D., Hausleitner, W., Maier, A., Krauss, S., Baur, O., Krasbutter, I., and Gruber, T., (2011). Combination of GOCE data with complementary gravity field information. Proc. of '4th International GOCE User Workshop' (ESA SP-696, July 2011), Munich, Germany.

Pavlis, NK, Holmes, SA, Kenyon, SC, Factor, JK, (2008). An Earth gravitational model to degree 2160: EGM2008, Oral presentation at EGU General Assembly 2008, Vienna, Austria, April 13–18.

Rajner, M., and Liwosz, T., (2011). Studies of crustal deformation due to hydrological loading on GPS height estimates, Geod. and Cart. Res., 143, Vol. 60, No 2, 2011, pp. 135-144.

Ramillien, G., F. Frappart, A. Cazenave, and A. Guntner (2005). Time variations of land water storage from an inversion of 2 years of GRACE geoids, Earth Planet. Sci. Lett., 235, 283–301, doi:10.1016/j.epsl.2005. 04.005

.

Reager, J., and J. Famiglietti (2009). Global terrestrial water storage capacity and flood potential using GRACE, Geophys. Res. Lett., 36, L23402, doi:10.1029/2009GL040826.

Rodell, M., et al. (2004). The global land data assimilation system, Bull. Am. Meteorol. Soc., 85(3), 381–394, doi:10.1175/BAMS-85-3-381.

Saria, E., (2007). Kinematics of the East African Rift System using long baseline GPS measurements in Tanzania. University of Dar es salaam (UDSM). Tanzania.

Schmidt, R., et al. (2006). GRACE observations of changes in continental water storage, Global Planet. Change, 50, 112–126, doi:10.1016/j.gloplacha.2004.11.018.

Schmidt, R., S. Petrovic, A. Guntner, F. Barthelmes, J. Wunsch, and J. Kusche (2008). Periodic components of water storage changes from GRACE and global hydrology models, J. Geophys. Res., 113, B08419, doi:10.1029/2007JB005363.

Seeber, G. (2003). Satellite Geodesy. 2nd Completely Revised and Extended Edition. Walter de Gruyter,Berlin, New York 2003.

Steckler, M. S., S. L. Nooner, S. H. Akhter, S. K. Chowdhury, S. Bettadpur, L. Seeber, and M. G. Kogan (2010). Modeling Earth deformation from monsoonal flooding in Bangladesh using hydrographic, GPS, and Gravity Recovery and Climate Experiment (GRACE) data, J. Geophys. Res., 115, B08407, doi:10.1029/2009JB007018.

Smith, W.H.F., and P. Wessel (1990). Gridding with continuous curvature splines in tension, Geophysics, 55,293-305.

Swenson, S., and Wahr, J., (2002). Methods for inferring regional surface-mass anomalies from Gravity Recovery And Climate Experiment (GRACE) measurements of time-variable gravity, J. Geophys. Res., 107 (B9), 2002.

Swenson, S., Wahr, J., Milly, PCD., (2003). Estimated accuracies of regional water storage anomalies inferred from GRACE, Water Resour. Res., 39(8), 1223.

Swenson, S., and Wahr J., (2006). Estimating Large-Scale Precipitation Minus Evapotranspiration from GRACE Satellite Gravity Measurements. J. Hydrometeor, 7, 252–270.

Syed TH, Famiglietti JS, Chen J, Rodell M, Seneviratne SI, Viterbo P, Wilson CR (2005). Total basin discharge for the Amazon and Mississippi River Basin from GRACE and A land atmosphere water balance, Geophys. Res., Lett., **32 (L24404)** , 2005.

Syed, T. H., J. S. Famiglietti, M. Rodell, J. Chen, and C. R. Wilson (2008). Analysis of terrestrial water storage changes from GRACE and GLDAS, Water Resour. Res., 44, W02433, doi:10.1029/2006WR005779.

Tapley, B., S. Bettadpur, J. Ries, P. Thompson, and M. Watkins (2004). GRACE measurements of mass variability in the Earth system, Science, 305, 503–505, doi:10.1126/science.1099192.

Tapley, B, Ries, J, Bettadpur, S, Chambers, D, Cheng, M, Condi, F, Poole, S. (2007). The GGM03 Mean Earth Gravity Model from GRACE. Fall AUG Meeting, San Francisco.

Tapley, B, Ries, J, Bettadpur, S, Chambers, D, Cheng, M, Condi, F, Gunter, B, Kang, Z, Nagel, P, Pastor R, Poole, S, Wang, F, (2005). GGM02-an improved Earth gravity field model from GRACE, Journal of Geodesy, 79:467–478.

Tamisiea, M. E., E. W. Leuliette, J. L. Davis, and J. X. Mitrovica (2005). Constraining Hydrological and cryospheric mass flux in southeastern Alaska using space-based gravity measurements, Geophys. Res., Lett., 32(L20501) , 2005.

Tesmer, V., P. Steigenberger, T. van Dam, and T. Mayer-Gurr (2011). Vertical deformations from homogeneously processed GRACE and global GPS long-term series, J. Geod., 85, 291 310, doi:10.1007/ s00190-010-0437-8.

Tregoning, P., C. Watson, G. Ramillien, H. McQueen, and J. Zhang (2009b). Detecting hydrologic deformation using GRACE and GPS, Geophys. Res. Lett., 36, L15401, doi:10.1029/2009GL038718.

Van Dam T., Wahr J., (1998). Modelling environment loading effects: a review, Phys. chem. Earth, No 23, pp. 1077–1087.

Van Dam, T., J. Wahr, and D. Lavalle´e (2007). A comparison of annual vertical crustal displacements from GPS and Gravity Recovery and Climate Experiment (GRACE) over Europe, J. Geophys. Res., 112, B03404, doi:10.1029/2006JB004335.

Wahr, J., M. Molenaar, and F. Bryan (1998). Time variability of the Earth's gravity field: Hydrological and oceanic effects and their possible detection using GRACE, J. Geophys. Res., 103, 30,205–30,229, doi:10.1029/98JB02844.

Wahr, J., S. Swenson, V. Zlotnicki, and I. Velicogna (2004). Time-variable gravity from GRACE: First results, Geophys. Res. Lett., 31, L11501, doi:10.1029/2004GL019779.

Wahr, J., S. Swenson, and I. Velicogna (2006). The Accuracy of GRACE Mass Estimates. Geophys. Res. Lett., 33, L06401, doi:10.1029/2005GL025305.

Wessel, P., and Smith, W. H. F (1998). New improved version of the Generic Mapping Tools Released, EOS Trans. AGU, 79, 579, 1998.

Winsemius HC, Savenije HHG, van de Giesen NC, van den Hurk BJJM, Zapreeva EA, Klees R (2006). Assessment of gravity recovery and climate experiment (GRACE) temporal signature over the upper Zambezi, Water Resour Res., 42(I2): Art. No.W12201 , 2006.

Zerbini, S., B. Richter, F. Rocca, T. van Dam, and F. Matonti (2007). A Combination of Space and Terrestrial Geodetic Techniques to Monitor Land Subsidence: Case Study, the Southeastern Po Plain, Italy, J. Geophys. Res., 112, B05401, doi:10.1029/2006JB004338.

Zhang, J., (2007). Precise Velocity and Acceleration Determination Using a Standalone GPS Receiver in Real Time. School of Mathematical and Geospatial Sciences, Royal Melbourne Institute of Technology, Australia.

Zhang, K., Hu, Y., Liu, G., Wu, F., and Deakin, R., (2005). Deformation monitoring and analysis using Victorian regional CORS data, Journal of GPS. Res., 129, Vol. 4, No. 1-2: 129-138, 2005.

DECLARATION

I, Bakari Mchila Hemedi declare that, this thesis on "A study of movement of IGS stations due to hydrological water loading using GRACE and GPS data (A case study of East Africa)" is my own writing and has never been presented and will not be presented in any other institution for any degree award.

SUBMITTED BY:

Bakari Mchila Hemedi _____ _____

Signature Date

CONFIRMATION:

Dr. Adissu Humegnaw _____ _____

Advisor(s) Signature Date

Dr. Tulu Besha Bedada _____ _____

Co-Advisor(s) Signature Date